

**HCN/h-channel deficiency in forebrain neurons  
impairs early postnatal development and  
alters neuronal network activity in mice  
(*Mus musculus*, Linnaeus 1758)**

Dissertation with the aim of achieving a doctoral degree  
at the Faculty of Mathematics, Informatics and Natural Sciences

Department of Biology  
of Universität Hamburg

submitted by Andrea Merseburg

2016 in Hamburg

**Day of oral defense:**

June 3<sup>rd</sup>, 2016

**The following evaluators recommend the admission of the dissertation:**

Prof. Dr. Arp Schnittger

Prof. Dr. Dirk Isbrandt

## Abstract

The activity of voltage-gated ion channels is instrumental in governing neuronal excitability and network activity patterns in the central nervous system (CNS). Developing neuronal networks undergo dramatic changes in the composition of voltage-gated ion channels in order to orchestrate the maturation of functional connectivity and are especially vulnerable to abnormal activity. Any perturbation in the function or expression pattern of voltage-gated ion channels that occurs during development can therefore potentially impair maturation of neuronal networks and result in abnormal brain activity and behavior.

Unlike the majority of voltage-gated channels, hyperpolarization-activated cyclic nucleotide-gated (HCN) channels are unique in their activation upon hyperpolarized potentials close to the resting membrane potential. Activated HCN channels conduct a depolarizing mixed  $\text{Na}^+/\text{K}^+$  current –  $I(h)$ , which critically influences the neuron's membrane potential, input resistance, and integrative properties. Accordingly,  $I(h)$  contributes to a wide range of physiological phenomena; such as pacemaker activity, dendritic integration, plasticity mechanisms and information processing underlying learning and memory, resonant and oscillatory behavior of single neurons and neuronal networks, complex behavior, and disease. Furthermore, a growing body of evidence is indicating that  $I(h)$  plays a significant role in neuronal development. The functional diversity of  $I(h)$  is met by four HCN channel subunits (HCN1-4) that form homo- or heterotetrameric HCN1-4 channels with individual expression patterns, gating properties, and regulation by cyclic nucleotides and auxiliary subunits. Consequently, currents yielded by HCN1-4 channels are functionally diverse. Commonly used mouse models for studying  $I(h)$  are usually targeted to a specific HCN channel subunit, but no models are yet available that are designed to restrict  $I(h)$  deficiency to specific developmental stages.

This study was aimed at investigating the physiological roles of HCN subunit-mediated currents, independent of the endogenous subunit composition, with specific focus on the functional roles of  $I(h)$  in early postnatal development. To this end, two mouse models with conditional loss of  $I(h)$  restricted to forebrain projection neurons or cerebellar

Purkinje neurons were characterized. I(h) was functionally ablated through expression of a non-conducting, i.e. dominant-negative, HCN channel subunit (HCN-DN).

Functional I(h) ablation caused intrinsic neuronal hyperexcitability *in vitro* that resulted in network hypoexcitability in immature and mature neuronal networks *in vivo*. I(h) attenuation was accompanied by behavioral hyperactivity, mild cognitive deficits, gait abnormalities and motor dysfunction. Of note, the behavioral phenotype observed was critically dependent on I(h) during early postnatal development because loss of I(h) at more mature stages had only mild effects.

# 1. Introduction

## 1.1. Hyperpolarization-activated cyclic nucleotide-gated cation channels

I(h) was originally observed in cat motor neurons (Araki et al., 1961; Ito and Oshima, 1965), and first described in rod photoreceptors as a Cs<sup>+</sup>-sensitive, depolarizing, inward current activated upon hyperpolarization (Bader et al., 1979), later termed I(h) (Yanagihara and Irisawa, 1980). Around the same time, sinoatrial node cells (Noma and Irisawa, 1976) and Purkinje fibers of the mammalian heart were found to express a similar cation current that conducts both, Na<sup>+</sup> and K<sup>+</sup> ions, and was termed funny current, or I(f) (Barbuti et al., 2007). The first equivalent of I(h) in the central nervous system (CNS) was recorded in hippocampal pyramidal neurons and termed queer current (I(q)) (Halliwell and Adams, 1982). Since their initial discovery 55 years ago, HCN channels have been extensively studied in the heart and CNS. By driving a depolarizing Na<sup>+</sup> current upon activation at hyperpolarized potentials that drives the membrane voltage toward the action potential firing threshold, I(h) critically determines the basic biophysical properties which control neuronal excitability, i.e. the neuron's resting membrane potential and input resistance. Accordingly, I(h) contributes to a wide range of physiological phenomena; such as pacemaker activity, dendritic integration, plasticity mechanisms and information processing underlying learning and memory, resonant and oscillatory behavior of single neurons and neuronal networks, as well as complex behavior, and disease (as reviewed in (Pape, 1996; Robinson and Siegelbaum, 2003; Biel et al., 2009; DiFrancesco and DiFrancesco, 2015)).

### 1.1.1. HCN channel-mediated currents – I(h)

The HCN channel-mediated current is a mixed Na<sup>+</sup> and K<sup>+</sup> current, and unlike the majority of other voltage-gated channels, HCN channels activate upon hyperpolarized potentials negative to resting membrane potentials of –50 to –60 mV. The ratio of K<sup>+</sup> to Na<sup>+</sup> permeability is (3-5):1, yielding reversal potentials between –25 and –40 mV. Consequently, I(h) activated at hyperpolarized potentials is driven by a depolarizing

inward  $\text{Na}^+$  current (Fig. 1-1 A). Under current clamp conditions, activation of  $I(h)$  with negative current injections is typically reflected by a depolarizing sag in the voltage response of the membrane that brings it back towards resting membrane potential, and often, at the end of the current pulse rebound depolarization that is driven by the remaining  $\text{Na}^+$  influx before HCN channels deactivate can be observed (Fig. 1-1 B). When rebound depolarization does not exceed the action potential firing threshold, deactivation of HCN channels (and concomitant activation of potassium currents) at depolarized potentials brings the membrane back to resting potential. In dynamic interaction with other ion channels,  $I(h)$  greatly determines the stability of a neuron's resting membrane potential (RMP) (Robinson and Siegelbaum, 2003). By being active at subthreshold levels (i.e., at potentials between RMP and firing threshold),  $I(h)$  acts like a leak current and reduces a neuron's input resistance. The current activation and deactivation kinetics range from milliseconds to seconds with half-maximally activated currents at voltages between  $-60$  and  $-90$  mV ( $V_{1/2}$ ). Current responses to hyperpolarizing voltages can be described by a sigmoidal curve (Fig. 1-1 C), and are significantly modulated by intracellular cyclic adenosine monophosphate (cAMP). Elevated cAMP levels facilitate  $I(h)$  activation by shifting the voltage dependence to more positive potentials (by 10 mV and more), and accordingly a decrease in intracellular cAMP reduces current activation by shifting the activation curve to more negative values (Accili et al., 2002; Robinson and Siegelbaum, 2003).  $I(h)$  can be blocked by low concentrations of external  $\text{Cs}^+$  and various organic compounds, including anesthetics (Chen et al., 2005a, 2005b) or ZD7288 (Gasparini and DiFrancesco, 1997), and the heart-rate reducing agents ivabradine (Bois et al., 1996) and zatebradine (DiFrancesco, 1994). Pharmacological upregulation of  $I(h)$  is achieved using the anticonvulsant drug lamotrigine (Poolos et al., 2002).

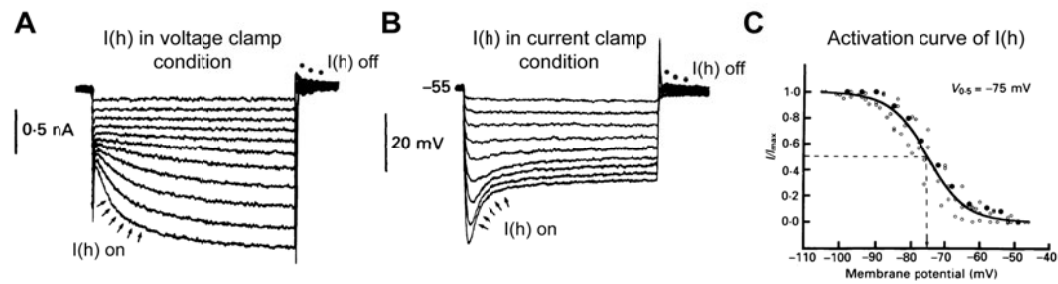


**Figure 1-1: Characteristics of I(h) conductance under experimental conditions.**

Thalamic relay neuron response to hyperpolarizing steps obtained under voltage clamp (A) and current clamp (B) conditions to demonstrate the conductance of I(h) (holding potential -55 mV, hyperpolarizing steps from -55 mV to -108 mV). **A:** Hyperpolarizing voltage steps elicit the slow inward conductance underlying I(h) (arrows, I(h) on). **B:** Hyperpolarizing current steps result in a hyperpolarized membrane voltage. Concomitant I(h) activation is voltage- and time-dependent and reflected by the depolarizing response or "sag" (indicated by arrows, I(h) on). **C:** Activation curve of I(h), obtained by tail current measurements (I(h) off marked by dots in A). The tail current amplitude upon return to holding potential is plotted as a function of hyperpolarizing voltage steps ( $I/I_{max}$ , i.e. tail current amplitudes normalized to the maximal amplitude). I(h) increases with increasing hyperpolarization voltage steps (x-axis, right to left), and is half-maximally activated ( $V_{0.5}$ ) at -75 mV. (Modified from McCormick and Pape, 1990).

The current is also diverse in its underlying HCN channel isoforms and their respective expression patterns and regulation in the central nervous system, which significantly contributes to the various functions of I(h), and will be described here in more detail (Pape, 1996; Accili et al., 2002; Robinson and Siegelbaum, 2003; Biel et al., 2009; He et al., 2014).

### 1.1.2. HCN channel family and regulation

The HCN channels belong to the superfamily of voltage-gated  $K^+$  channels and are encoded by four mammalian genes, *HCN1-4* (Santoro et al., 1997, 1998; Ludwig et al., 1998, 1999; Seifert et al., 1999). Each isoform consists of six transmembrane segments (S1 to S6) with a positively charged voltage sensor in S4, and a pore-forming P region containing the glycine-tyrosine-glycine (GYG) motif responsible for  $K^+$  selectivity, which is located between S5 and S6 (Macri et al., 2012). The cytoplasmic carboxy terminus harbors the cyclic nucleotide-binding domain (CNBD), which mediates the channel's responsiveness to cAMP. HCN1-4 subunits assemble into homo- or heteromeric tetramers (Xue et al., 2002) with subunit-specific voltage-dependence of activation, current kinetics, and regulation by cAMP (Fig. 1-2) (Wahl-Schott and Biel, 2009). The HCN1 channel isoform activates at the most depolarized membrane potentials ( $V_{1/2}$  of  $-70$  mV) with the fastest kinetics (100-300 milliseconds) and the lowest response to cAMP (shift in  $V_{1/2}$  by about 2-4 mV); HCN2 to HCN4 channel isoforms gradually exhibit more hyperpolarized activation potentials ( $V_{1/2}$  between  $-80$  and  $-100$  mV) and slower kinetics (2.5-10 seconds), and HCN2 and HCN4 channels show the highest cAMP-mediated facilitation of I(h) activation by shifting the voltage-dependence to more positive potentials (up to 10 mV and more). HCN3 channels are not regulated by cAMP (Santoro et al., 1998; Ludwig et al., 1999; Altomare et al., 2001; Chen et al., 2001; Moosmang et al., 2001; Stieber et al., 2005). The extent to which the binding of cAMP to HCN channels modulates their gating properties was shown to be dependent on the efficacy of CNBD-mediated inhibition (i.e., gating is shifted to more negative potentials), which varies among isoforms (Wainger et al., 2001). Besides the modulation by cyclic nucleotides, HCN channels are influenced by many more factors (as reviewed in (He et al., 2014)), including: i) small molecules (phosphatidylinositol-4, 5-bisphosphate (PIP<sub>2</sub>), acidic lipids, intracellular protons (pH)), ii) protein kinases (serine/threonine kinases, PKA and PKC, Ca<sup>2+</sup>/calmodulin-dependent protein kinase II (CAMKII)), and iii) auxiliary proteins (tetratricopeptide repeat-containing Rab8b interacting protein (TRIP8b), scaffolding proteins, min-K related protein (MiRP1)), and vi) a repertoire of neurotransmitters (acetylcholine, glutamate, serotonin, dopamine, norepinephrine), glutamate, nitric oxide, and neuropeptides. For example, TRIP8b targets HCN1 and HCN2 channels to distal dendrites of hippocampal and cortical neurons (Lewis et al., 2011; Huang et al., 2012), and regulates HCN channel gating and kinetics (Lewis et al., 2009; Santoro et al., 2009).

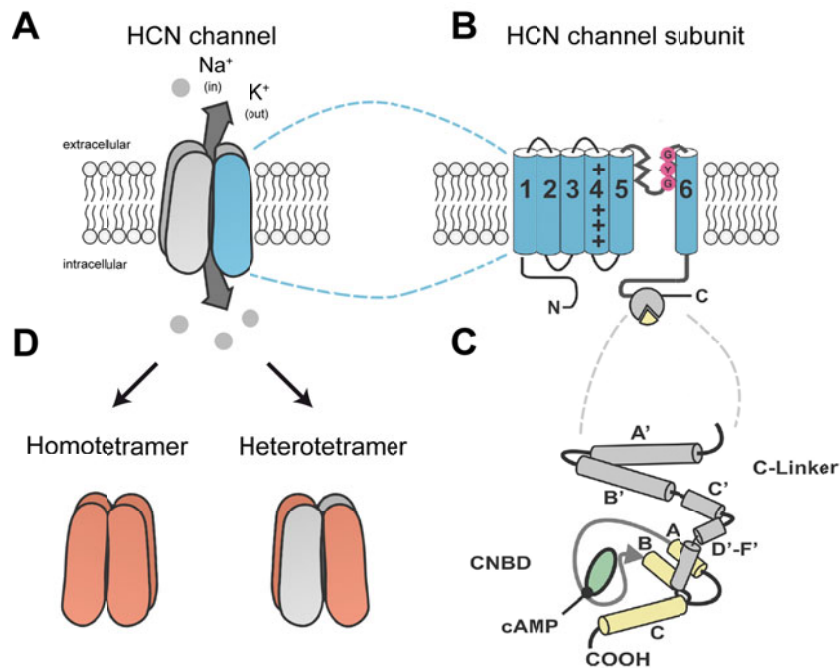


**Figure 1-2: Structure of HCN channels.**

**A:** HCN channels are tetrameric channels composed of four subunits that conduct  $\text{Na}^+$  and  $\text{K}^+$  ions. At physiological membrane potentials,  $\text{Na}^+$  flows into and  $\text{K}^+$  out of the cell. One subunit is highlighted in blue and shown in **B**: One subunit consists of six transmembrane segments (S1-6), a positively charged voltage sensor in S4 (indicated by "+"), and a pore-forming P region between S5 and S6 that comprises the glycine-tyrosine-glycine motif (GYG, highlighted in pink) responsible for  $\text{K}^+$  selectivity. The amino (N) and carboxy (C) termini are located in the intracellular cytoplasmic site. **C:** The C-terminus (COOH) of the HCN channel subunit comprises the C-linker and the cyclic nucleotide-binding domain (CNBD, highlighted in yellow). The C-linker consists of six alpha-helices (A' to F'). The CNBD consists of three alpha-helices (A to C, yellow), with a  $\beta$ -roll between helices A and B (indicated by the arrow). The CNBD binds cAMP (highlighted in green). **D:** Four subunits assemble into either homotetramers composed of one HCN channel isoform (red), or heterotetramers of two different isoforms (red and grey). (Modified from Wahl-Schott and Biel, 2009).

### 1.1.3. HCN channel expression pattern

The expression pattern of the HCN channel isoforms varies on many levels: between brain regions and cell types, within one cell at the subcellular location, and during the course of brain development (immature slow vs. mature fast currents).

Between different regions of the brain, the four HCN channel isoforms have been shown to have individual but partially overlapping expression patterns (Notomi and Shigemoto, 2004). HCN1 expression is distinct and prominently found in neocortex, hippocampus, cerebellum, brainstem, spinal cord, and dorsal root ganglion (DRG) (Moosmang et al., 1999, 2001; Santoro et al., 2000; Lörincz et al., 2002; Milligan et al., 2006). The HCN2 isoform can be ubiquitously found throughout the brain, with the highest expression in thalamus and brainstem nuclei, and it is expressed in small nociceptive DRG neurons

(Moosmang et al., 1999; Santoro et al., 2000). HCN3 can only be detected at very low levels, but is mostly found in the olfactory bulb and hypothalamus (Moosmang et al., 1999). HCN4 is selectively expressed in thalamic nuclei, distinct basal ganglia populations, and olfactory bulb (Moosmang et al., 1999; Santoro et al., 2000; Chan et al., 2004).

Within one cell, I(h) expression also varies depending on the subcellular localization. For example, in neocortical layer 5 pyramidal neurons (Stuart and Spruston, 1998; Lörincz et al., 2002) and hippocampal CA1 pyramidal neurons (Magee, 1998), I(h) is expressed in a somatodendritic density gradient, with current density increasing with distance from the soma. In contrast, interneurons of the medial septum, hippocampus, and cerebellum were shown to preferentially express HCN channels at the soma or axon terminals (Maccaferri and McBain, 1996; Luján et al., 2005; Aponte et al., 2006; Bender et al., 2007; Brewster et al., 2007). In cases in which HCN channel isoforms overlap in their expression pattern, e.g. HCN1 and HCN2 channels in pyramidal neurons of the neocortex and hippocampus, the resulting I(h) may be mediated either by separate homomeric channels formed by HCN1 and HCN2, or by heteromultimeric channels (He et al., 2014). This further adds to the variance in I(h). Evidence for heteromerization of HCN channel isoforms first came from studies in heterologous expression systems, including *Xenopus laevis* oocytes (Chen et al., 2001; Ulens and Tytgat, 2001) and human embryonic kidney (HEK) cells (Much et al., 2003). Coexpression of the HCN1 and HCN2 subunits in oocytes has been reported to yield currents with intermediate features to those expressed by HCN1 or HCN2 homomeric channels alone (Chen et al., 2001; Ulens and Tytgat, 2001). Of note, each subunit may exert specific dominant effects on the voltage dependence of activation and on the regulation of channel gating by cAMP of heteromeric channels (Accili et al., 2002). For example, HCN1 and HCN2 heteromers were shown to have HCN1-like activation potentials and HCN2-like regulation by cAMP (Chen et al., 2001; Ulens and Tytgat, 2001). HCN1 and HCN2 channels were co-immunoprecipitated from whole mouse brain lysates (Much et al., 2003), as well as from lysates of subdissected hippocampal CA1 area (Lewis et al., 2011). Finally, pathological brain states were shown to induce heteromerization of HCN channels, as shown for HCN1 and HCN2 channels in rat hippocampus when developmental seizures were induced (Brewster et al., 2005).

Another contributor to the high variance is development. The HCN subunit expression changes during embryonic and postnatal development, with immature stages characterized by slow  $I(h)$  and mature stages by prominent fast currents. The postnatal developmental expression profile of HCN channels has been studied in substantia nigra (Washio et al., 1999), hippocampus (Bender et al., 2001), and olfactory sensory cortex (Sciancalepore and Constanti, 1998), and can differ in terms of age of onset of expression, density, and subunit composition of HCN channels. In the mouse hippocampus, for instance, the HCN channel expression patterns evolve in the first three postnatal weeks before reaching mature states, and are differently regulated in CA1, CA3, and dentate gyrus (DG) pyramidal neurons and interneurons (Bender et al., 2001; Brewster et al., 2007). In CA1 pyramidal neurons, an increase in HCN1 expression is accompanied by downregulation of the HCN4 subunit. Although HCN2 levels stay relatively constant, their subcellular localization changes from somatic to dendritic during the developmental period. In CA3, HCN2 and HCN4 were shown to increase with age, whereas HCN1 channels disappear. Lastly, HCN1 and HCN2 protein levels in DG increased with age, whereas HCN4 levels did not change much during the developmental period. Additionally, pyramidal neurons precede interneurons in HCN channel expression, and it was found that interneurons in hippocampal layers CA1 and CA3 precede interneurons in the DG at the onset of HCN channel expression (Bender et al., 2001; Brewster et al., 2007).

As described above, HCN channel-mediated currents are highly versatile. Depending on subunit composition, subcellular localization, maturational state, and on the respective environment,  $I(h)$  exerts various heterogeneous physiological roles that influence a neuron's excitability and communication within a network.

## **1.2. Physiological roles of $I(h)$**

### **1.2.1. From excitability to behavior**

The stabilizing and depolarizing effects of  $I(h)$  on the membrane potential endows it with its most prominent role as a pacemaker current,  $I(f)$ , in sinoatrial node cells and Purkinje fibers in the heart (Barbuti et al., 2007); and in thalamocortical relay neurons (McCormick and Pape, 1990), brainstem inferior olive neurons (Bal and McCormick,

1997), substantia nigra dopaminergic neurons (Franz et al., 2000; Neuhoff et al., 2002), or hippocampal interneurons located in stratum oriens of CA1 (Maccaferri and McBain, 1996) in the CNS.

In spontaneously active cells, I(h) stabilizes the resting membrane potential to promote ongoing firing activity, such as in cerebellar Purkinje neurons (Raman and Bean, 1999), and hippocampal interneurons in stratum lacunosum moleculare (Chapman and Lacaille, 1999). Cerebellar Purkinje neurons, for instance, usually fire tonically at high frequencies, but when I(h) was blocked, their activity was shown to switch between high firing episodes and states of relative silence (Williams et al., 2002). These findings demonstrate the important function of I(h) by limiting the extent of membrane hyperpolarization brought about by inhibitory postsynaptic potentials (IPSPs) in order to keep the membrane close to firing threshold (Robinson and Siegelbaum, 2003). The ability to maintain persistent spiking in cerebellar Purkinje neurons and, concomitantly, their integrative properties associates HCN channel-mediated currents with a role in motor learning (Nolan et al., 2003). The authors showed that a general *Hcn1* deletion impairs learning of coordinated movements, whereas mice with forebrain-restricted *Hcn1*<sup>-/-</sup> had normal motor performance. Similar deficits in the expression of motor functions were also observed in *Hcn2*<sup>ap/ap</sup> and TRIP8b<sup>-/-</sup> mice (Chung et al., 2009; Lewis et al., 2011). In addition, I(h) is implied to play a role in working memory by a mechanism not yet fully resolved but shown to be orchestrated by the interaction of HCN1 channel-mediated currents, cAMP, and alpha2-adrenergic receptors (Wang et al., 2007; Barth et al., 2008; Thuault et al., 2013).

In neurons that are not spontaneously active, I(h) critically contributes to the dendritic integration of incoming excitatory postsynaptic potentials (EPSPs) (Magee, 1998, 1999). Active I(h) at subthreshold hyperpolarized levels reduces the input resistance and thus affects the summation of local dendritic EPSPs. As a result, I(h) exerts a shunting effect on EPSP summation that increases with current density (Magee, 1999). This led to the assumption that I(h) constrains hippocampus-dependent learning and memory, since mice with a forebrain-restricted *Hcn1* deletion exhibited a better performance in the hippocampus-dependent water maze task (Nolan et al., 2005). I(h) suppression in CA1 pyramidal neurons was shown to increase long term potentiation (LTP) at perforant path synapses on CA1 stratum lacunosum moleculare, but not Schaffer collateral input to stratum radiatum (Nolan et al., 2005). Facilitation of LTP is thought to be a result of the

hyperpolarized membrane potential upon *Hcn1* deletion, which decreases the steady-state inactivation of T- and N-type voltage-gated calcium channels, leading to elevated calcium spikes and LTP induction upon depolarizing inputs (Tsay et al., 2007). Furthermore, presynaptic HCN channels may influence information processing, since they regulate glutamate release on entorhinal cortex layer 3 pyramidal neurons by suppressing voltage-gated calcium channel activity (Huang et al., 2011). Besides, HCN channels influence the size and stability of the firing fields of place cells of the hippocampus and grid cells of the entorhinal cortex, which encode the spatial location of an animal and thereby contribute to spatial learning and memory (Giocomo et al., 2011; Hussaini et al., 2011).

In addition to influencing the firing behavior of a neuron,  $I(h)$  also contributes to subthreshold membrane potential oscillations, and to the oscillatory activity of neuronal networks (Nolan et al., 2007; Giocomo and Hasselmo, 2009). The basis for network oscillations is provided by intrinsic resonant properties of the neuron's membrane potential, which is known to be determined by  $I(h)$  (Pike et al., 2000; Hu et al., 2002) and other active membrane conductances, such as Kv7 channels (Peters et al., 2005). In CA1 pyramidal neurons,  $I(h)$  mediates theta resonance at hyperpolarized potentials (Hu et al., 2002), and resonance frequency correlates with current density (Narayanan and Johnston, 2007). Entorhinal cortex stellate neurons also show a clear resonant peak at theta frequency, which is shifted to lower values ( $< 4$  Hz) in the absence of HCN1 channel-mediated currents (Nolan et al., 2007). At the network level, theta oscillations are a prominent feature of the hippocampal and entorhinal cortex activity patterns (Chrobak, 2000; Buzsáki, 2002; Buzsáki and Draguhn, 2004). It has repeatedly been shown that suppression of HCN1 channel-mediated currents increases the power of theta oscillations in hippocampal CA1 pyramidal neurons (Nolan et al., 2005; Hussaini et al., 2011). In the entorhinal cortex, theta oscillations exhibit a frequency gradient along the dorsal to ventral axis that is disrupted in mice with a global *Hcn1* deletion (Giocomo and Hasselmo, 2008, 2009), indicating a contribution of HCN channels to the theta gradient. Considering that theta oscillations are involved in memory functions,  $I(h)$ -mediated changes in frequency or power of theta can also affect learning and memory mechanisms (Buzsáki, 2005; Buzsáki and Moser, 2013).

### 1.2.2. HCN channel dysfunction is associated with disease

I(h) mediated by HCN4 channels is crucial for pacemaking: global or cardiomyocyte-restricted *Hcn4* deletion is embryonically lethal due to the lack of pacemaking potentials in the developing sinoatrial node (SAN) (Stieber et al., 2003). Mice with a global deletion of *Hcn2* are viable, but have cardiac sinoatrial dysrhythmia (Ludwig et al., 2003). In humans, dysfunction of HCN4 channels is linked to sinus node dysfunction (Schulze-Bahr et al., 2003; Milanesi et al., 2006). I(h) has been intensely studied in association with epilepsy, one of the most common neurological disorder that affects approximately 3% of the general population (Aylward, 2008). Several findings in human epileptic patients demonstrate a contribution of I(h) to the pathophysiology of epilepsy. A direct link between HCN channel dysfunction and epilepsy was found very recently in human patients with early infantile epileptic encephalopathy (EIEE), revealing *de novo* mutations in *HCN1* (Nava et al., 2014a). Patients with generalized idiopathic epilepsy (IGE) were found to have functional variants of the *HCN1* and/or *HCN2* (Tang et al., 2008; Dibbens et al., 2010; Difrancesco et al., 2011). In addition, the HCN1 channel subunit has been shown to be upregulated in patients with temporal lobe epilepsy (TLE) (Bender et al., 2003). In the last years, studies in rodent models have shed light on the potential mechanisms by which altered HCN channel expression and function can promote seizure activity in the brain. When induced in neonatal rats, febrile seizures, the most common seizure type in childhood, were accompanied by long-term alterations of the neuronal network that caused a reduction in the threshold of pharmacologically induced seizures in adulthood (Dube et al., 2000). Thereby, changes in the expression pattern of HCN1 and HCN2 channels in the hippocampus, such as seizure-induced downregulation of HCN1 channels or heteromerization of HCN1 and HCN2 subunits (Brewster et al., 2002, 2005), were found to be associated with increased excitability of CA1 pyramidal neuron dendrites (Dyhrfeld-Johnsen et al., 2008), suggesting that an “acquired channelopathy”, i.e. deregulation of HCN channels upon pathological activity, contributes to disease susceptibility (Richichi et al., 2008). Likewise, pharmacologically induced status epilepticus in rat models of TLE was accompanied by deregulated HCN channels and altered excitability of hippocampal and entorhinal cortex neurons (Shah et al., 2004; Jung et al., 2007). Besides, mice with a global deletion of *Hcn2* (Ludwig et al., 2003) and mice with a spontaneous mutation in *Hcn2* that truncates the protein (apathetic, *HCN2<sup>ap/ap</sup>* (Chung et al., 2009)) displayed spontaneous absence seizures. Absence seizures resulted from changes in the firing mode of thalamocortical neurons

when of HCN2 channel-mediated current is deficient. Normally, thalamocortical neurons either fire bursts of spikes that are triggered by voltage-gated T-type calcium channels, or they exhibit a tonic firing of single action potentials. Without  $I(h)$ , the firing mode of thalamocortical neurons was shifted from tonic to burst state, which was due to the hyperpolarized membrane potential and concomitant decrease in the steady-state inactivation of T-type calcium channels. As a consequence, depolarization elevated calcium currents and triggered spikes, resulting in typical spike-and-wave discharges in absence epilepsy (Ludwig et al., 2003). In comparison, a global deletion of *Hcn1* in HCN1<sup>-/-</sup> mice caused increased cortical excitability and increased susceptibility to pharmacologically induced seizures, but spontaneous seizures were not observed (Huang et al., 2009; Santoro et al., 2010).

Besides epilepsy, HCN channels have also been implicated to play a role in Parkinson's disease (PD), a neurodegenerative disorder that is characterized by loss of dopamine neurons in substantia nigra pars compacta (SNc) and accompanied by progressive motor symptoms (Rivlin-Etzion et al., 2006). Animal models of PD revealed that HCN2 channel-mediated currents are important to maintain rhythmicity in neurons of the globus pallidus external segment (GPe), and become downregulated upon induction of the parkinsonian state in mice (Chan et al., 2011). Furthermore, a deletion in *HCN1* was found in humans with autism spectrum disorders (ASD) and intellectual disability (Nava et al., 2014b). Of note, *HCN1* mutations in human patients were also associated with other conspicuous traits, such as absence of language, behavioral disturbances, attention deficit/hyperactivity disorder (ADHD), motor delay and ataxia (Nava et al., 2014a, 2014b). Suppression of  $I(h)$  mediated by HCN1 and HCN2 channels exerts antidepressant- and anxiolytic-like behaviors in mice (Lewis et al., 2011; Kim et al., 2012).

### 1.2.3. Role of $I(h)$ in CNS development

Developing networks need to adapt to a series of changes in the external and internal environment, which are influenced by spontaneous activity guiding maturation and connectivity. Intracellularly recorded GABA-mediated giant depolarizing potentials (GDPs) are a hallmark of the spontaneous activity in immature networks (Ben-Ari et al., 1989; Ben-Ari, 2001). In immature hippocampal slices, GDPs are generated by population bursts in CA3 and present in the first two postnatal weeks (Khazipov and

Khalilov, 2004; Sipilä et al., 2005).  $I(h)$ , due to its large variety as described above, may play a critical role in meeting the various requirements of developmental activity changes and is thus proposed to influence the development of neuronal networks to a substantial degree (Rocha et al., 2006; Bender and Baram, 2008). Indeed, blocking  $I(h)$  in the developing hippocampus has been shown to reduce the frequency of GDPs in rat hippocampal slices (Strata et al., 1997; Bender et al., 2005), and thereby modifying their regularity (Agmon and Wells, 2003). HCN channel-mediated currents thus participate in the generation of early network activity patterns in the hippocampus. Of note, the hippocampal expression pattern of HCN channels changes remarkably within the first three postnatal weeks of life with respect to subunit composition and density of the underlying current. The neonatal stage is the period during which the highest number of hippocampal neurons express  $I(h)$  (Bender et al., 2005). Especially in CA3,  $I(h)$  density is highest during the first postnatal week and declines thereafter (Vasilyev and Barish, 2002). In contrast, CA1 pyramidal neurons were shown to switch from slow HCN2- and HCN4- to fast HCN1-mediated currents (Brewster et al., 2007), together with a strong increase in current amplitude between postnatal days 1 and 20 (Vasilyev and Barish, 2002). However, not only the subunit composition and density of HCN channels located in CA1 and CA3 pyramidal neuron dendrites are subjected to developmental regulation, but also the presynaptic localization in axon terminals of entorhinal cortex perforant path projections (Bender and Baram, 2008). The perforant path provides the major input to the hippocampus, and in immature rats, HCN1 channel expression in axonal terminals were was pronounced during the developmental period and contributed to synaptic activity in the immature hippocampus, whereas it decreased with maturation (Bender et al., 2007). Adult EC neurons still express HCN1 channels at their perforant path neurons, but additional dendritic HCN1 (Nolan et al., 2007; Huang et al., 2011; Wilkars et al., 2012). These data demonstrate that HCN channel expression and function are highly regulated during postnatal development, suggesting a significant influence on development-dependent activity and concomitant maturation of neuronal networks. Neuronal activity itself can affect HCN channel regulation as well. This becomes especially evident in the presence of abnormal activity, such as seizures, to which developing networks are very susceptible (Ben-Ari and Holmes, 2006). Febrile seizures have been shown to substantially and persistently deregulate the expression of HCN channels in the hippocampus, which even increases the predisposition to epileptogenesis when induced later in life (Dube et al., 2000; Brewster et al., 2002, 2005; Zhang et al.,

2006; Richichi et al., 2008). In addition to the hippocampus, immature cortical layer 5 pyramidal neurons undergo significant increases in I(h) during postnatal maturation (Zhu, 2000). In a rat model of absence seizures, HCN1 protein expression was markedly reduced and accompanied by decreased I(h) in cortical layer 2/3 and 5 pyramidal neurons that caused hyperexcitability (Strauss et al., 2004). As HCN channelopathy was prevented by early neonatal treatment with the anticonvulsant ethosuximide (Blumenfeld et al., 2008), deregulated HCN channels in immature networks are very likely to promote further abnormal activity that might contribute to disease predisposition in adulthood.

Furthermore, the age-dependent changes in I(h) overlap with network activity changes observed in hippocampal and cortical slices (Garaschuk et al., 1998, 2000) and in the developing neocortex and hippocampus *in vivo* (Khazipov and Luhmann, 2006; Mohns and Blumberg, 2008; Yang et al., 2009; Seelke and Blumberg, 2010). Neonatal network activity is characterized by a transformation from discontinuous to continuous electroencephalogram (EEG) patterns (Khazipov and Luhmann, 2006). In neonatal rodent somatosensory and visual cortex, early network activity during the first two weeks changes from slow immature to more fast mature oscillations that are characterized by early network oscillations (ENOs (Adelsberger et al., 2005)), slow activity transients (SATs (Colonnese and Khazipov, 2010)), spindle bursts (SB, 5-25 Hz (Khazipov and Luhmann, 2006)) and gamma oscillations (30-40 Hz (Yang et al., 2009)). Given that I(h) and its underlying subunit composition seem to be very susceptible to external influences during neonatal development and mutations in HCN1 are linked to infantile epileptic encephalopathy in humans (Nava et al., 2014a), abnormal I(h) is likely to contribute to altered spontaneous activity *in vivo* during a critical developmental period, which might manifest in persistent abnormal neuronal activity and behavior in the adult. However, studies of the consequence of I(h) deficiency for *in vivo* network oscillations in the neonatal brain have yet to be performed.

### 1.3. Aims of the study

Hyperpolarization-activated cyclic nucleotide-gated (HCN) channels are voltage-gated ion channels that are unique in their activation upon hyperpolarization to potentials close to the resting membrane potential. Activated HCN channels conduct a depolarizing mixed  $\text{Na}^+/\text{K}^+$  current –  $I(h)$  that critically influences the neuron's membrane potential, input resistance, and integrative properties.  $I(h)$  acts like a leak current by stabilizing the RMP and preventing it from excessive hyperpolarization. As a consequence,  $I(h)$  contributes to a wide range of physiological phenomena. The functional diversity of h-currents is mediated by the underlying four different HCN channel subunits (HCN1-4) that form homo- or heterotetramers with specific expression patterns, gating properties, and regulation by cyclic nucleotides and auxiliary subunits. Currents yielded by HCN1-4 channels thus comprise functionally heterogeneous effects. Growing evidence further supports the notion of  $I(h)$  as a critical contributor to postnatal developmental processes. Mouse models for studying  $I(h)$  in the CNS include a general or region-restricted knockout of the HCN1 channel subunit (HCN1<sup>-/-</sup> general, HCN<sup>ff,cre</sup> in forebrain, HCN<sup>ff,L7cre</sup> in cerebellar Purkinje neurons (Nolan et al., 2003, 2005; Rinaldi et al., 2013)), a general knockout of HCN2 (HCN2<sup>-/-</sup> (Ludwig et al., 2003)), or mice with a spontaneous mutation in HCN2 (HCN2<sup>ap/ap</sup> (Chung et al., 2009), and TRIP8b-knockout mice that exhibit reduced HCN1 and HCN2 channel surface expression in the neocortex and hippocampus (Lewis et al., 2011). However, these models are restricted to specific HCN channel subunits and report residual  $I(h)$  expression.

This study was aimed at investigating the physiological roles of HCN subunit-mediated currents *per se*, i.e. independent of the endogenous subunit composition. To this end, a dominant-negative (i.e., non-conducting) transgenic approach was used to ablate  $I(h)$ , which is similar to the one applied by our laboratory for studying  $I(f)$  in mouse heart (Alig et al., 2009; Mesirca et al., 2014) or Kv7/M-currents in mouse brain (Peters et al., 2005; Marguet et al., 2015). The human *HCN4* pore mutant transgene construct (hereafter referred to as HCN-DN) contains a mutation in the pore motif that changes GYG to GYS (G480S), which is known to exert dominant-negative effects in KCNQ2 channels (Schroeder et al., 1998), and was modeled based on a mutation identified in the human *KCNQ1* gene in patients with congenital long QT syndrome (Russell et al., 1996). KCNQ and HCN channels share the GYG selectivity filter in the pore region. Thus, GYS

was applied to HCN channels and the corresponding transgene expressed in mice (Sandke, 2006). By using the CaMKII $\alpha$  promoter to drive HCN-DN expression, this study, which was focused on neurons that are not spontaneously active, was aimed at examining the effects of I(h) on somatodendritic integration and population activity in the forebrain. Another focus was on the functional roles of I(h) in early postnatal development. We previously showed that mice with functional I(h) ablation in the forebrain exhibit several behavioral abnormalities, such as delayed sensorimotor reflex development at neonatal ages, hyperactive behavior, motor dysfunctions, and moderate cognitive deficits in adults (Sandke, 2006; Merseburg, 2011). To be able to discriminate between effects resulting from either the homeostatic roles of I(h) in the adult brain, or from the consequences of I(h) deficiency during early postnatal period of brain development, a conditional system driving HCN-DN expression was used. Temporal control of I(h) deficiency was mediated by the Tet-Off system through a doxycycline-dependent transgene expression.

In the following study, the effects of I(h) deficiency at different stages of brain maturity (i.e., during early postnatal brain development and at adult ages) on neuronal activity and behavior were investigated. Electrophysiological acute and chronic recordings were performed to assess the consequences of suppressed I(h) for neuronal excitability and neuronal population activity. At the behavioral level, mice deficient in I(h) at different developmental stages were analyzed with respect to their general activity, cognitive performance, and motor functions.

## 2. Material and Methods

### 2.1. Animals and husbandry

All experimental procedures were approved by the Ministry of Science and Public Health of the City State of Hamburg, Germany (46/07). Animals (mice, *Mus musculus*) were kept in type II long plastic cages under standard housing conditions ( $21 \pm 2^\circ\text{C}$ , 40 to 60% relative humidity, rodent chow (ssniff Spezialitäten GmbH) and water *ad libitum*, nesting material provided). Mice were kept on an inverted 12:12 light:dark cycle (light on at 20:00 h) and once per week transferred to clean cages. Transgenic mice carrying human HCN4 (C57BL/6J-Tg(tetO-HCN4<sup>G480S</sup>,-EGFP) (Krestel et al., 2001)) were cross-bred with a line expressing the regulative tetracycline-responsive transcriptional transactivator (tTA) under control of either the calcium-calmodulin-dependent kinase II alpha (CaMKII $\alpha$ ) promoter (C57BL/6J-Tg(CamK2 $\alpha$ -tTA)Mmay/J (Mayford et al., 1996)), or the Purkinje cell protein-2 (PCP2) promoter (FVB-Tg(Pcp2-tTA)3Horr/J (Zu, 2004)), to obtain double-transgenic (mutant) mice. Littermates carrying only one of the transgenes were used as controls. All behavioral tests and *in vivo* depth recordings in behaving mice were performed during the dark cycle between 8:30 h and 18:00 h.

### 2.2. Genotyping

#### 2.2.1. Isolation of genomic DNA from tail biopsies

Tail biopsies were lysed overnight at  $54^\circ\text{C}$  by constant shaking in 100  $\mu\text{l}$  DirectPCR-Tail lysis reagent (Viagen Biotech) containing 0.2 mg/ml Proteinase K. Then, lysed tail biopsies were incubated for 30 min at  $87^\circ\text{C}$  to inactivate Proteinase K.

#### 2.2.2. Isolation of genomic DNA from ear biopsies

Ear biopsies were lysed overnight at  $54^\circ\text{C}$  under constant shaking in 70  $\mu\text{l}$  lysis buffer (100 mM NaCl, 50 mM Tris HCl pH 8.0, 1 mM EDTA, 0.2% Nonidet P-40, 0.2% Tween 20, 0.1 mg/ml Proteinase K).

### 2.2.3. Polymerase chain reaction

Polymerase chain reaction (PCR) was performed to detect both, the region coding for the transcriptional transactivator (tTA) and the hHCN4-G480S transgene (sequences are given in Tab. 2-1). For the tTA transgene a touchdown protocol was followed, instructing a stepwise reduction of the hybridization temperature, approaching the expected melting temperature  $T_m$  of the primers. In addition, simultaneous amplification of the *Terd* (coding for the conserved part of the delta chain of the T cell receptor) was performed, which functioned as internal control over the quality of the genomic DNA. Reactions were performed in a thermoblock (T3 Thermocycler, Biometra®) with a reaction volume of 50  $\mu$ l. Programs applied are given in Tab. 2-2 and 2-3.

### 2.2.4. Agarose gel electrophoresis

After PCR reaction 10  $\mu$ l of 5x loading dye (50% glycerine, 60 mM EDTA, 0.025% Xylene cyanol, 0.025% bromophenol blue) was added to 50  $\mu$ l PCR product, and 15  $\mu$ l PCR product containing loading dye was loaded into agarose gel wells (1.5% agarose in 1x TAE buffer (40 mM Tris, 10 mM acetic acid, 1 mM EDTA pH 8.0)) and electrophoretically separated in 1x TAE buffer at 100-130 V.

**Table 2-1: Nucleotide sequences of oligonucleotides used for PCR and expected product size.**

Primer	Sequence	Product size
Terd_1	5'- CAA ATG TTG CTT GTC TGG TG -3'	200 bp
Terd_2	5'- GTC AGT CGA GTG CAC AGT TT 3'	
tTA_6c	5'- CGC TGT GGG GCA TTT TAC TTT AG -3'	450 bp
tTA_7nc	5'- CAT GTC CAG ATC GAA ATC GTC -3'	
HCN4_PCR_1c	5'- GGC ATG TCC GAC GTC TGG CTC AC -3'	350 bp
HCN4_PCR_2nc	5'- TCA CGA AGT TGG GGT CCG CAT TGG -3'	

**Table 2-2: Touchdown PCR protocol to amplify the tTA transgene.**

Cycle	Step description	Temperature	Duration
1	initial denaturation	94°C	3 min
	denaturation	94°C	30 s
2-13	annealing	64°C - 0.5°C/cycle	45 s
	elongation	72°C	45 s
	denaturation	94°C	35 s
14-39	annealing	58°C - 0.5°C/cycle	30 s
	elongation	72°C	45 s
40	final elongation	72°C	5 min

Hybridization temperatures were gradually lowered by 0.5°C per cycle.

**Table 2-3: PCR protocol to amplify hHCN4-G480S transgene.**

Cycle	Step description	Temperature	Duration
1	initial denaturation	94°C	3 min
	denaturation	94°C	30 s
2-30	annealing	60°C	30 s
	elongation	72°C	30 s
31	final elongation	72°C	5 min

### 2.3. *In situ* hybridisation

The *in situ* hybridization procedure was performed in collaboration with Susanne Fehr of the service unit Morphology (ZMNH, Hamburg) as described (Fehr et al., 1987).

#### 2.3.1. Preparation of probe

A 280 bp long fragment of the mutated human HCN4 channel subunit (hHCN4-G480S) was amplified from tail/ear biopsies via PCR with primers shown in Table 2-4, prepared as described (Schlusche, 2011) and kindly provided by Anna Katharina Schlusche (Experimental Neurophysiology, DZNE & UzK Cologne). Radioactively labeled cRNA probes were made with the DIG RNA labeling method using DIG RNA labeling kit for transcription with <sup>35</sup>S-UTP (T7, Boehringer).

#### 2.3.2. Hybridisation protocol

Mice were decapitated, the brain was carefully removed, embedded in Tissue Tek and immediately frozen on dry ice. 16 µm cryostat-cut sections were mounted on cold *SUPERFROST® PLUS* slides (Thermo scientific) and stored at -80°C. For fixation, slides were then incubated for 10 min in freshly prepared and cold 4% paraformaldehyde (PFA) in phosphate buffered saline (PBS; 150 mM NaCl, 8 mM Na<sub>2</sub>HPO<sub>4</sub>, 2 mM KH<sub>2</sub>PO<sub>4</sub>), and washed twice in PBS for 5 min each. To block unspecific binding, slides were incubated for 10 min in freshly prepared, cold acetylation buffer (PBS, 0.1 M Triethanolamine (Sigma), 0.9% 5 M NaCl, 2.5 ml/l acetic anhydride (Sigma)). Slides were then dehydrated by placing them for 5 min each in 60%, 80%, 90%, 95% and 100% ethanol, and then for 5 min in chloroform, and dried at room temperature. Prehybridisation was performed by applying 1 ml of prehybridisation buffer (50% deionized formamide, 5X hybridization salts (0.75 M NaCl, 0.025 M EDTA, 0.025 M Pipes, pH 6.8), 5X Denhardt's (0.1% Ficoll, 0.1% polyvinylpyrrolidon, 0.1% bovine serum albumin (BSA)), 0.2% SDS, 10 mM dithiothreitol (DTT), 250 µg/ml denatured herring sperm DNA, 250 µg/ml yeast tRNA) to the slides and incubating them for 3 hours at 50°C in a chamber containing filter paper that was soaked with 50% formamide. The prehybridisation buffer was drained and the hybridization step followed. For hybridization, 100 µl hybridization buffer (prehybridisation buffer plus 10% dextran

## MATERIAL AND METHODS

sulfate) containing 1  $\mu$ l of the probe ( $2 \times 10^6$  cmp) was applied, sections were covered with a cover slip, and slides incubated overnight at 50°C in a closed chamber. After hybridization cover slips were removed, the slides were dipped into 4X SSC, and then washed three times for 5 min each in 4X SSC. Incubation for 30 min at 37°C in 40  $\mu$ g/ml RNase A (Boehringer)-containing buffer (0.5 M NaCl, 10 mM Tris-HCl pH 7.5, 1 mM EDTA) followed. Then the slides were washed again in the same buffer but without RNase A for 30 min at 37°C, and dehydrated through 60%, 80%, 90%, 95% and 100% ethanol, and dried at room temperature. The dried slides were exposed to X-ray film (Kodak Biomax MR) or dipped into Kodak NTB-3 nuclear track emulsion at 42°C. After exposure at 4°C overnight, autoradiograms were developed with Kodak chemicals at 16°C: 5 min Kodak D19, 1 min H<sub>2</sub>O, 3 x 5 min Kodak Unifix, 3 x 5 min H<sub>2</sub>O. The slides were then counterstained with hematoxylin eosin solution, rinsed in H<sub>2</sub>O, and then 1% HCl in 70% ethanol to remove excess staining solution. Dehydration with 60%, 80%, 90%, 95% and 100% ethanol was followed by 2 x 10 min incubation in xylol and slides were coverslipped.

**Table 2-4: Primer for *in situ* hybridization probe specific to hHCN4-G480S**

Primer	Sequence	Product size
HCN4_ISH_4c	5'-TGT CGG AAG CTG GTG GCC TCC A -3'	
HCN4_ISH_4nc	5'- TAA TAC GAC TCA CTA TAG GGG GCC GCG TTG CTG GCG TTT TTC CAT AGG CAG TAG GTG TCG GCC CTC ACG CT -3'	280 bp

## 2.4. Western blot

The western blot technique was used to detect the HCN-DN protein via the attached N-terminal hemagglutinin tag (HA-tag, 132 kDa). Mice were decapitated and brains were carefully removed. Separation of forebrain and cerebellum tissue was performed on ice in cold 0.9% NaCl. The tissue was then homogenized dissolved in 500  $\mu$ l ice cold extraction buffer containing protease inhibitors, and gently agitated for 10 min at 4°C. A centrifugation step for 5 min at 1000 x g and 4°C followed, and the resulting supernatant was kept as cytosolic fraction. The pellet was dissolved in 1 ml ice cold PBS, and centrifuged again for 5 min at 1000 x g/rcf and 4°C. The supernatant was discarded and the pellet dissolved in 200  $\mu$ l extraction buffer to obtain the membrane fraction. Incubation for 15 min at 4°C with gentle agitation followed, another centrifugation step for 15 min at 16000 x g and 4°C, and the supernatant was kept as membrane fraction. Protein concentrations were determined with the bicinchoninic acid (BCA) assay. Proteins (40  $\mu$ g) were then separated with SDS-PAGE (150 V, 30 min), and electrophoretically transferred (2h at 80 V and 30 min at 90 V) to PROTAN nitrocellulose membranes (Whatman) in transfer buffer (150ml MeOH, 850 ml buffer). Membranes could be stored at 4°C in TBS-Tween (10 mM Tris pH 7.5, 150 mM NaCl, 0.05% Tween) before further use. Blocking was performed with blocking solution (5% milk powder in TBS-Tween) for 1 hour at room temperature. Then, primary antibody (rat anti-HA antibody, Roche) was applied in a 1:500 dilution (in 5% milk powder in TBS-Tween) and incubated for 1 hour at room temperature. The antibody was then removed and could be stored at -20°C for further use. A washing procedure in TBS-Tween followed for once shortly and 3 x 5 min at room temperature. The secondary antibody (anti-rat horse radish peroxidase (HRP), Vector Laboratories) was applied in a 1:2000 dilution (in 1% milk powder in TBS-Tween). Washing for 3 x 5 min was followed by application of 2 ml of the Luminata™ Crescendo Western HRP Substrate (Millipore), incubation for 5 min at room temperature and signal detection with a CCD camera using LAS 4000 min (Fujifilm).

## 2.5. Histology

### 2.5.1. Perfusion

For transcardial perfusion animals were anaesthetized via intra peritoneal (i.p.) injection of 1  $\mu$ l/gb.w. anaesthetic (12% Ketanest, 8% Sedaxylan in 0.9% NaCl solution). A thoracotomy was performed and the right atrium was perforated. The mouse was perfused by pumping 150 ml of PBS into the left ventricle. For tissue fixation, 50 ml of 4% PFA (Roti® Histofix, Roth) was injected afterwards. Mice were then decapitated and the brain was carefully removed, fixed overnight in 4% PFA at 4°C, and stored in PBS at 4°C.

### 2.5.2. Slice preparation

For vibratome sections, brains were glued to a socket, submerged in PBS and 50  $\mu$ m or 100  $\mu$ m sagittal sections were cut using a vibratome (VT1000S, Leica). Slices were kept at 4°C in 24-well plates filled with PBS. For cryosections, brains were incubated in 15% and 30% sucrose (in PBS) each overnight at 4°C and then frozen on dry ice in tissue glue. 20  $\mu$ m coronal or sagittal sections were mounted on *SUPERFROST® PLUS* (Thermo scientific) microscope slides and stored at -20 °C.

### 2.5.3. Immunolabeling

Cryosections were washed 3 x 5 min each in PBS. Antigen retrieval was performed in 10 mM sodium citrate buffer (pH 9) at 70°C for 30 min. After cooling down at room temperature, slides are washed 4 x 5 min each in PBS. The tissue was blocked in 5 % normal goat serum, 0.2 % Triton X-100 in PBS for 1 h at room temperature. The primary antibody CaMKII $\alpha$  (monoclonal mouse antibody, Sigma) was diluted 1:1000 in PBS-Carrageenan and applied overnight at 4°C. Brain slices were washed 3 x 15 min each in PBS before application of the secondary antibody Alexa Fluor® 546 Goat Anti-Mouse IgG (Molecular Probes®) which was diluted 1:500 in 0.5 % Triton X-100 in PBS at room temperature. Slides were washed 4 x 5 min each in PBS and embedded in DAPI Fluoromount-G® (Biozol).

#### 2.5.4. Microscopy

Brain sections were investigated with a Zeiss AX10 microscope using an AxioCam MRC colour camera and the corresponding software AxioVision (Zeiss), and with an Olympus Fluoview FV1000 confocal laser-scanning microscope and corresponding software (Olympus).

### 2.6. Whole-cell patch clamp recordings

#### 2.6.1. Electrophysiological recordings from neonatal CA1 pyramidal neurons

Recordings in neonatal brain slices were performed by PD Dr. Axel Neu (Experimental Neuropediatrics, ZMNH, Hamburg). For *in vitro* patch clamp recordings from neonatal CA1 pyramidal neurons, neonatal P7-8 mice were decapitated and brains rapidly transferred to ice-cold sucrose-solution (in mM: 85 NaCl, 1.25 NaHPO<sub>4</sub>, 2.5 KCl, 0.5 CaCl<sub>2</sub>, 4 MgCl<sub>2</sub>, 25 glucose, 75 sucrose, 25 NaHCO<sub>3</sub>) oxygenated with carbogen (95% O<sub>2</sub>/ 5% CO<sub>2</sub>). Coronal sections (300 µm) were cut with a vibratome (Leica VT1200s), incubated for at least 30 min in 31-33°C sucrose-solution and then transferred to artificial cerebral-spinal fluid (ACSF, in mM: 126 NaCl, 1.25 NaHPO<sub>4</sub>, 2.5 KCl, 2 CaCl<sub>2</sub>, 2 MgCl<sub>2</sub>, 25 glucose, 25 NaHCO<sub>3</sub>) at room temperature (20-22°C). For electrophysiological recordings, slices were transferred to a chamber continuously perfused with ACSF at room temperature containing bicuculline (10 µM) and CNQX (10 µM). Intracellular recording solutions contained: in mM 135 K-gluconate, 5 KCl, 10 HEPES, 0.1 EGTA, 2 MgCl<sub>2</sub>, 2 MgATP, 0.2 NaGTP, pH 7.3 with KOH). Whole-cell patch-clamp recordings were filtered at 4 kHz and digitized at 10 kHz using an EPC9 amplifier and PULSE software (HEKA Elektronik, Germany). CA1 pyramidal cells were voltage-clamped from a holding potential of -60 mV to test potentials of -50 to -120 mV in steps of 10 mV followed by a voltage step to -120 mV. Series resistances were below 20 MegaOhm and electronically compensated by 60%. For current-clamp recordings, cells were clamped to -60 mV and then hyperpolarized by current injections of -20 pA until -120 mV were reached.

### 2.6.2. Electrophysiological recordings from adult CA1 pyramidal neurons

The recordings were performed by Prof. Dr. Dirk Isbrandt (DZNE Research Team Experimental Neurophysiology, DZNE Bonn and University Cologne) and Prof. Dr. Jochen Roeper (NEUROSCIENCE CENTER, Goethe University, University Hospital Frankfurt). Coronal hippocampal slices (250  $\mu$ m) of adult mice were sectioned after intracardial perfusion with ice-cold sucrose–artificial cerebrospinal fluid (ACSF) (in mM: 50 sucrose, 75 NaCl, 25 NaHCO<sub>3</sub>, 2.5 KCl, 1.25 NaH<sub>2</sub>PO<sub>4</sub>, 0.1 CaCl<sub>2</sub>, 6MgCl<sub>2</sub>, and 2.5 glucose, oxygenated with 95% O<sub>2</sub>/5% CO<sub>2</sub>). After 90 min of recovery, slices were transferred to a recording chamber and perfused continuously at 2–4 ml min<sup>-1</sup> with oxygenated ACSF (2.5 mM glucose, 22.5 mM sucrose) at 36 °C. Fast excitatory and inhibitory synaptic transmission was inhibited by 20 mM CNQX (6-cyano-7-nitroquinoxaline-2,3-dione) and 10 mM gabazine. CA1 pyramidal neurons were visualized by infrared–differential interference contrast (IR-DIC) video microscopy and epifluorescence for detection of EGFP. Whole-cell recordings, data acquisition and analysis were essentially as described (Neuhoff et al., 2002; Liss et al., 2005).

### 2.6.3. Electrophysiological recordings from adult entorhinal cortex layer III pyramidal neurons

Whole-cell recordings of entorhinal cortex layer III pyramidal neurons were performed by Z. Huang in the laboratory of Prof. Mala Shah, UCL School of Pharmacy, London, UK (collaboration) as described (Huang et al., 2009). Adult 6-9 week old mice were anesthetized and perfused intracardially with ice-cold modified ACSF (in mM: 110 choline chloride, 2.5 KCl, 1.25 NaH<sub>2</sub>PO<sub>4</sub>, 25 NaHCO<sub>3</sub>, 0.5 CaCl<sub>2</sub>, 7 MgCl<sub>2</sub>, 10 dextrose, 1.3 ascorbic acid), bubbled continuously with 95% O<sub>2</sub> / 5% CO<sub>2</sub> to maintain pH at 7.2. The brain was then removed, and 400  $\mu$ m thick slices were prepared with a vibratome (Leica VT 1000S). The slices were incubated in a holding chamber at 36°C for 10-15 min followed by 1 hour at room temperature. The holding chamber contained external recording solution (in mM: 125 NaCl, 2.5 KCl, 1.25 NaH<sub>2</sub>PO<sub>4</sub>, 25 NaHCO<sub>3</sub>, 2 CaCl<sub>2</sub>, 2 MgCl, 10 dextrose, bubbled continuously with 95% O<sub>2</sub> / 5% CO<sub>2</sub> to maintain pH at 7.2). Whole-cell recordings were obtained from both the soma and dendrites of entorhinal cortex layer 3 (EC L3) pyramidal neurons. For recording purposes, slices were placed in a chamber containing external recording solution (supplemented with 0.05 mM APV,

0.01 mM CNQX, 0.01 mM bicuculline, 0.001 mM CGB 55845) maintained at 34-36°C. The internal recording pipette solution contained, in mM: 120 KMeSO<sub>4</sub>, 20 KCl, 10 HEPES, 2 MgCl<sub>2</sub>, 0.2 EGTA, 4 Na<sub>2</sub>ATP, 0.3 Tris-GTP, 14 Tris-phosphocreatine; pH adjusted to 7.3 with KOH. Pipettes had resistances of 5-12 MΩ. Whole-cell current clamp recordings were obtained using a bridge-mode amplifier (AxoClamp 2B, Molecular Devices, UK), filtered at 10 kHz and sampled at 50 kHz. αEPSPs were generated by current injection of the order:

$$A = (t/\tau) * \exp(1-(t/\tau)).$$

A is the amplitude of the current injected and  $\tau$  is the rise time constant. Tungsten electrodes (A-M systems) were placed in EC LI to elicit EPSPs by extracellular stimulation. ZD7288 (15μM) was bath applied, effects occurred within 15 min and recordings were usually made within 25 min of application. For analysis, pClamp software was used. The input resistance was calculated from 400 ms hyperpolarizing pulses of 100 pA applied from a holding potential of -70 mV. The αEPSP decay time constants were obtained by fitting the double exponential function:

$$A_1 e^{(-t/\tau_1)} + A_2 e^{(-t/\tau_2)}.$$

$\tau_1$  and  $\tau_2$  represent time constants of initial and falling phase of the αEPSPs. Since I(h) is activated during the falling phase of the αEPSP, only  $\tau_2$  was used. The summation ratio of EPSPs was calculated as the ratio of the peak of the fifth EPSP to that of the first EPSP. Action potential threshold was determined as the point before the first derivative of the trace was no longer equal to zero.

## 2.7. *In vivo* depth recordings

### 2.7.1. *In vivo* depth recordings in neonatal head-fixed mice

Neonatal mice at postnatal day (P) 6-8 were anesthetized with 1.5-2% isoflurane in 100% oxygen. A midline skin incision was made on the skull. The periosteum was denatured using 10% H<sub>2</sub>O<sub>2</sub> and subsequently removed. The skull bone was rinsed with 0.9% NaCl solution and dried. Skin incisions were treated with a bupivacaine solution (Bucain®-Actavis 0.25%). A silver wire as common ground and reference electrode was inserted into a hole drilled above the cerebellum and fixed with dental cement. The

following stereotaxic coordinates were used (Paxinos, G., Hallyday, G., Watson, C., Koutcherov, Y. & Wang, 2007): for primary visual cortex silicone probes, burr holes were placed at 0.1 mm anterior to lambda and 2.0-2.1 mm left from the midline. For somatosensory cortex and hippocampal silicone probes, burr holes were placed 1.4-1.6 mm anterior from bregma and 1.5-1.6 mm left from the midline. All coordinates were adjusted according to the distance between lambda and bregma for each individual animal. After surgery isoflurane anesthesia was turned off. Awake mice were recorded while being head fixed and resting in the stereotaxic instrument. Body temperature was maintained at ambient nest temperature of about 34°C using a homeothermic heating pad (Stoelting). Linear 16- or 32-site silicon probes with 50 µm spacing (A1x16/32-50-5mm-703-A16/32, NeuroNexus Technologies) were lowered vertically into the primary somatosensory cortex and hippocampus, and with a lateral tilt of 10° into the primary visual cortex. The silicon probe was connected to a 1x preamplifier (Neuralynx) mounted to the stereotaxic instrument (Stoelting). Data were digitally filtered (0.5-9000 Hz bandpass) and digitized as 16-bit integers with a sampling rate of 32 kHz using a Digital Lynx data acquisition system (Neuralynx). Animal movements were detected by a piezoelectric sensor placed under the animal's thorax. Data acquisition was started about 15-30 minutes after probe insertion when recording conditions were stable. Probe positions were marked by silicone probes covered with fluorescence dye (DiI, Molecular Probes, Life Technologies) and verified in DAPI (Fluoromount-G®, Biozol)-stained coronal slices.

### 2.7.2. *In vivo* depth recordings in adult behaving mice

Adult male mice (> 8 weeks old) were anesthetized with 3.5-4% isoflurane in 100% oxygen and kept at 0.8-1.5% isoflurane throughout the surgery. For analgesia mice subcutaneously received 0.05 mg/kg buprenorphine (Temgesic) and 5.0 mg/kg Caprofen (Rimadyl), and 7.5 mg/kg of the antibiotic Enrofloxacin (Baytril). Mice were placed in a stereotaxic apparatus (Stoelting) and the body temperature was maintained at 36.5°C using a homeothermic heating pad and rectal thermometer (ATC 1000, World Precision Instruments). The head was then shaved and povidon iodine (Betaisodona®, Mundipharma GmbH) was applied. A midline skin incision was made on top of the skull. The periosteum was denatured using 10% H<sub>2</sub>O<sub>2</sub>, removed, and rinsed with 0.9% NaCl. A single component self-etch dental adhesive (OptiBond™ All-In-One, Kerr) was

applied to the skull and dried with UV light (Woodpecker) for 15 seconds. Two wires, each soldered to a skull screw, were implanted above the cerebellum and used for ground and reference. The stereotaxic coordinates for the hippocampus electrode were 1.7-2.0 mm posterior to bregma and 1.5-1.6 mm right from the midline (Franklin and Paxinos, 2007). A 16-site linear silicone probe with 100  $\mu\text{m}$  spacing (CM16LP, 177  $\mu\text{m}^2$  site area, NeuroNexus) was lowered vertically into the dorsal hippocampus along the CA1-dentate gyrus axis (2.0-2.2 mm depth) and fixed to the skull with a wooden framework and dental cement (Tetric EvoFlow A3, Dentsply). Copper mesh was used to surround and protect the implant. It was fixed to the skull with dental cement, and used to solder the electrode's and animal's ground wire on to. The electrode's reference wire was soldered to the animal's reference wire. Then the skin incision was sutured together and covered with povidon iodine. Mice were allowed to recover for at least 3 days.

### 2.7.3. Data acquisition and analysis

Amplifying headstages (2x or 20x, Plexon) were attached to the silicone probe and connected to the Digital Lynx data acquisition system (Neuralynx). Data were digitally filtered (0.5-9000 Hz bandpass) and digitized as 16-bit integers with a sampling rate of 32.552 kHz. Two LEDs were attached to the headstage and used to simultaneously video record the position of the mouse. For analysis, the 32.552 kHz broadband signal was downsampled to 1.252 kHz. Current-source-densities (CSDs) were built from the second spatial derivative of 1-200 Hz filtered local field potential (LFP) signal. All *in vivo* data were analyzed and visualized in Matlab (Mathworks) or Neuroscope (neuroscope.sourceforge.net). Multitaper spectrograms were computed using Chronux ([www.chronux.org](http://www.chronux.org)); for visualization wavelets were also used. In neonatal recordings, sharp waves (SPW) were considered the point of maximum negativity in deep hippocampus after automatically detecting high variance across CSD traces; SPW amplitudes were quantified by the maximum peak to minimum trough in the LFP. Stratum radiatum oscillations (SROs), cortical spindle bursts, and slow activity transients were detected by hand and verified by independent observers.

## 2.8. Telemetric electrocorticogram recordings

### 2.8.1. Implantation of radio transmitters

Telemetric electrocorticogram (ECoG) analyses were performed using implantable radio transmitters (models TA10EA-F20, TA10ETA-F20, or TA11ETA-F10, Data Sciences International). Adult male mice received 0.1 mg/kg<sub>body weight</sub> buprenorphine for analgesia and were anesthetized with 0.5-4% isoflurane in 100% oxygen. Additionally, animals received 5.0 mg/kg<sub>b.w</sub> of the analgesic Caprofen (Pfizer) and 7.5 mg/kg<sub>b.w</sub> of the antibiotic Baytril (Bayer HealthCare) subcutaneously during surgery. Body temperature was maintained by placing the animal on 37°C heating pad during the surgery. A midline skin incision was made on top of the skull. The transmitter body was implanted subcutaneously in a pouch made in the loose skin of the back. The two lead wires were tunneled subcutaneously through the incision on the skull. The pericranium was mechanically removed and the bone was dried with compressed air. Using a dental drill a skull hole was drilled above the cortex and dorsal hippocampus (1.8 mm lateral and 1.8 mm caudal from bregma) for the recording electrode. The reference electrode was placed above the cerebellum. The tips of the EEG leads were wrapped around the two skull screws that served as cortical surface electrodes (1.0 mm in diameter). The electrode wires and screws were sealed with dental cement (Grip cement, Dentsply). Radio transmitters allowed the simultaneous recording of ECoG and motor activity in undisturbed, freely moving mice while housed in their home cages. Animals were allowed to recover from surgery for 2-3 days. Telemetric data recording was started no earlier than one week after surgery. A receiver board placed underneath the cage was used to detect the ECoG signal and synchronized video recordings of the mice were digitally stored using ART-Acquisition 4.2 software (Data Sciences International (DSI)) and visualized with NeuroScore (DSI™, St. Paul, Minnesota).

### 2.8.2. Data analysis

Telemetric ECoG recordings in adult mice allowed for continuous recording of neuronal activity and behavior over multiple days. Behavioral states were scored by means of power in specific frequency (delta frequency 1-4 Hz, theta frequency 4-9 Hz) bands, activity counts made by the transmitter, and periods of high-amplitude and high-

frequency signals in the ECoG. The 100-200 Hz filtered ECoG signal was thereby used for artefact detection. The NeuroScore rodent sleep scoring detector (NeuroScore, DSI™, St. Paul, Minnesota) was used to automatically assign a behavioral state to each epoch (epoch duration of 10 seconds), and manual corrections were performed when necessary and based on video monitoring. The detector discriminated between four different behavioral states: wake, active wake, slow wave sleep and paradoxical or REM sleep. Epochs were scored as wake if delta power was high, theta power low, and activity levels below threshold for active wake activity levels. Active wake was assigned if delta power was low, theta power high, and activity levels above the previously set threshold. Slow wave sleep was scored when delta power was high, theta power low, and activity levels low. Paradoxical or REM sleep was assigned when delta power was low, theta power high, and activity levels low. Thresholds for activity and artefact detection were set individually for each mouse, due to high variations in the signal amplitude and noise ratio between individual radio transmitters.

### **2.9. Behavioral analysis**

#### 2.9.1. Home cage activity

Mice were continuously monitored in their home cage over three consecutive days to assess their general activity in a familiar environment. Individual animals were kept in type II long plastic cages under standard housing conditions. One day prior to recording the food pellets were transferred into the cage to allow detection of the mouse from the top of the cage. A metal rack was placed on top of the cage. Movement was recorded with an infrared sensing data logger (Mouse-E-Motion, Infra-e-motion, Henstedt-Ulzburg, Germany) that was placed in the metal rack. The sensor detects body movement (at least 1.5 cm from one sample point to the next one) by sensing the animal's body heat.

#### 2.9.2. Grip strength

The grip strength test was used to measure the forelimb strength of the mice with a GripStrengthMeter system (TSE Systems, Bad Homburg, Germany) and performed as described (Morellini and Schachner, 2006). Mice were suspended by the tail and allowed

to grasp a stainless steel grip attached to a dynamometer with the front paws. Mice were pulled back until they released the grip. The maximal force applied was recorded. Mice underwent 4 sessions of 3 trials each (intertrial interval (ITI) = 5 sec, intersession interval (ISI) = 60 min). The mean of the 4 maximal values among 3 trials within each session was used for analysis.

### 2.9.3. Pole test

In the Pole test mice were placed head upward on the top of a vertical wooden rod (60 cm long, 7 mm diameter) so that they grasp the rod with all four paws, and had to climb down the rod in a headfirst position. For motivation to climb down nest material was placed at the bottom of the pole. To test motor learning, mice were scored 3 times with an ITI of 30 seconds, during which they were placed into their home cage. Maximum trial duration was 120 seconds. Time needed to reach the floor with all four paws and the manner by which mice descended from the top of the pole (falling, climbing down after 180° body rotation at levels 1, 2 or 3) was assessed as described (Freitag et al., 2003).

### 2.9.4. Rotarod

In the accelerated Rotarod test mice had to walk on a turning, corrugated rod (3.2 cm diameter, Jones & Roberts, TSE Systems), and performance was evaluated by scoring the latency to fall. Mice were allowed to make one passive rotation. After a second passive rotation, mice were gently pulled off the Rotarod and the trial was considered completed. Mice with forebrain-restricted I(h) deficiency underwent 5 trials with an ITI of 45 min. Trials 1 and 2 were done to familiarize the mice to the Rotarod and performed at slow, constant speed (4 rpm) for a maximum duration of 3 min. In trials 3 to 5 mice were subjected to the accelerating protocol (4 rpm to 40 rpm in 4 min, 5 min maximum duration). Mice underwent a 6<sup>th</sup> trial on the accelerating rod (4-40 rpm, 5 min trial duration) at the next day as described (Morellini and Schachner, 2006).

Mice with cerebellar Purkinje cell-restricted I(h) deficiency underwent a different training protocol. Mice were trained for 4 days with 4 trials per day on the accelerating rod (4-40 rpm in 5 min, 5.5 min maximum duration, ITI = 20 min). Mice that did not fall off the Rotarod within 5 min were allowed to continue for another 30 sec at constant

speed (40 rpm). On the 5<sup>th</sup> day, mice underwent one trial at constant speed (40 rpm, 3 min trial duration).

### 2.9.5. Beam walk

In the Beam walk test mice were trained to cross a wooden beam (100 cm long, elevated at a height of 50 cm) to reach their home cage. Familiarization was performed with a 4.5 cm-wide beam. At the following 2 days mice were tested over 2 sessions of 3 trials each (ITI = 30 sec). A 2 cm-wide beam was used in sessions 1 and 4, a 1 cm-wide beam was used in sessions 2 and 3. Latency to cross the beam and number of hind limb faults were recorded. A fault was defined as any foot slip off the top surface. Sessions 2 and 3 were used for analysis. A mean foot fault score was calculated by averaging the 3 trials per session and normalized by the total number of steps, as described (Morellini and Schachner, 2006).

### 2.9.6. Catwalk

For the automated gait analysis system Catwalk mice had to run on an enclosed walkway on a glass plate. Run duration variation was set to 0.5-20 sec, with a maximum speed variation of 60%, and a minimum of ten consecutive steps. A minimum of eight runs per mouse was collected. Runs were classified with the Catwalk XT software (Noldus, Wageningen, The Netherlands). Foot prints were detected automatically by the software and manually corrected by visual inspection. The following parameters were used for analysis: running speed, stand (duration in seconds of contact of a paw with the glass plate), stride length (distance between successive placements of the same paw in centimeter), step cycle (the time in seconds between two consecutive paw placements), base of support (BOS, the average width between the hind paws), step sequence (contains information on the order in which four paws are placed), and regularity index (expresses the number of normal step sequence patterns relative to the total number of paw placements in percent).

### 2.9.7. Open field

The open field was performed in a box (50 x 50 x 40 cm) illuminated with 100 lux. Mice were placed in one corner of the arena and could freely move for 15 min. Tracks were recorded and analyzed with the software EthoVision (Noldus) and the following parameters were obtained: distance moved, running velocity, number of rotations, time in border (an imaginary 5 cm wide border around the arena), and time in center (an imaginary inner square of 20 x 20 cm).

### 2.9.8. Spontaneous alternation

Spontaneous alternation in the Y maze was performed to test for working memory performance. The maze consisted of three equally sized arms (34 x 5 x 30 cm) made of transparent Plexiglas. Mice were placed in the center of the maze and allowed to freely explore the maze until they performed 27 transitions. An entry into any arm was considered as transition. An entry into a new arm after having visited the two other arms was considered as alternation. Maximum trial duration was 20 minutes.

### 2.9.9. Water maze

The maze consisted of a circular pool (145 cm in diameter, 40 cm walls above water surface area, 22.0°C ± 1.0°C water temperature, non-toxic white paint was used to make the water opaque) placed in the corner of the experimental room and surrounded by two white walls and two black curtains. For orientation 4 landmarks with different black/white patterns were attached to the walls of the maze. The arena was homogeneously illuminated with white light. Mice underwent two pre-training days with 4 trials per day (maximum trial duration 60 seconds, inter-trial interval (ITI) of 10 minutes) for familiarization. To avoid any interference with learning, familiarization took place under red light in a different maze (42.5 x 26.5 cm and 15.5 cm high, circled by a black curtain) than that used for learning in the water maze. The position of the platform (diameter of 10 cm, 1 cm below the water surface) was unpredictable, since its location was randomized and did not provide any information that could guide the animals. Thus, mice had to swim at random to escape from the water. After the pre-training mice underwent 3 learning days during which they had to learn the location of a hidden platform. Starting position and direction from which mice were taken out of the

maze were randomized. At learning day (LD) 1 mice underwent 4 learning trials (maximum duration 90 seconds, ITI of 20 minutes. LD 2 consisted of 5 trials. Trials 1, 2, 4 and 5 were learning trials. Trial 3 was a so-called probe trial during which the platform was removed. LD 3 consisted of 1 probe trial. The probe trials had a fixed duration of 60 seconds. All trials were video recorded and the position of the mice was tracked using the software EthoVision (Noldus).

### 2.9.10. Contextual fear conditioning

Mice had to learn the association between unconditioned (electric foot shock) and conditioned (context) stimuli. The conditioned stimulus was a chamber (23.5 x 23.5 x 19.5) with Plexiglas walls and ceiling and a stainless steel grid floor. The chamber was surrounded by three black plastic sheets with different white patterns. The set up was illuminated with 8 lux. At day 1 mice were placed in the chamber and received three foot shocks (0.35 mA, 1 seconds duration) at 120, 160 and 200 seconds. After 240 seconds the recording was terminated and mice were immediately returned to their home cage. 24 hours later mice underwent a recall phase by being placed in the conditioning chamber for 4 minutes without receiving a foot shock. The time the mice spent freezing was used as a read-out for the conditioned response. Freezing was defined by the absence of body movement for at least 1 second. Motion was automatically analyzed using the movement detector Mouse-E-Motion (Infra E-Motion). The sensor detects body movement (at least 0.5 cm from one sample point to the next one) by sensing the animal's body heat.

### 2.10. Statistics

Unless otherwise stated, group measures are given as mean  $\pm$  standard error of the mean (S.E.M.) Statistical analysis was performed using the software STATISTICA (StatSoft, Tulsa, Oklahoma) and GraphPad Prism (GraphPad Software, Inc., La Jolla, California). Mutant mice and their respective treatment and littermate controls were compared with a Student's *t* test, or Mann-Whitney *U* test when data did not meet the requirements for parametric analysis. For multifactorial analysis of paired values (different time intervals for open field, and fear conditioning; different trials for water maze and Rotarod), a mixed ANOVA for repeated measures was performed. When appropriate, *post hoc* Newman-Keuls analysis followed. To compare between controls and mutants the

## MATERIAL AND METHODS

proportion of mice showing a particular performance, as in the Pole test, a Fisher's exact probability test was used. To compare values to expected chance, either a parametric one-sample  $t$  test or a nonparametric Wilcoxon signed-rank test was applied. All tests were unpaired, two-tailed and significance accepted at  $P < 0.05$ .

### 3. Results

In the following study, I investigated the consequences of dysfunctional hyperpolarization-activated currents, i.e. I(h) deficiency, for brain development and behavior. The study was based on earlier findings that forebrain-restricted I(h) deficiency causes strong behavioral abnormalities, including delayed reflex development in neonatal mice and behavioral hyperactivity, impairments in motor function, and cognitive deficits in adult mutant mice (Sandke, 2006; Merseburg, 2011). It was not clear, however, which abnormalities resulted from a lack of homeostatic roles of I(h) in the adult brain, and which from I(h) deficiency during the early postnatal period of brain development. This study was thus aimed at investigating the physiological roles of the HCN channel-mediated currents in neuronal network activity and behavior at different stages of brain maturity, i.e. during early postnatal brain development and at adult ages. The Tet-Off system, in which the activity of the transcriptional transactivator (tTA) is regulated by doxycycline administration (Fig. 3-1 A), was used to obtain temporal control of I(h) deficiency. Without doxycycline, the transcriptional transactivator induces I(h) deficiency. Doxycycline will reversibly inactivate the transcriptional transactivator, and thus restore I(h). Doxycycline treatment will further be referred to as ON condition and no treatment as OFF. Three different doxycycline treatment groups were compared in this study (Fig. 3-1 B): The OFF group never received doxycycline, and mutant mice were thus always deficient in I(h) throughout development and adulthood. Data included in the OFF group was partially generated during my previous study (Merseburg, 2011), but is required for comparison and was extended here to include results obtained from additionally tested mice . A second group of control and mutant littermates received doxycycline after weaning (weaning age is postnatal day 21), affecting early brain development by I(h) deficiency, which was restored by continuous doxycycline treatment from postnatal day 21 throughout adulthood. This group will further be referred to as OFF/ON, and may provide an estimate about the requirements for I(h) during early postnatal brain development, that cannot be compensated by restored I(h) at the juvenile stage. In the third group, mutants had an intact early postnatal development due to doxycycline treatment until weaning age of postnatal day (P) 21, and were deficient in I(h) only after early postnatal development of the CNS was completed. Mice were thus receiving an ON/OFF doxycycline treatment. Results obtained from this group may allow an insight into functional roles of I(h) in the mature brain.

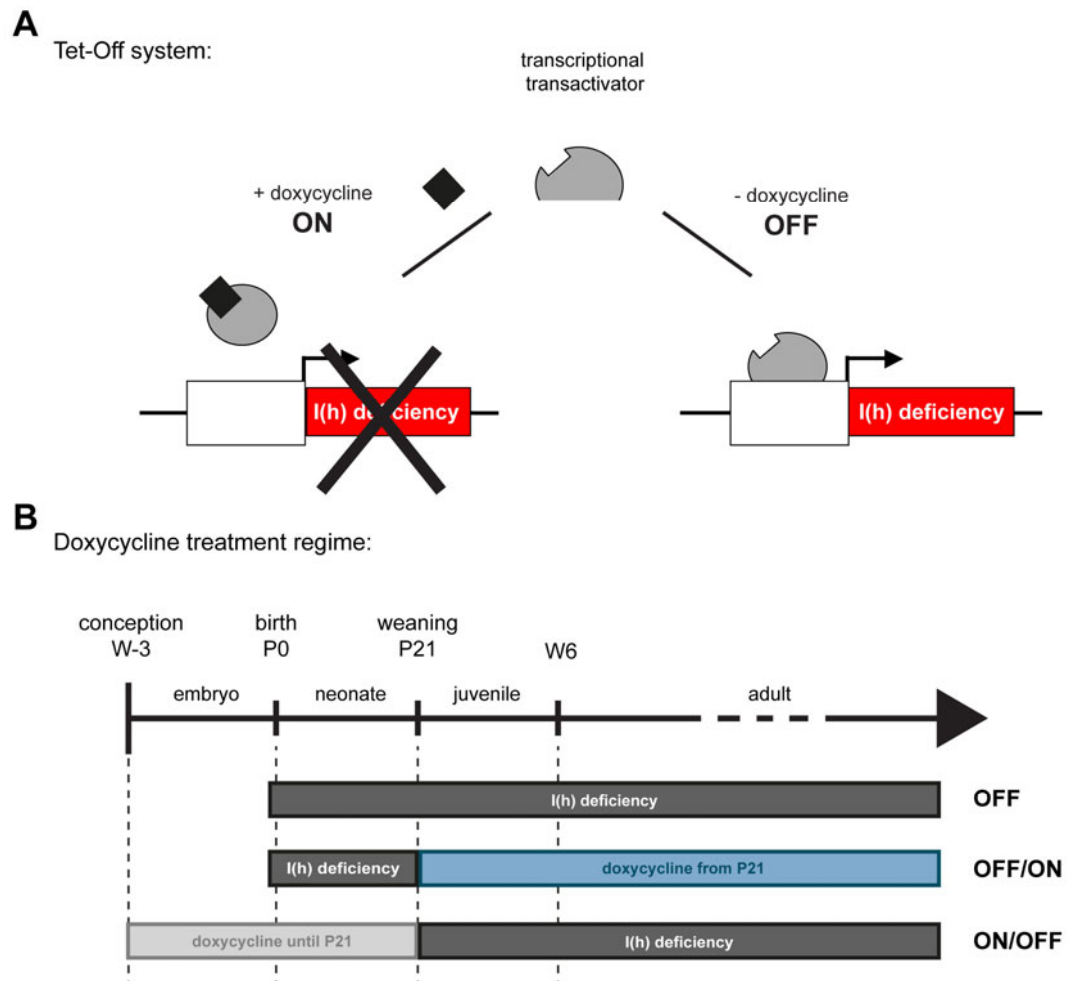


**Figure 3-1: Tet-Off system to study I(h) deficiency at different developmental stages.**

**A:** Scheme of the Tet-Off system to obtain temporal control of I(h) deficiency via doxycycline treatment. The transcriptional transactivator is regulated by doxycycline administration (further referred to as ON, left). Doxycycline causes conformational changes of the transcriptional transactivator and thus, prevents it from inducing I(h) deficiency. Without doxycycline (further referred to as OFF, right), the transcriptional transactivator induce I(h) deficiency. **B:** Doxycycline treatment regime to induce I(h) deficiency at different time points during development. The timeline depicts developmental stages from conception (W-3, around 3 weeks before birth), to birth (P0, postnatal day 0), weaning (P21) and through juvenile (until W6, 6 weeks of age) and adult ages. Mutant animals without doxycycline treatment (OFF) are deficient in I(h) from around birth throughout life (depicted by the dark grey bar). OFF/ON animals did not receive doxycycline during the neonatal period (OFF until P21) and mutants OFF/ON were therefore deficient in I(h) during the early postnatal development until weaning; doxycycline treatment started with weaning (ON from P21, blue bar) and I(h) was restored in mutants. ON/OFF animals received doxycycline until weaning (ON until P21, light gray bar) and had normal I(h) during the early postnatal period until weaning; doxycycline treatment ended with weaning (OFF from P21), which induced I(h) deficiency in mutant ON/OFF.

### **3.1. I(h) deficiency causes hyperexcitability in forebrain projection neurons**

#### **3.1.1. Mice with forebrain-restricted I(h) deficiency in projection neurons**

In order to suppress the HCN/h channel-mediated currents – I(h), mice with conditional expression of a non-conductive (dominant-negative) HCN channel subunit were used, in which HCN-DN subunits can co-assemble with endogenous subunits to suppress HCN channel-mediated currents in a subunit-unspecific manner. The Tet-Off system allowed for regional control of transgene expression via the promoter mouse, as well as temporal control via doxycycline administration (Fig. 3-2 A). Double-transgenic (mutant) mice were obtained by cross-breeding mice that expressed the tetracycline transactivator (tTA) under control of the CaMKII $\alpha$  promoter (Fig. 3-2 A, promoter line) with mice that carried a human HCN4 pore mutant construct (hHCN4-G480S, further called dominant-negative HCN subunit, HCN-DN), fused to a bidirectional promoter containing the tetracycline-response element (TRE) (Fig. 3-2 A, response line). The G480S pore mutation changed the GYG motif to GYS, which is known to exert dominant-negative effects (Schroeder et al., 1998). The bidirectional promoter allowed for simultaneous expression of HCN-DN and enhanced green fluorescent protein (EGFP) (Krestel et al., 2001). The CaMKII $\alpha$  promoter restricted transgene expression to the forebrain, including cortex, hippocampus, striatum, and olfactory bulbs, as visualized via EGFP autofluorescence (Fig. 3-2 B) (Mayford et al., 1996). HCN-DN mRNA levels in forebrain projection neurons were detected by *in situ* hybridization with a probe specific for the human HCN4 transgene in mutant mice (Fig. 3-2 C). In brains of mutant mice receiving doxycycline (mutant ON dox), no mRNA was detectable (Fig. 3-2 C), demonstrating that transgene expression is prevented by doxycycline administration. The intracellular expression of EGFP allowed for indirect localization of HCN-DN-expressing cells (Fig. 3-2 B). To detect the HCN-DN protein on the subcellular level, immunolabeling of the N-terminal HA-tag attached to the transgene was used (Fig. 3-2 A). The results demonstrated that HA-immunostaining was located at distal dendrites of hippocampal CA1 pyramidal neurons (Fig. 3-2 D), indicating that the HCN-DN is localized to sites of endogenous HCN channel subunits. Whole-cell voltage and current-clamp recordings in adult hippocampal slices revealed a strong attenuation of I(h) in mutant CA1 pyramidal neurons that express HCN-DN (Fig. 3-2 E-G). In control CA1 pyramidal neurons, hyperpolarization of the membrane activated I(h), visible by the typical depolarizing voltage

sag under current-clamp conditions (Fig. 3-2 E left), and by increasing current amplitudes upon increasing hyperpolarizing voltage steps under voltage-clamp conditions (Fig. 3-2 E right). In contrast, mutant HCN-DN expressing pyramidal neurons showed no depolarizing voltage sag in response to hyperpolarizing currents (Fig. 3-2 F left), and current amplitudes were strongly reduced (Fig. 3-2 F right). In ON mutants, I(h) amplitudes were at control levels (Fig. 3-2 G), demonstrating effective suppression of HCN-DN expression by doxycycline treatment. In addition, recordings in neonatal P7-8 hippocampal slices revealed that I(h) was functionally ablated in neonatal mutant mice at P7-8 (Fig. 3-2 H-I). CA1 pyramidal neurons of neonatal mutant mice had a hyperpolarized RMP (control:  $n_{\text{cells}} = 15$ ,  $V_m = -57.4 \pm 0.6$  mV; mutant  $n_{\text{cells}} = 10$ ,  $V_m = -59.6 \pm 0.8$  mV;  $P = 0.042$ , Student's  $t$  test), and a significantly increased input resistance (control:  $n_{\text{cells}} = 15$ ,  $R_{\text{in}} = 669 \pm 48$  pA; mutant  $n_{\text{cells}} = 10$ ,  $R_{\text{in}} = 939 \pm 61$  pA;  $P < 0.01$ , Student's  $t$  test). The time course of doxycycline-dependent HCN-DN expression was previously analyzed in our lab and demonstrated that HCN-DN mRNA levels were detectable as early as three days after doxycycline withdrawal, and reached full expression levels within three weeks (Sandke, 2006).

In summary, the data demonstrate that I(h) was functionally ablated by HCN-DN expression in a region- and time-dependent manner in neonatal P7 and adult mutant hippocampal CA1 pyramidal neurons. Furthermore, HCN-DN was shown to be localized to distal dendrites of CA pyramidal neurons, which is the site of endogenous HCN channel subunit localization. In a next step, the distribution of EGFP autofluorescence among the CaMKII $\alpha$ -expressing population was analyzed in more detail.

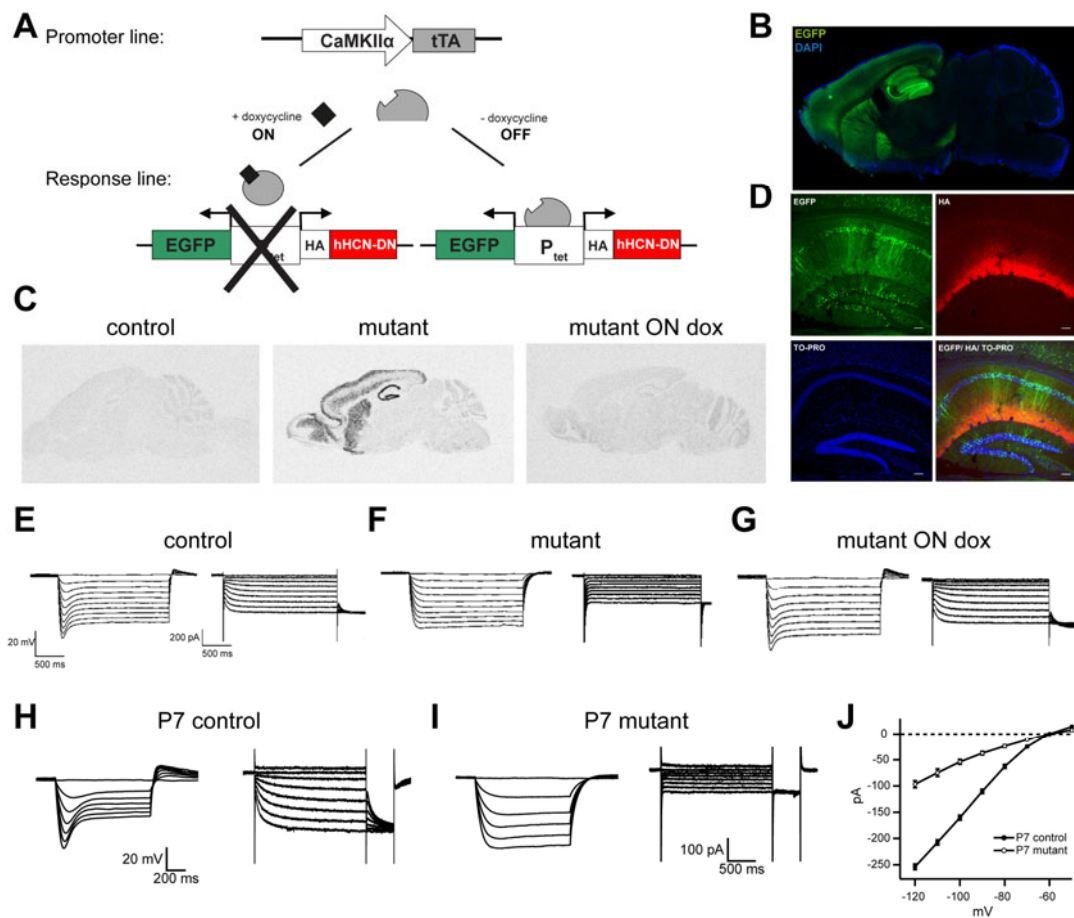


**Figure 3-2: Mice with forebrain-specific I(h) ablation.**

**A:** Region-specificity of transgene expression is achieved via the promoter line that drives the expression of the tetracycline-responsive transcriptional transactivator (tTA). The CaMKII $\alpha$  promoter limits tTA expression to forebrain projection neurons. The response line carries the dominant-negative HCN channel subunit (HCN-DN, red). Double-transgenic mutant mice are obtained by cross-breeding promoter and response lines. Doxycycline administration prevents transcription of HCN-DN due to a conformational change of the tTA upon binding of doxycycline. HCN-DN is tagged with a hemagglutinin (HA)-tag and driven by a bidirectional promoter for simultaneous expression of enhanced green fluorescent protein (EGFP, green). **B:** Sagittal brain section showing forebrain-specific HCN-DN expression visualized by EGFP expression (green). Cell nuclei are stained with DAPI (blue). **C:** HCN-DN expression depends on genotype and doxycycline administration, as shown for control (left), mutant (middle), and mutant ON dox (right) via *in situ* hybridization with a HCN-DN specific probe. **D:** Immunofluorescence images of the adult mutant hippocampal CA1 region. Transgene expression localized via intracellular EGFP autofluorescence (green, top left). Immunostaining of the HCN-DN-attached HA-tag (red, top right) demonstrating that HCN-DN is localized to distal dendrites. Cell nuclei are stained with TO-PRO (blue, bottom left). Bottom right shows merged image. Images in C and D were modified with permission from Sandke (2006). **E-G:** *In vitro* whole-cell current (left) and voltage (right) clamp recordings obtained from adult CA1 pyramidal neurons in hippocampal acute slices, showing the response of **E:** control, **F:** mutant and **G:** mutant ON dox mice to hyperpolarizing current and voltage steps. I(h) is only absent in mutants without doxycycline treatment, and completely restored in mutants ON doxycycline. Patch-clamp recordings shown in E-G were obtained by Prof. Dirk Isbrandt and Prof. Jochen Roeper. **H-J:** Whole-cell current (left) and voltage clamp (right) recordings from neonatal P7 CA1 pyramidal neurons in acute hippocampal slices of **H:** control and **I:** mutant neonatal mice, displaying the absence of functional I(h) in mutant neonates. **J:** Quantification of tail currents recorded from control (closed circles) and mutant (open circles) CA1 pyramidal neurons showing strongly reduced currents in mutant cells. (Patch-clamp recordings in P7 hippocampal slices shown in H-J were performed by PD. Dr. Axel Neu, ZMNH, Hamburg.)

### 3.1.2. Localization of HCN-DN expression via EGFP in forebrain regions

The bidirectional promoter driving HCN-DN expression allowed for simultaneous intracellular expression of EGFP. Immunolabeling with an antibody against CaMKII $\alpha$  was used to compare EGFP expression with endogenous CaMKII $\alpha$  expression in double-transgenic brains. According to Mayford *et. al* (1996), the CaMKII-alpha promoter-mediated expression of tTA and hence, HCN-DN is expected to be present in forebrain regions, including the cortex, striatum, hippocampal CA1 and CA3 regions, and the dentate gyrus (Mayford et al., 1996). As shown in Fig. 3-2 B, EGFP expression was seen throughout the cortex. However, EGFP expression was restricted to specific layers. For example, in the primary and secondary motor area, EGFP expressing cell bodies were located in layer 2/3 and 6a, and co-immunolabeled with CaMKII $\alpha$ -positive neurons (Fig. 3-3 A). In layer 5 of the motor cortex, CaMKII $\alpha$ -expressing cell bodies showed no overlay with EGFP (Fig. 3-3 A). In the somatosensory hind limb area (S1HL), EGFP expression was prominent in layers 2/3, 4 and 6a, but again absent in layer 5 projection neurons (Fig. 3-3 B). In both cortical regions, the neuropil in layer 1 also showed an EGFP signal that was colocalized with CaMKII $\alpha$ -immunoreactivity (Fig. 3-3). The hippocampal formation displayed the strongest EGFP signal and prominent CaMKII $\alpha$  immunostaining (Fig. 3-4). In CA1, EGFP labeling was seen in deep cell bodies of the pyramidal cell layer and their distal dendrites in radiatum and lacunosum moleculare (Fig. 3-3 A), whereas in the CA3 region especially the neuropil in stratum lucidum showed strong EGFP fluorescence (Fig. 3-4 B), presumably coming from mossy fibers of dentate granule cells, which also showed strong EGFP fluorescence (Fig. 3-4 C). In subcortical brain areas, the caudoputamen of the striatum showed prominent EGFP labeling, in particular in cell bodies and neuropil in the matrix, with strong CaMKII $\alpha$  co-staining (Fig. 3-5 A). In the dorsal globus pallidus, EGFP-positive cells and neuropil were detected and colocalized with CaMKII $\alpha$  immunolabeling (Fig. 3-5 B). In accordance with the lack of HCN-DN in layer 5 pyramidal neurons of the motor cortex, the pyramids of the corticospinal tract did not express HCN-DN (Fig. 3-5 C). A few EGFP-positive cells were found in the raphe nucleus region, but did not colocalize with the CaMKII $\alpha$  signal. In the cerebellum, EGFP-expressing afferent projections were detected in the granule cell layer, but there was no overlay with CaMKII-alpha positive Purkinje cells, or their dendrites in the molecular layer (Fig. 3-5 D). In all brain regions examined it was observed that a proportion of CaMKII $\alpha$ -positive cell bodies of presumed projection neurons did not express EGFP, and

that EGFP-positive cells differed from each other regarding their EGFP fluorescence intensity, which was indicative of a cell-to-cell difference in transgene expression.

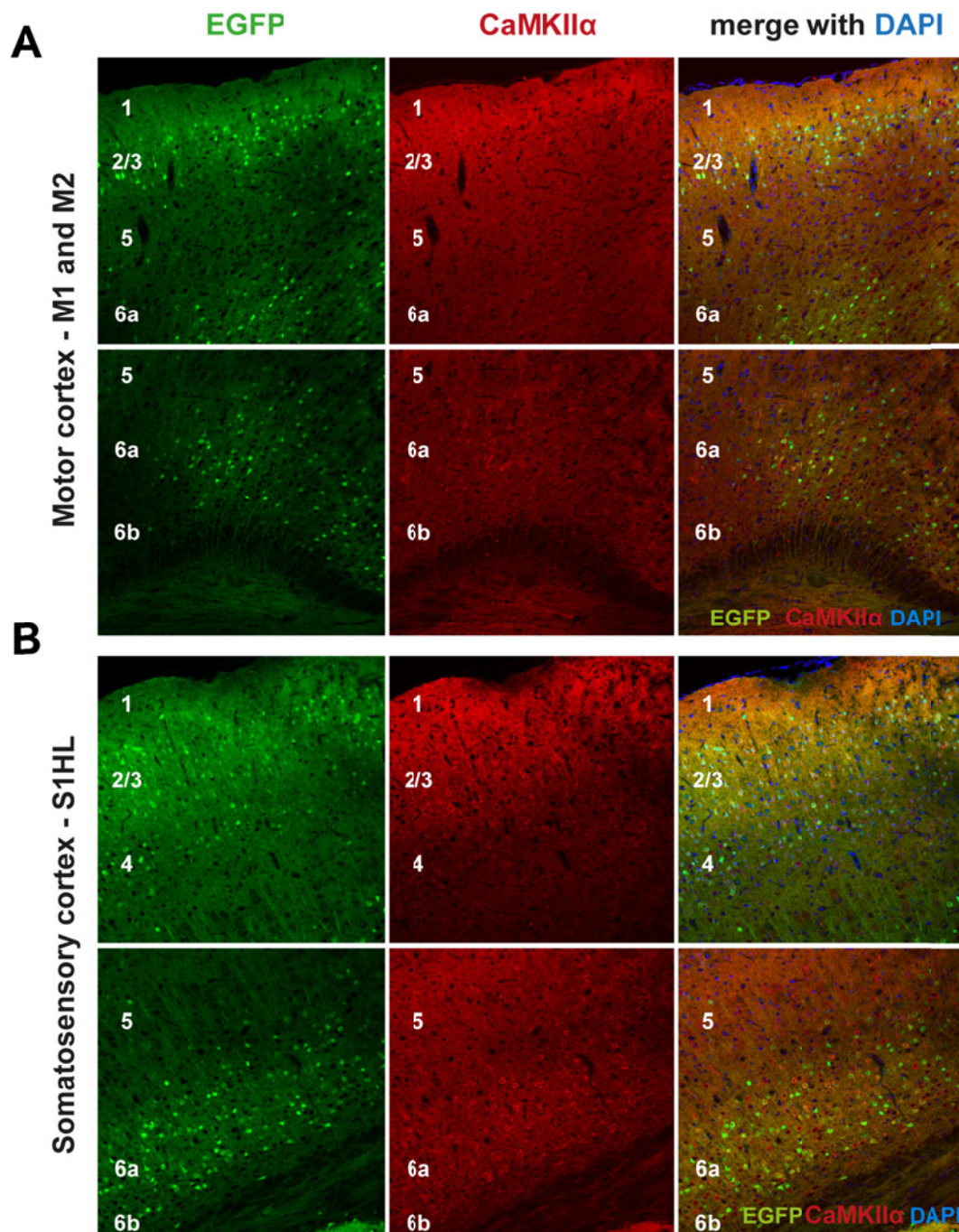


**Figure 3-3: EGFP expression in cortical regions.**

EGFP expression (left, green) and immunostaining of endogenous CaMKII $\alpha$  (middle, red) in the cortex. Overlay with cell nucleus stain (DAPI, blue) is shown on the right. **A:** In primary (M1) and secondary (M2) motor cortex, EGFP (left, green) was localized to layers 2/3 (top) and layer 6a (bottom), and absent in layer 5. CaMKII $\alpha$ -positive projection neurons were detected in layers 2/3, 5 and 6a (middle, red). **B:** In the hindlimb area of the primary somatosensory cortex hind limb region (S1HL), EGFP was localized to layers 2/3, 4 and 6a, but absent in layer 5 CaMKII $\alpha$ -positive neurons.

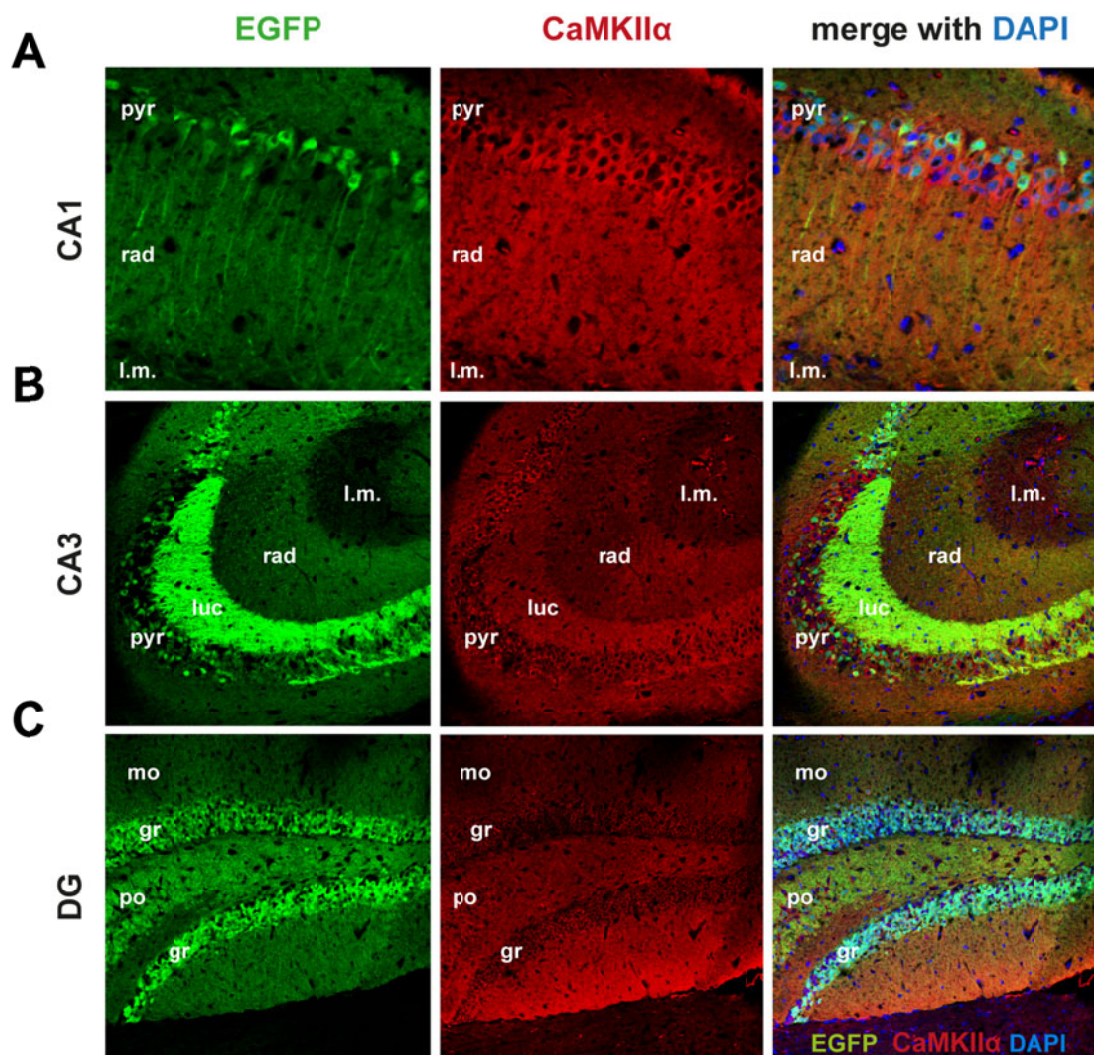


**Figure 3-4: EGFP expression in the hippocampus.**

EGFP expression (left, green) and immunostaining of endogenous CaMKII $\alpha$  (middle, red) in the hippocampal formation. Overlay with cell nucleus stain (DAPI, blue) is shown on the right. **A:** EGFP signal of cell bodies in the pyramidal cell layer (pyr) and neuropil in stratum radiatum (rad) of CA1 was colocalized with CaMKII $\alpha$ -immunoreactivity. Note prominent EGFP expression in deep pyramidal layer and lack of EGFP-positive cell bodies in the superficial CaMKII $\alpha$ -positive cells. **B:** Within the CA3 area, strong EGFP fluorescence was detected in stratum lucidum (luc) of presumed mossy fibers of dentate granule cells. Only a few cell bodies in the pyramidal layer (pyr) were EGFP positive. **C:** In the dentate gyrus, EGFP expression was located in cell bodies of the granule cell layer (gr) and neuropil in molecular (mo) and polymorphic (po) layers.

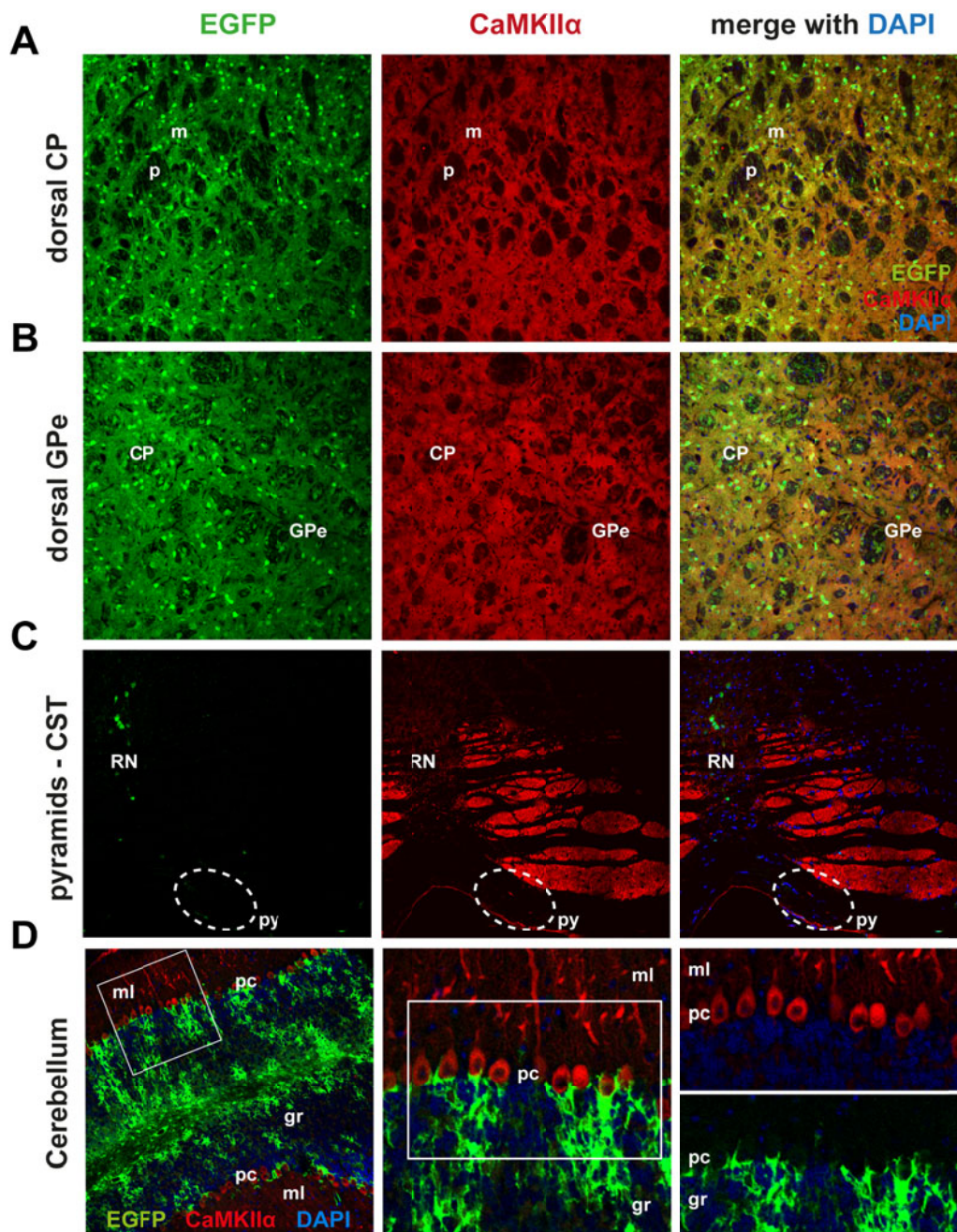


**Figure 3-5: EGFP expression in subcortical regions.**

EGFP expression (left, green) and immunostaining of endogenous CaMKII $\alpha$  (middle, red) in subcortical structures. Overlay with cell nucleus stain (DAPI, blue) is shown on the right. **A:** The caudoputamen (CP) of the striatum, with its patch (p) and matrix (m) organization, showed EGFP expressing cells in the matrix (left, green) with CaMKII $\alpha$  overlay (middle, red). Cell nuclei were stained with DAPI (right, blue). **B:** EGFP fluorescence detected in the dorsal globus pallidus external segment (GPe). **C:** In the raphe nucleus region (RN) EGFP-expressing cells were detected, but not colocalized with CaMKII $\alpha$  immunolabeling. The pyramids (py, dotted ellipse) of the corticospinal tract (CST) did not express EGFP (left). **D:** In the cerebellum, EGFP-expressing afferents were detected in the granular layer (gr, left). Box depicts region shown in the middle. EGFP-positive afferents reach close onto the Purkinje cells (pc). Box depicts region shown on the right, demonstrating that there was no overlay with CaMKII $\alpha$ -positive Purkinje cells or their dendrites in the molecular layer (ml).

### 3.1.3. HCN-DN expression causes hyperexcitability in brain slices

To further examine how HCN-DN expression affects cellular excitability, *in vitro* whole-cell current clamp recordings were performed (collaboration with Prof. Mala Shah, UCL London). The membrane voltage response of adult entorhinal cortex layer 3 (EC L3) pyramidal neuron dendrites (Fig. 3-6 A-F) and somata (Fig. 3-6 G-L) to current injections ranging from -150 pA to +200 pA was recorded in acute slice preparations. In control EC L3 neuron dendrites, hyperpolarizing current steps activated I(h), which was reflected by the voltage sag response (Fig. 3-6 A left). Depolarizing current injections evoked action potential firing in control EC L3 neurons (Fig. 3-6 A left and B). Application of the HCN channel blocker ZD7288 (ZD) to control neurons hyperpolarized the RMP at the dendrites (Fig. 3-6 A middle and E), caused elevated action potential firing upon depolarization (Fig. 3-6 A middle and B), and increased the input resistance of the neurons (Fig. 3-6 F). Thus, blocking HCN channels with ZD increased the excitability of control EC L3 neurons. In contrast to control cells in the absence of ZD, mutant HCN-DN-expressing neurons had a hyperpolarized membrane potential at rest (Fig. 3-6 C left and E), an increased input resistance (Fig. 3-6 F), did not show a voltage sag response to hyperpolarizing currents (Fig. 3-6 C left), and elicited more action potentials upon depolarizing current pulse injections as compared to control neurons (Fig. 3-6 C left and D). In other words, mutant EC L3 pyramidal cells showed responses similar to those obtained for control neurons upon ZD-mediated block of HCN channels. In addition, mutant EC L3 pyramidal neurons were not affected by ZD application (Fig. 3-6 C right). The somatic response of control and mutant EC L3 pyramidal neurons was similar to the above-described dendritic response (Fig. 3-6 G-L). This indicates that HCN-DN expression functionally blocked I(h), thereby causing neuronal hyperexcitability *in vitro*.

Changes in RMP and input resistance can affect the integration of incoming excitatory postsynaptic potentials (EPSPs). It was thus examined whether HCN-DN expression affects the integration of incoming single EPSPs or a train of EPSPs (Fig. 3-7). When recorded at the dendrites of control EC L3 pyramidal neurons, single EPSPs (Fig. 3-7 A top) had a greater amplitude (Fig. 3-7 C) and decay time (Fig. 3-7 D) upon blocking I(h) with ZD. In addition, the summation ratio of a train of five EPSPs (Fig. 3-7 A bottom) was increased in control neurons in the presence of ZD (Fig. 3-7 E). HCN-DN-expressing mutant neurons had a larger EPSP amplitude and decay time, as well as a larger summation ratio under baseline conditions, and were not altered by ZD administration (Fig. 3-7 B-E). The responses obtained

at the soma were again similar to those obtained at the dendrites of EC L3 pyramidal neurons (Fig. 3-7 F-J).

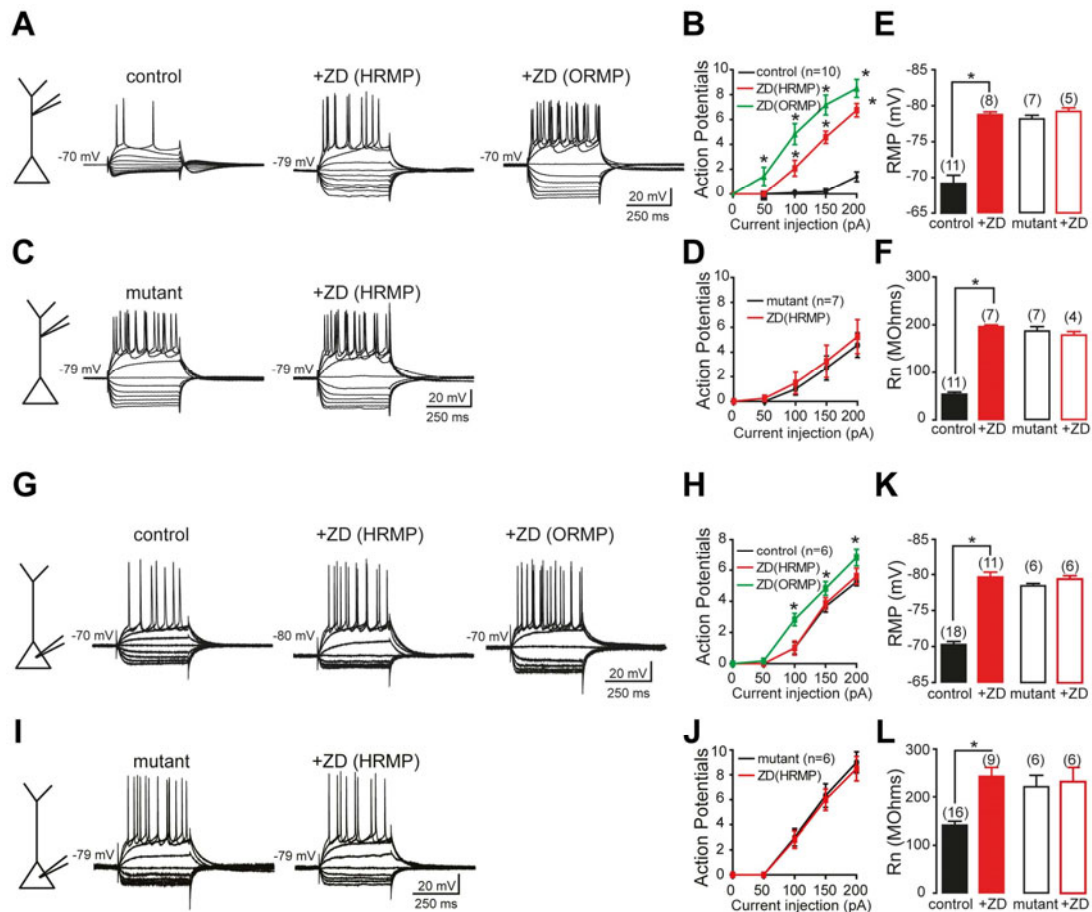


**Figure 3-6: Lack of I(h) increases entorhinal cortex layer 3 pyramidal neuron excitability *in vitro*.**

**A:** Example traces obtained from dendritic whole-cell current clamp recordings of control entorhinal cortex layer III pyramidal neurons in response to current injections from -150 pA to +200 pA under control conditions (left) and following bath application of 15  $\mu$ M ZD7288 (ZD, middle). ZD application in control cells caused a hyperpolarization of the membrane potential (HRMP), therefore recordings were made at the original RMP (ORMP, right) for comparison. **B:** Number of action potentials elicited upon 400 ms depolarizing current injections in the absence (black) and presence of ZD (red for HRMP, green for ORMP) in control neurons. Note elevated action potential firing in control cells upon ZD application. **C:** Mutant neuron dendrites had a hyperpolarized RMP, fired more action potentials (left) and did not respond to ZD application (right). **D:** Elevated action potential firing in mutant cells in the absence (black) and presence (red) of ZD. **E:** RMP of control and mutant neurons in the absence and presence of ZD. **F:** Input resistance ( $R_n$ ) of control and mutant neurons in the absence and presence of ZD. Note that mutant HCN-DN-expressing cells had a hyperpolarized RMP and that  $R_n$  was not further affected by ZD application. **G-L:** Recordings obtained from the soma of EC L3 neurons revealed responses similar to those described for dendritic recordings. Data represent mean  $\pm$  S.E.M. \*  $P < 0.05$  with Student's  $t$  test. The data shown were generated in collaboration with Prof. Mala Shah, UCL School of Pharmacy, London.

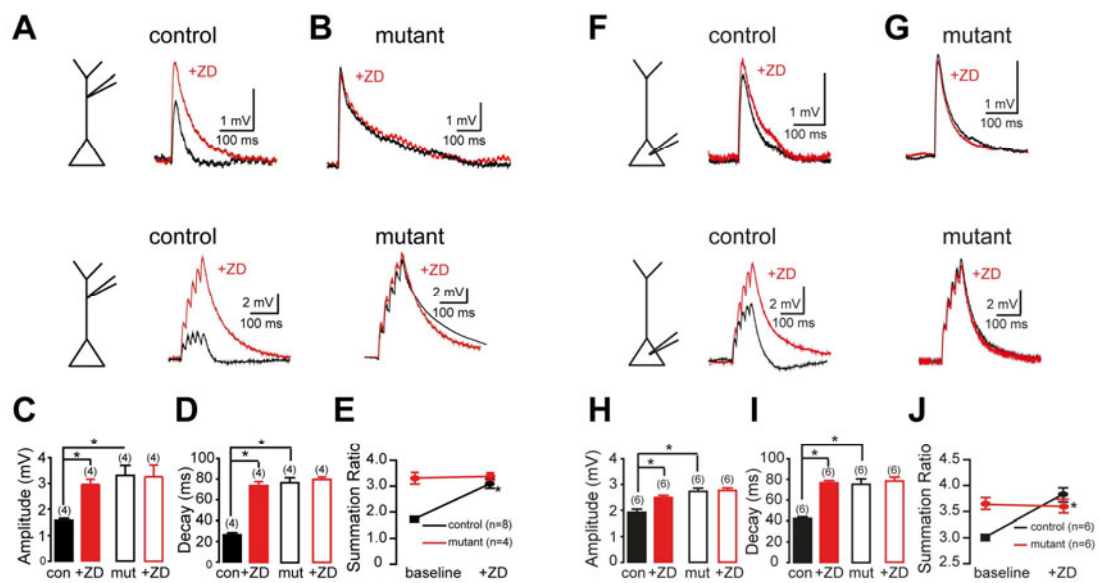


**Figure 3-7: I(h) ablation affects integration of EPSPs.**

**A:** Example of a single dendritic EPSP (top) or a train of EPSPs (bottom) recorded from control and **B:** mutant dendrites under baseline conditions (black traces) and after application of ZD (red traces). Blocking HCN channels with 15  $\mu$ M ZD in control dendrites increased the amplitude and summation ratio of EPSPs. ZD had no effect on HCN-DN-expressing mutant dendrites. **C:** Quantification of EPSP amplitude and **D:** decay time of single EPSPs before (black) and after (red) ZD application in control (filled bars) and mutant (open bars) dendrites; and **E:** the summation ratios of trains of EPSPs before and after ZD application in control (black) and mutant (red) dendrites. **F-J:** Recordings obtained from the soma of EC layer III pyramidal neurons for **F:** control and **G:** mutant cells. Data represent mean  $\pm$  S.E.M. \*  $P < 0.05$  with Student's  $t$  test. The data shown were generated in collaboration with Prof. Mala Shah, UCL School of Pharmacy, London.

Taken together, these data show that HCN-DN expression successfully ablates the current in a time- and region-dependent manner. The HCN-DN protein was localized to sites of endogenous HCN subunit expression (Sandke, 2006), and HCN-DN transgene expression mimicked the effects of the specific HCN channel blocker ZD. I(h) attenuation changed the intrinsic electrophysiological properties of EC L3 neurons, i.e. the resting membrane potential, input resistance and dendritic integration, causing neuronal hyperexcitability *in vitro*.

Next, the question was addressed of whether HCN-DN-mediated neuronal hyperexcitability was reflected in the behavior of neuronal network activity *in vivo*.

### **3.2. *In vivo* cortical and hippocampal activity is affected by I(h) deficiency**

Local field potentials (LFPs) were recorded in awake and behaving mice to study the effect of ablated I(h) on neuronal population activity. In my previous study, I observed the earliest phenotypic abnormality at P6, which was expressed as delayed sensorimotor reflex development in mutant neonatal mice (Merseburg, 2011). Thus, hippocampal and cortical activity was recorded in awake mice at P6-P8.

#### **3.2.1. Functional suppression of I(h) alters spontaneous local field potential activity in neonatal mice**

LFPs were recorded with extracellular 16-channel silicon probes placed in hippocampus (Fig. 3-8 A), and somatosensory (Fig. 3-9 A) and visual (Fig. 3-10 A) cortices in head-restrained, awake neonatal mice.

Hippocampal LFPs were recorded along the dorsal CA1-dentate gyrus axis (Fig. 3-8 A), and were characterized by sharp waves (SPWs) and stratum radiatum oscillations (SROs) with intermittent periods of silence. SPWs were short field events, characterized by negative deflections that were largest in channels located in stratum lacunosum moleculare of apical dendrites, a phase reversal in CA1 pyramidal layer, and positive deflections in stratum oriens of basal dendrites (Fig. 3-8 B). SPWs either occurred alone or in combination with SROs, 10-30 Hz oscillations that were most prominent in channels located below the phase reversal in stratum radiatum and lacunosum moleculare (Fig. 3-8 C). Quantification of the properties of SPWs and SROs, including mean SPW rate and amplitude; mean SRO rate and length, and time mice spent in SROs during the recording epoch (~ 1.5 hours), and the number of SPWs co-occurring with SROs revealed no significant differences between control and mutant mice (Fig. 3-8 D-F) (Table 6-1). However, mutant mice tended to have lower SPW rates and amplitudes (Fig. 3-8 D), as well as lower SRO rates of slightly longer duration (Fig. 3-8 E).

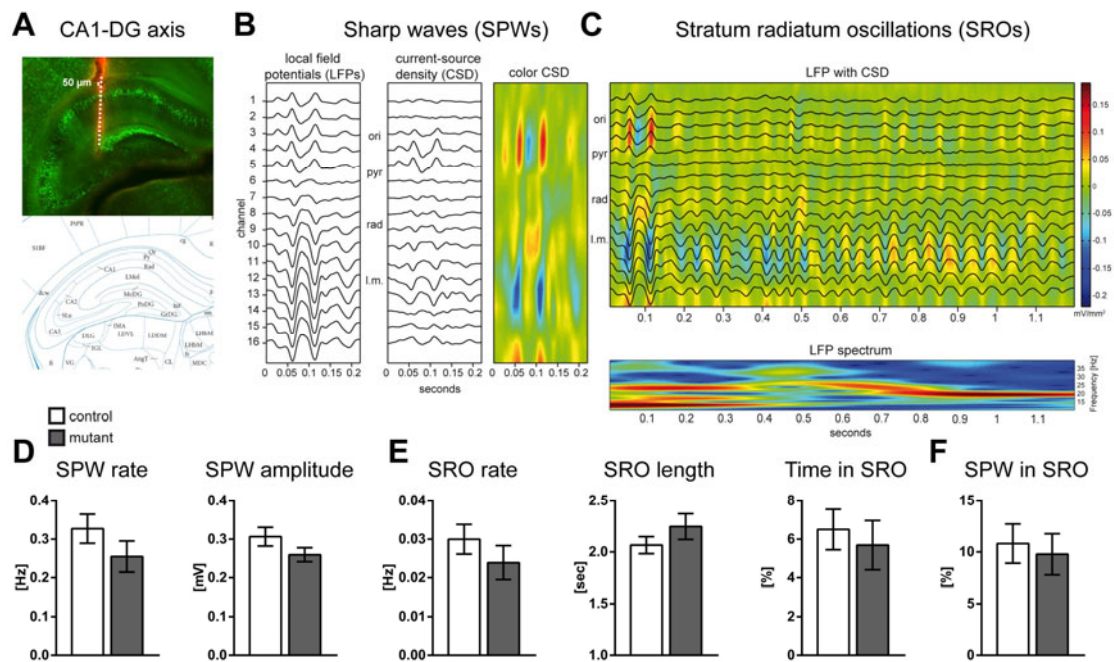


**Figure 3-8: Hippocampal local field potential activity is not affected by I(h) ablation.**

**A:** Position of the 16-channel (white dots, 50  $\mu\text{m}$  spacing) linear electrode (marked with Dil in red) along the CA1-dentate gyrus (DG) axis of the hippocampus in a mutant mouse (EGFP expression in green), with corresponding reference atlas picture below. **B:** Representative local field potential recording during two sharp waves (SPWs, left). The depth-profile shows negative deflections in lacunosum moleculare (l.m.) and radiatum (rad), phase reversal in pyramidale (pyr), and positive deflections in oriens (ori). Current-source density (CSD, middle) demonstrates the most negative deflections in lacunosum moleculare (current sink), and most positive deflections in oriens (current source). Color CSD (right) demonstrating the current sinks in lacunosum moleculare (cold colors), and corresponding current sources in oriens (warm colors). **C:** Representative LFP with color CSD recording during two SPWs followed by stratum radiatum oscillations (SROs). Below the corresponding 10–40 Hz LFP spectrum of channel 13 is shown. **D:** SPW rate and SPW amplitude in radiatum. **E:** SRO rate, mean length, and time in SRO as percentage of total recording duration. **F:** Amount of SPWs co-occurring with SROs. Control  $n = 19$ , mutant  $n = 9$ . Data represent mean  $\pm$  S.E.M. Mann-Whitney  $U$  test revealed no statistically significant differences between control and mutant mice (Table 6-1).

In both, somatosensory and visual cortex, the LFP was characterized by two types of activity, slow activity transients (SATs) and beta oscillations. Based on their depth profiles, SATs were further subdivided into type I (SAT I) and type II (SAT II) that were observed on single or multiple channels up to 500  $\mu\text{m}$  deep in the cortex. SAT I events were prominent positive LFP changes recorded on superficial cortical channels of the probe (Fig. 3-10 B), and carried negative components of lower amplitude in underlying channels (Fig. 3-9 B). SAT II events were characterized as solely negative LFP deflections and recorded on various channels (Fig. 3-9 B and 3-10 B). Beta oscillations (spindle bursts, SBs) were 10–30 Hz oscillations on superficial channels around 300  $\mu\text{m}$  deep in the cortex (Fig. 3-9 C and 3-10 C). In somatosensory cortex, quantification of SATs and SBs revealed no significant differences when I(h) was deficient (Fig. 3-9) (Table 6-2). SAT I rates were similar in control and mutant mice (Fig. 3-9 D), but mutants tended to display lower SAT II (Fig. 3-9 E) and SB rates

(Fig. 3-9 F), due to the absence of detectable events in a higher number of mutant than control mice (Fig. 3-9 G, F). In contrast, suppression of I(h) in visual cortex was found to exert a more pronounced effect (Fig. 3-10) (Table 6-3). The overall occurrence rate of SATs was significantly reduced in mutant mice (Fig. 3-10 D). This reduction was attributable to a significant decrease in SAT I rates, with the majority of mutant mice having no detectable SAT I events (Fig. 3-10 E). In contrast, SAT II events occurred with similar rates in control and mutant mice (Fig. 3-10 F). SB occurrence was also significantly reduced, but the mean length was not changed (Fig. 3-10 G). Again, a high proportion of mutant mice did not show any SB activity during the recording epochs of up to 1.5 h.

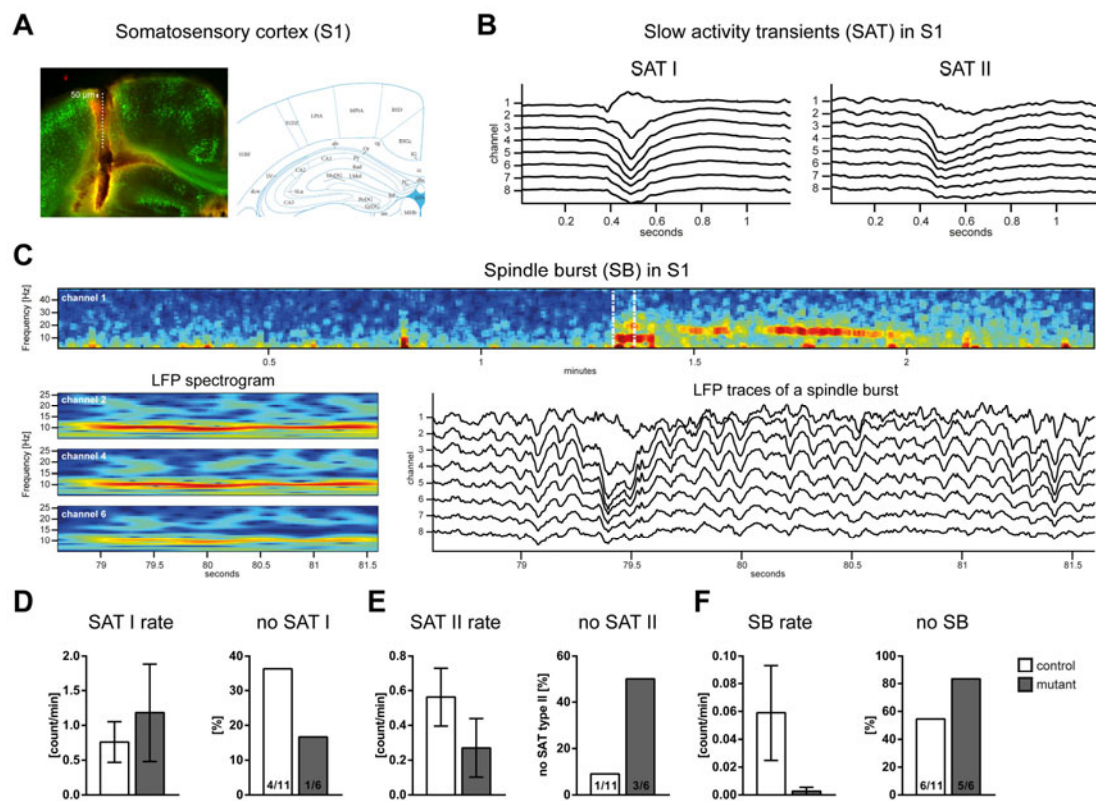


**Figure 3-9: Activity in somatosensory cortex is slightly affected by suppressed I(h).**

**A:** Position of the 16-channel (white dots, 50  $\mu$ m spacing) linear electrode (marked with Dil in red) in somatosensory cortex (S1) of a P7 mutant mouse (EGFP, green), with corresponding atlas reference picture. **B:** Representative traces of slow activity transients (SAT) of type I (left) and type II (right). **C:** (Top) 0-50 Hz spectrogram of the current-source density (CSD) constructed from the first recording channel of the electrode (channel 1), showing three spindle burst (SB) events between 1.3 and 2 minutes. The first SB highlighted by white rectangular ticks is shown in more detail below. (Bottom left) 5-25 Hz LFP spectrogram of the SB highlighted above for channels 2, 4 and 6. (Bottom right) Corresponding LFP traces of the top 8 recording channels. **D:** SAT I rate and proportion of mice without any SAT I events. **E:** SAT II rate and proportion of mice without any SAT II events. **F:** SB rates and proportion of mice without any SBs in S1 over the recording epoch of  $\sim$ 1.5 hours. Control  $n = 11$ , mutant  $n = 6$ . Data represent mean  $\pm$  S.E.M. Mann-Whitney  $U$  test for SAT and SB rates and Fisher's exact probability test for proportion of mice without SATs and SBs revealed no statistically significant differences between control and mutant mice (Table 6-2).

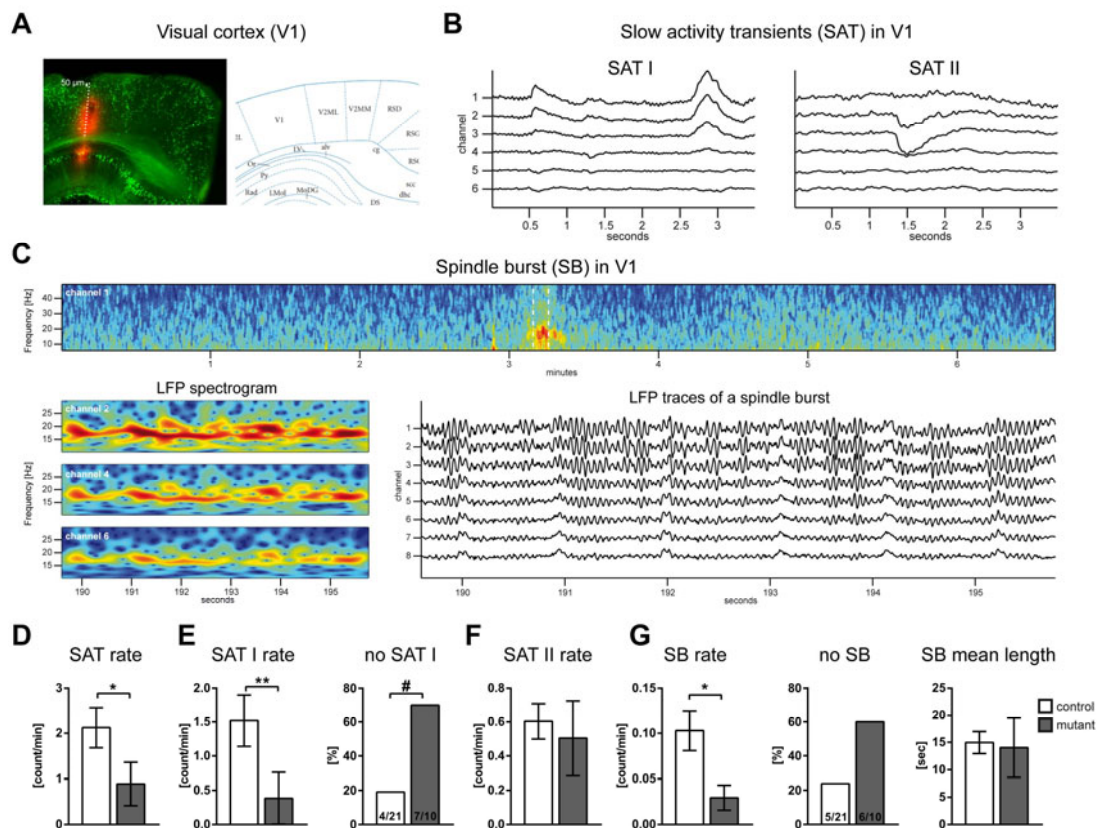


**Figure 3-10: Spontaneous activity in visual cortex is attenuated upon I(h) deficiency.**

**A:** Position of the 16-channel (white dots, 50  $\mu\text{m}$  spacing) linear electrode (marked with Dil in red) in visual cortex (V1) of a P7 mutant mouse (EGFP, green), with corresponding atlas reference picture. **B:** Example traces of slow activity transients (SAT) of type I (left) and type II (right). **C:** (Top) 0-50 Hz spectrogram of the current-source density (CSD) constructed from the first recording channel of the electrode (channel 1), showing a spindle burst (SB, marked by white rectangular ticks). (Bottom left) 10-30 Hz LFP spectrogram of the SB shown above for channels 2, 4 and 6. Bottom right shows corresponding LFP traces of the top 8 recording channels. **D:** The overall SAT rate was reduced in mutant neonatal mice. **E:** SAT I rate was reduced (left) due to a higher proportion of mutant mice without SAT I events. **F:** SAT II rates were unchanged. **G:** Mutant mice had lower SB rates of similar mean length. Control  $n = 21$ , mutant  $n = 10$ . \*  $P < 0.05$ , \*\*  $P < 0.01$  with Mann-Whitney  $U$  test. #  $P < 0.01$  Fisher's exact probability test (Table 6-3).

In summary, it was observed that attenuated I(h) tended to reduce network activity in the hippocampus and cortex of neonatal mutant mice, with the strongest effects seen on visual cortex activity. Therefore, in neonatal mice, the neuronal hyperexcitability characterizing mutant neurons in acute slices *in vitro* (Figs. 3-6, 3-7), did not result in neuronal network hyperactivity, but rather showed the opposite. Next it was determined, whether adult neuronal network activity was altered when I(h) was deficient.

### 3.2.2. Adult network activity is affected by I(h) deficiency

To investigate whether suppressed I(h) causes changes in brain activity in adulthood, hippocampal LFPs were recorded in adult behaving mice implanted with a 16-site linear probe along the dorsal hippocampal CA1-DG axis (Fig. 3-11 A). Since the behavior of animals during sleep is less variable than during wake states, sleep brain activity was considered to be more representative of the internal network properties. Therefore, recordings were performed while mice were sleeping in their home cages. Hippocampal LFP patterns were found to show characteristics as had been described for adult mice (Buzsáki et al., 2003). During slow-wave sleep, the most prominent activity pattern was the sharp wave-ripple complex (SPW-Rs) (Fig. 3-11 B). Ripples were short high frequency oscillations (120-180 Hz), with their highest amplitude in the pyramidal layer, which were accompanied by a negative sharp wave (SPW) in stratum radiatum of CA1 (Fig. 3-11 B). REM sleep was characterized by theta oscillations (4-12 Hz) with nested gamma oscillations (30-80 Hz) (Fig. 3-12 C). Theta oscillations changed their phase gradually and reached full reversal in stratum lacunosum moleculare. Accordingly, gamma oscillations along the CA1-DG axis occurred at the peak of the theta wave in stratum oriens and pyramidal layer, and at the trough in layers below the pyramidal layer (Fig. 3-12 C).

For each mouse multiple recordings of sleep activity were performed, but not every sleep recording contained both, slow-wave sleep and REM episodes. In addition, the animal number per group was limited. Therefore, analysis of the number of recordings obtained per genotype was performed. Slow-wave sleep episodes were analyzed regarding the specific properties of SPW-R, including ripple frequency and duration, SPW amplitude in stratum radiatum, and SPW-R occurrence rate over the course of a slow-wave sleep epoch (Table 6-4). Quantification of SPW-R properties revealed strongly reduced ripple peak frequencies in mutant mice (Fig. 3-12 A-B). When comparing the average spectral ripple peak for each recording performed in control and mutant mice, a strong peak was seen at around 150 Hz in control mice, whereas the majority of ripples recorded in mutant mice had lower peak frequencies that averaged around 130 Hz (Fig. 3-12 B-C). Together with significantly shorter frequencies, mutant SPW-R were of significantly shorter duration and showed higher SPW amplitudes, as well as lower occurrence rates during the slow-wave sleep (Fig. 3-12 D).

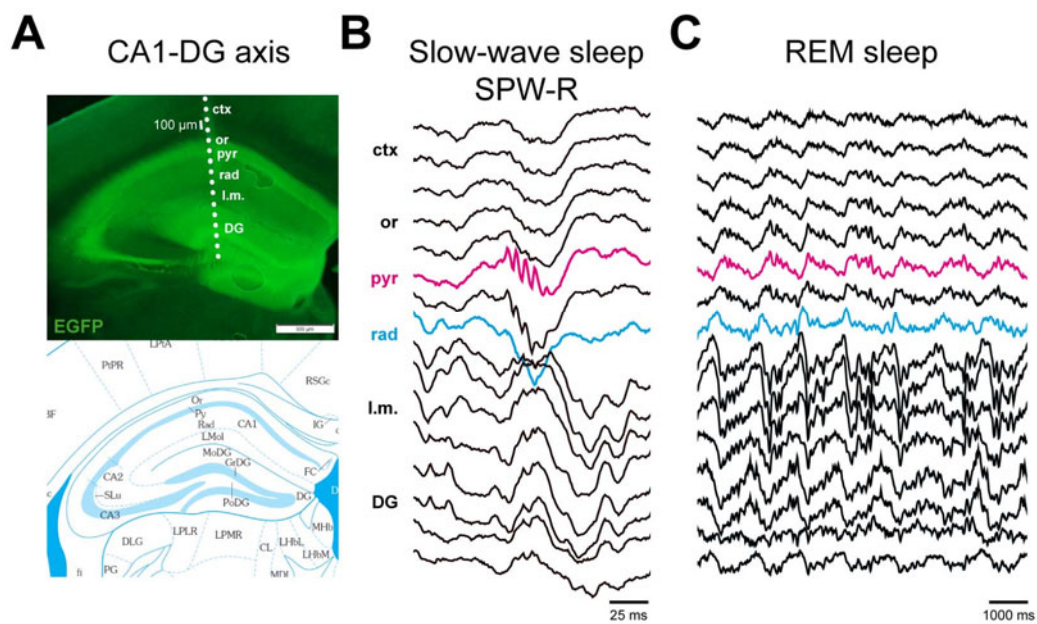


**Figure 3-11: Hippocampal LFP sleep patterns in adult mice.**

**A:** Position of the 16-site (100 µm spacing) linear recording electrode (implanted at bregma -1.9) along the CA1-DG axis in a mutant mouse, with corresponding reference atlas picture below. Ctx, cortex; or, stratum oriens; pyr, stratum pyramidale; rad, stratum radiatum; l.m., stratum lacunosum moleculare; DG, dentate gyrus. **B:** Example LFP traces recorded from a control mouse during a sharp wave/ripple (SPW-R). Ripples had the highest amplitude in the pyramidal layer (pink) and were accompanied by a negative SPW in stratum radiatum (blue). **C:** Example LFP traces obtained during REM sleep of a control mouse, demonstrating 4-12 Hz theta waves with nested 30-80 Hz gamma oscillations. Note that theta oscillations change their phase along the CA1-DG axis, reaching full reversal in stratum lacunosum moleculare. The same colors as in C.

Changes in SPW-R properties might be the cause of an abnormal early postnatal development due to attenuated I(h). To study the effect of functional I(h) ablation independently of I(h) deficiency during the early postnatal developmental period, adult mice were recorded receiving doxycycline until P21 (mutant ON/OFF animals). Mutant ON/OFF mice had functional I(h) until weaning age, and were deficient in I(h) from juvenile ages onward. In contrast to the significant changes found in mutant mice, ripple peak frequencies of mutant ON/OFF animals were not affected (Fig. 3-12 C). In mutant ON/OFF animals, too, SPW-R properties were not changed in terms of either ripple frequency and duration, or SPW amplitude as compared to control mice, but the SPW-R occurrence rate was significantly lower, as was similarly seen in mutant OFF animals (Fig. 3-12 D). This indicated that suppression of I(h) during the postnatal developmental period (mutant OFF mice) caused persistent changes in hippocampal network activity of adult mice, whereas post-developmental I(h) suppression (mutant ON/OFF mice) had only mild effects on SPW-R properties during slow-wave sleep.

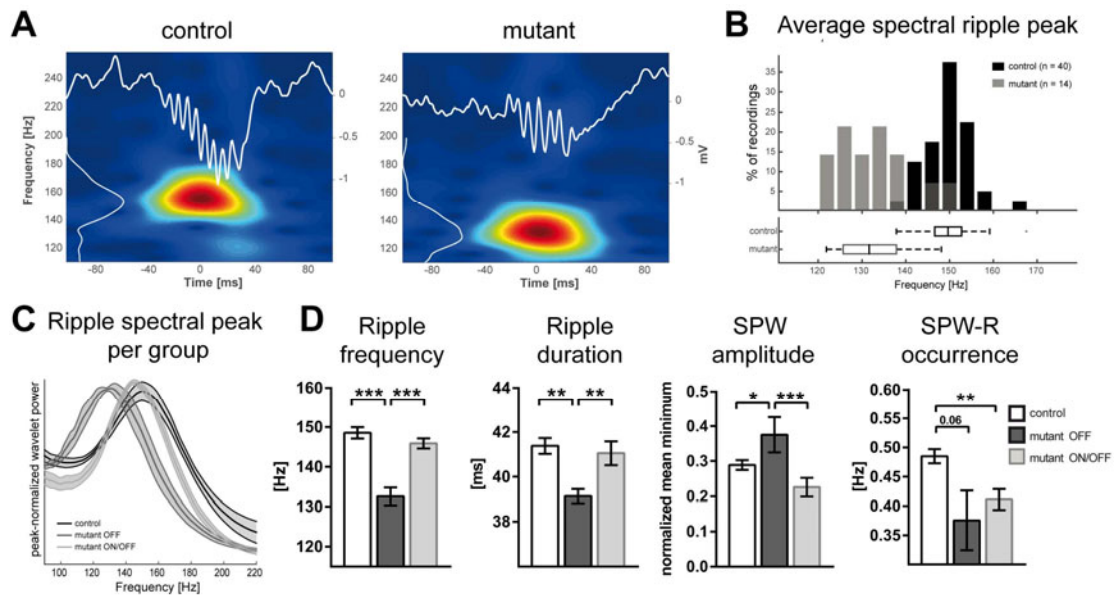


**Figure 3-12: Ripple frequency is reduced upon developmental I(h) attenuation.**

**A:** Representative LFP trace of a ripple recorded from the pyramidal layer of a control (left) and mutant (right) animal. The spectral peak in ripple frequency (left axis) is indicated by a white line on the left (color coded background with warm colors demonstrating the frequency peak). The ripple midpoint is set to 0 ms. Right axis shows the amplitude range (in mV) of the ripple LFP trace. Control ripple peak frequency was at around 150 Hz. Ripple frequency was lower in the mutant animal (right), indicated by the downshift of the spectral peak from 150 Hz to 130 Hz. **B:** Histogram of the average ripple peak frequency expressed as percentage of the total number of ripple events recorded from control ( $n = 40$  recordings/8 mice) and mutant ( $n = 14$  recordings/3 mice). Quantification of the average spectral ripple peak is shown in the boxplot below. **C:** Average normalized ripple peak frequency per group for control, mutant OFF, and mutant ON/OFF mice demonstrating a clear reduction in the ripple frequency seen in OFF mutants, but not in ON/OFF mutants. **D:** Quantification of SPW-R properties; ripple frequency and mean length were significantly reduced in mutant OFF animals. The normalized SPW amplitude was higher in mutant OFF mice. The SPW-R occurrence rate was lower in mutant OFF and ON/OFF mice. Control  $n = 42$  recordings/8 mice, mutant OFF  $n = 14$  recordings/4 mice, mutant ON/OFF  $n = 17$  recordings/4 mice. \*  $P < 0.05$ , \*\*  $P < 0.01$ , \*\*\*  $P < 0.001$  Newman-Keuls post hoc comparison after one-way ANOVA. (Table 6-4) Four of the eight control animals belonged to a different promoter mouse line (C57BL/6J-Tg(Nop-tTA)Mmay) and were recorded by Kolja Meier (ZMNH, Hamburg).

The analysis of REM sleep episodes was focused on peak theta frequencies across layers of CA1 and on interlaminar coherence (Fig. 3-13) (Table 6-4, 6-5). Theta frequencies in stratum oriens, radiatum, and moleculare were similar among groups, but in pyramidal layer of CA1 the peak theta frequency tended to be slightly increased in mutant OFF mice, and to a larger extent in mutant ON/OFF animals as compared to controls (Fig. 3-13 A). Coherence is a measure of the phase relationship of two oscillations of a certain frequency, e.g. between theta or gamma in the pyramidal layer and theta or gamma in stratum lacunosum moleculare, respectively. The coherence in both theta and low-gamma frequencies between stratum lacunosum moleculare and pyramidal layer was significantly increased in mutant OFF and ON/OFF animals (Fig. 3-13 B left). Stratum radiatum and pyramidal layer theta coherence was also significantly increased in both mutant groups; low-gamma coherence in mutant OFF

mice tended to be higher, and was significantly higher in mutant ON/OFF animals (Fig. 3-13 B middle). The phase relationship of oscillations in strata lacunosum moleculare and radiatum was not affected by suppressed I(h) (Fig. 3-13 B right).

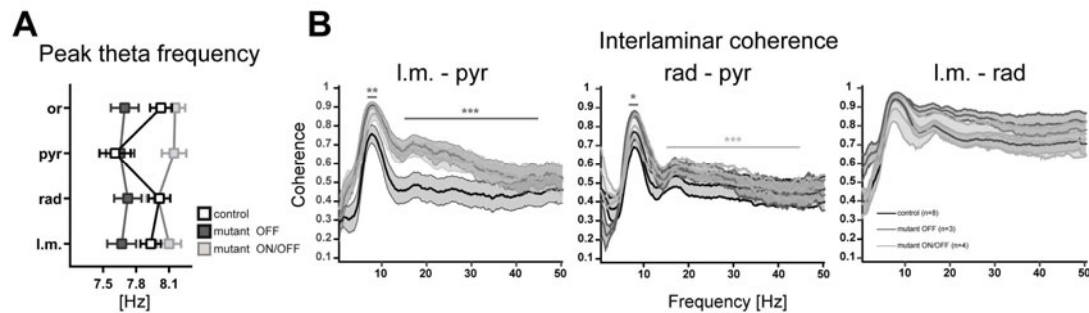


**Figure 3-13: Theta oscillations during REM sleep are affected by I(h) deficiency .**

**A:** Peak theta frequency along layers in CA1; strata oriens (or), pyramidale (pyr), radiatum (rad) and lacunosum moleculare (l.m.), tended to be increased in mutant OFF and ON/OFF animals. **B:** Interlaminar coherence between l.m. and pyr (left) and rad and pyr (middle) was increased for theta and low gamma frequencies in mutant OFF and ON/OFF animals, but not affected between l.m. and rad (right). Control n = 33 recordings/7 mice, mutant OFF n = 11 recordings/4 mice, mutant ON/OFF n = 17 recordings/4 mice. \*\*  $P < 0.01$ , \*\*\*  $P < 0.001$  after one-way ANOVA (Table 6-4, 6-5).

### 3.3. I(h) deficiency causes behavioral abnormalities

To test for behavioral correlates of neuronal hyperexcitability and altered neuronal network activity, behavioral experiments were performed to analyze waking and sleeping behavior, cognitive performance, including working memory, and spatial learning and memory, gait, coordination and motor learning. Control and mutant mice of all doxycycline-treated groups consisted of both genders. Unless otherwise stated, mice in control and mutant groups were compared independent of sex.

#### 3.3.1. General behavioral hyperactivity

It was previously observed that mutant mice OFF doxycycline show hyperactive behavior in their home cages (Sandke, 2006; Merseburg, 2011) (Fig. 3-14 A). As mice are nocturnal animals, they are active during the night while sleeping during the day. Compared to control OFF mice, mutant OFF and ON/OFF mice spent significantly more time moving during the active phase, and the effect was more prominent in mutant OFF than mutant ON/OFF animals OFF (Fig. 3-14 A) (Table 6-6). During the inactive sleeping phase, no differences in

the time spent moving were obtained. This indicated that I(h) attenuation causes general hyperactive movement behavior during waking. In a next step, motor activity and exploratory/anxiety-like behavior in the open field were assessed (Table 6-7, 6-8). Motor activity was indicated by the distance moved, and running speed of the mice. With increasing time in the arena, a decline in the distance moved was observed in all control mice indicating a reduction in locomotion with increasing familiarization with the open field environment (Fig. 3-14 D). Control mice of all groups showed anxiety-like behavior (thigmotaxis), in that they preferentially stayed in the border zone of the arena and avoided the center area (Fig. 3-14 G-H), but crossed it occasionally (Fig. 3-14 B). In contrast, mutant OFF mice covered significantly longer distances (Fig. 3-14 C), and exhibited increased locomotion over time (Fig. 3-14 D). Mutant OFF mice also moved faster (Fig. 3-14 E) and expressed their high motility drive as rapid circling, which was reflected by a significant increase in the number of rotations per minute (Fig. 3-14 F). Compared to control OFF littermates, mutant OFF mice covered the whole arena (Fig. 3-14 B), spent less time in the border zone (Fig. 3-14 G) and more time in the center of the arena (Fig. 3-14 H), which indicates reduced anxious behavior in the open arena. Results obtained for mutant OFF/ON animals were similar. Although not generally hyperactive in terms of total distance moved (Fig. 3-14 C), mutant OFF/ON mice showed tended to rotate more per minute (Fig. 3-14 F), and increased their activity over time similarly to OFF mutants, but not significantly different when compared to control OFF/ON littermates (Fig. 3-14 D). As seen in mutant OFF mice, mutants OFF/ON also spent significantly less time in the border zone, and more in the center area of the open field (Fig. 3-14 G-H), which is indicative of a reduction in anxiety-like traits. In contrast, the behavior of mutant ON/OFF mice in the open field was not distinguishable from control littermates motor activity and exploratory and anxiety-like behavior, except for a significantly lower mean running speed (Fig. 3-14 D).

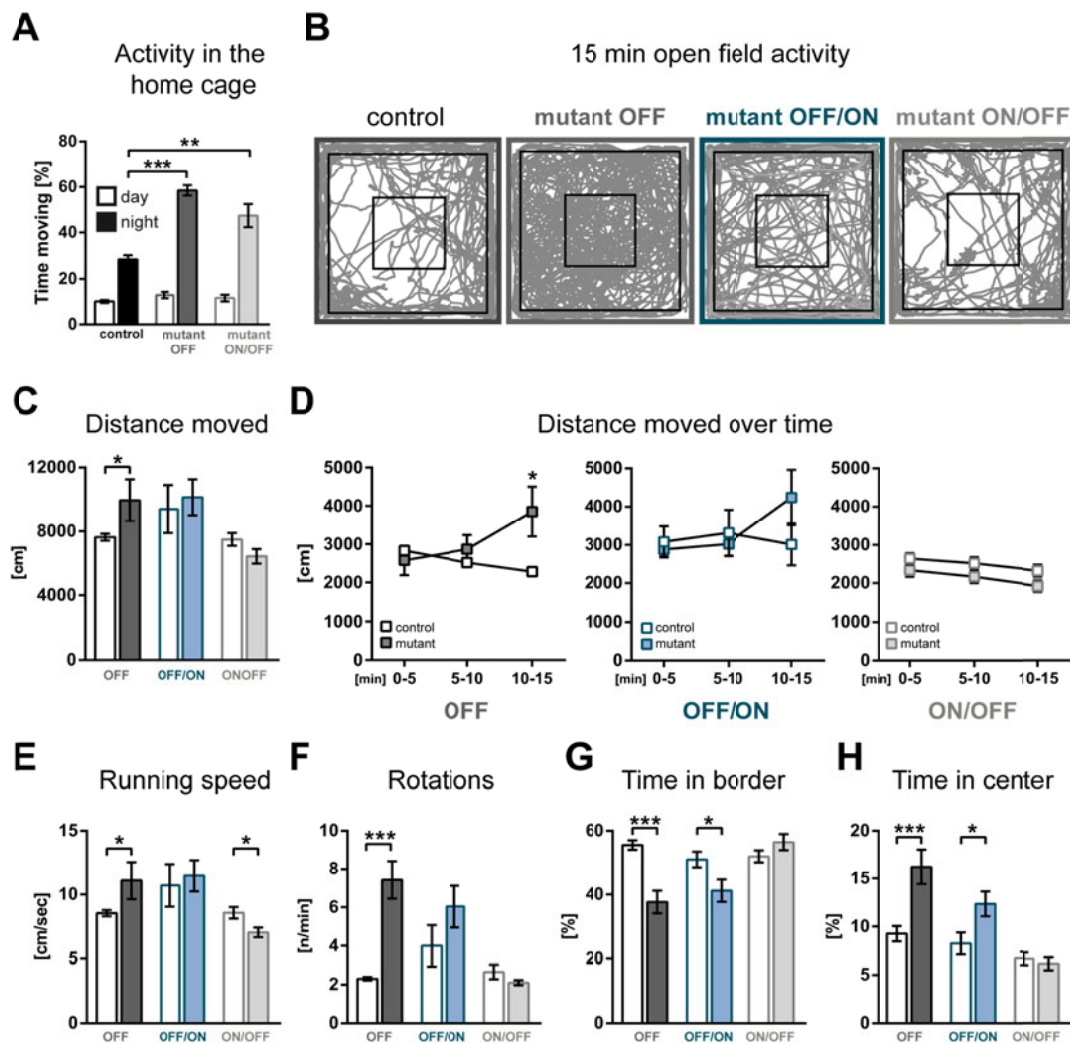


**Figure 3-14: Behavioral hyperactivity upon I(h) deficiency.**

**A:** Time spent moving in the home cage, expressed as percentage of 12 hours of day (open bars) or night (filled bars) and was increased during the active phase (night) in mutant OFF and ON/OFF animals. Control OFF:  $n = 14$ , mutant OFF:  $n = 14$ , mutant ON/OFF:  $n = 13$ . **B:** Sample activity patterns of 15-min open field experiments for a control animal and a mutant OFF, OFF/ON, and ON/OFF mouse. **C:** Total distance moved during a 15-min trial was increased in mutant OFF mice, but not in mutant OFF/ON or ON/OFF mice. **D:** Distance moved over time, shown for 5-min time bins, increased in mutants OFF (left) and OFF/ON (middle). Mutant ON/OFF decreased locomotion (right). **E:** Mean running speed was higher for OFF, and lower for ON/OFF mutants. **F:** Circling activity, expressed as rotations per minute, was increased in mutant OFF mice. Mutant OFF/ON animals showed a similar trend. **G:** Time spent in border zone, expressed as percentage of total time in the open field, was decreased in mutants OFF and OFF/ON. **H:** Mutant OFF and OFF/ON mice spent more time in the center of the arena. Control OFF:  $n = 29$ , mutant OFF:  $n = 18$ , control ON/OFF:  $n = 21$ , mutant ON/OFF:  $n = 27$ , control OFF/ON:  $n = 19$ , mutant OFF/ON:  $n = 17$ . Data represent mean  $\pm$  S.E.M. In **D** \*  $P < 0.05$  Newman-Keuls *post hoc* comparison after two-way mixed ANOVA; otherwise \*  $P < 0.05$ , \*\*  $P < 0.01$ , \*\*\*  $P < 0.001$  with Student's *t* test (Table 6-6 to 6-8).

### 3.3.2. Sleep behavior

Telemetric electrocorticogram (ECoG) recordings and simultaneous video monitoring in adult mice allowed for ECoG-based scoring of behavioral states over multiple days. Four behavioral states were distinguished: wake and active wake behavior, and slow-wave sleep and paradoxical (REM) sleep behavior. Wake periods included behaviors such as eating, grooming, and building a nest. Running and climbing activities were scored as active wake behavior. Sleeping episodes were behaviorally accompanied by very low to no movement activity. The distribution of the four behavioral states over time of the day (mean of three days per animal) showed highest wake and active wake periods during the active dark phase, and highest proportion of slow-wave sleep and REM sleep during the sleeping or light phase of the day (Fig. 3-15 A). Mutant mice seemed to stay up longer, and entered prolonged slow-wave sleep periods later in the day as compared to control animals (Fig. 3-15 A). Comparing the times spent in a certain state (Table 6-9) showed a tendency for mutant mice to have more wake and REM states and less slow-wave sleep. Times in active wake periods were similar between control and mutant animals (Fig. 3-15 B). The mean duration of the behavioral states (i.e. bout duration) showed a trend for mutant mice to have shorter active wake periods, whereas REM sleep bouts tended to be longer (Fig. 3-15 C). The overall number of wake, and active wake states seemed to be higher in mutants (Fig. 3-15 D). Due to the high variance in signal to noise ratio of the ECoG signal obtained for individual animals, as well as poor statistical performance on small groups, a definite conclusion as to whether I(h) suppression affects the distribution or amount of certain behavioral states was not possible.

Ablation of I(h) in the forebrain thus changes general behavioral traits, which was reflected by hyperactive behavior and slight changes in the sleep pattern of mutant mice. Next, it was tested whether loss of functional I(h) in forebrain pyramidal neurons alters cognitive abilities of mutant mice. Cognition was tested in terms of working memory, spatial learning and memory, and contextual fear learning.

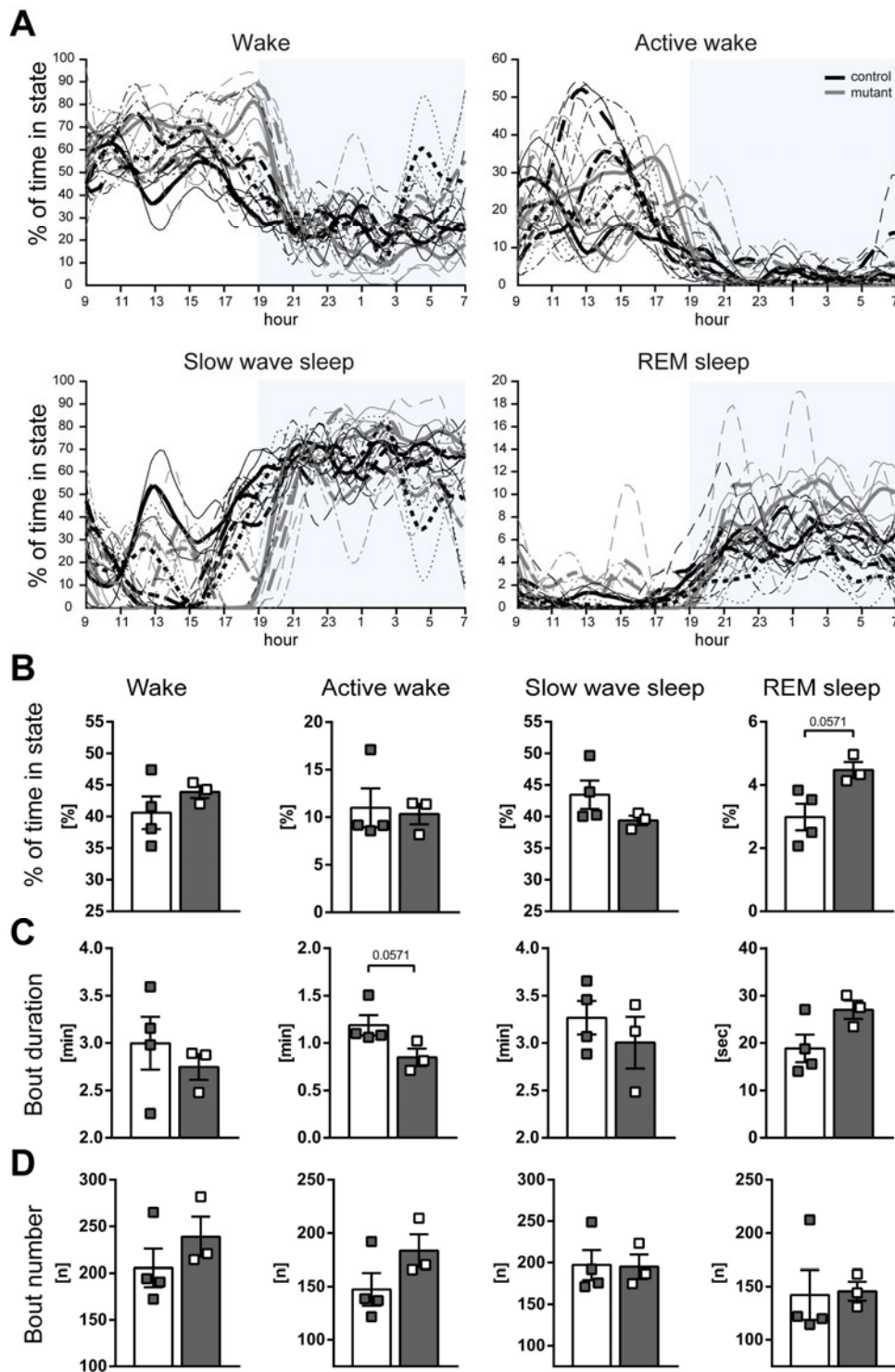


**Figure 3-15: Distribution of waking and sleeping behavior over the day.**

**A:** Distribution of wake (top left), active wake (top right), slow-wave sleep (bottom left), and REM sleep (bottom right) behavioral states; expressed as percentage of time in each state over time of the day (24 hours). The active waking phase started at 7 a.m., the inactive sleeping phase at 7 p.m. (indicated by the blue box). Thick lines indicate the mean of three days per mouse, thin lines represent individual days per mouse. **B:** Quantification of the percentage of time spent in wake, active wake, slow-wave sleep and REM sleep behavior. Mutant OFF mice tended to spend more time in REM sleep. **C:** Mean bout duration of wake, active wake, slow-wave sleep, and REM sleep episodes. Data represent mean  $\pm$  S.E.M. Mann-Whitney  $U$  test to compare groups. Control OFF  $n = 4$ , mutant OFF  $n = 3$  (Table 6-9).

### 3.4. Cognitive deficits are dependent on age of onset of I(h) deficiency

#### 3.4.1. Working memory

Working memory, which is needed to plan and execute behavior, is a cognitive function relying on attention, short-term memory and processing of information (Morellini, 2013). It was tested by scoring the spontaneous alternation in the Y maze task. The Y maze consisted of three identical arms (A, B, and C; as depicted in Fig. 3-16 A) that the mice could freely explore. For example, when visiting arms A and B, the mouse is expected to next enter a novel and unexplored arm C, i.e. to make a novel arm choice. A preference for the novel arm was indicated by values higher than chance (50%). The percentage of novel arm choices was above chance for control and mutant mice of all groups (Fig. 3-16 B). Mutant mice, however, tended to make fewer novel arm choices, which was significant in the OFF/ON group. In addition, mutant mice of the OFF and ON/OFF group needed significantly more time for the total number of required alternations than their control littermates (Fig. 3-16 C) (Table 6-10).

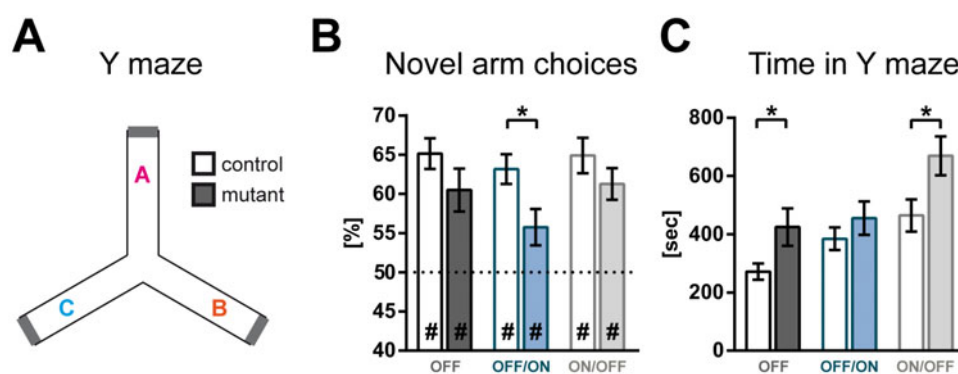


**Figure 3-16: Working memory performance in the spontaneous alternation task.**

**A:** The Y maze consisted of three identical arms (A-C), which the mice could freely explore during the trial. **B:** Novel arm choices are expressed as percentage of total transitions in the maze. Control and mutant mice of all treatment groups showed a preference for the novel arm, but mutant mice made fewer novel arm choices, which was significant in the OFF/ON group. **C:** The time mice needed for the required amount of alternations was significantly increased in mutants of the OFF and ON/OFF group. Control OFF n = 31, mutant OFF n = 21, control OFF/ON n = 19, mutant OFF/ON n = 16, control ON/OFF n = 23, mutant ON/OFF n = 32. Data represent mean  $\pm$  S.E.M. #  $P < 0.05$  as compared to chance level of 50% with Wilcoxon signed-rank test. \*  $P < 0.05$  with Student's  $t$  test (Table 6-10).

### 3.4.2. Spatial learning and memory in the water maze

The water maze task was used to test for spatial learning and long-term memory. In learning trials, mice had to find a hidden platform by using distal landmarks. A reduction in both the distance moved to find the platform, and the escape latency over trials was an indicator of spatial learning (Fig. 3-17 A-C) (Table 6-11, 6-12). Over two learning days, control OFF mice showed a reduction in distance moved and latency to reach the platform over trials, which thus reflected spatial learning of the hidden platform position. In comparison, mutant OFF mice covered greater distances and had longer escape latencies over all trials, without showing a clear reduction in both parameters, which is indicative of difficulties in learning the position of the platform (Fig. 3-17 B, and C left). In the OFF/ON treatment group, learning of the platform position was less obvious in control mice, especially during the first learning day (trials 1-4). Over the course of the second learning day (trials 5-8), control OFF/ON mice showed a reduction in their distance moved and concomitantly in escape latencies. However, the mixed two-way ANOVA did not reveal an effect of the interaction group x trial on distance moved or escape latency. Mutant OFF/ON animals were not significantly different from control littermates, but tended to move longer distances moved and have longer latencies to find the platform, which was similar to mutant OFF mice (Fig. 3-17 B, C middle). A reduction in both parameters was not seen over trials for mutant OFF/ON mice, again indicating a similar learning deficit as seen in mutant OFF mice. In comparison, control and mutant mice of the ON/OFF group performed equally well and improved their performance over trials, though mutants ON/OFF tended to perform worse during the second learning day (trial 5) as compared to control ON/OFF littermates (Fig. 3-17 B, C right). Long-term spatial memory of the platform position was further tested in the recall trial after two learning days. The platform was removed and time periods spent by the mice in the quadrant of the former platform location (i.e. target quadrant) were compared. A preference for the target quadrant over the other quadrants (left, right, opposite) is indicated by occupation times higher than expected by chance of 25% (Fig. 3-17 D). Control mice of all groups had a clear preference for the target quadrant. Mutant mice of the OFF and OFF/ON group, but not the ON/OFF group, tended to spend less time in the target quadrant as compared to respective control littermates. Mutants OFF/ON also did not exceed chance level (Fig. 3-17 E). Together, the results are suggestive of deficits in learning and remembering the spatial location of the hidden platform in mutant OFF and OFF/ON mice.

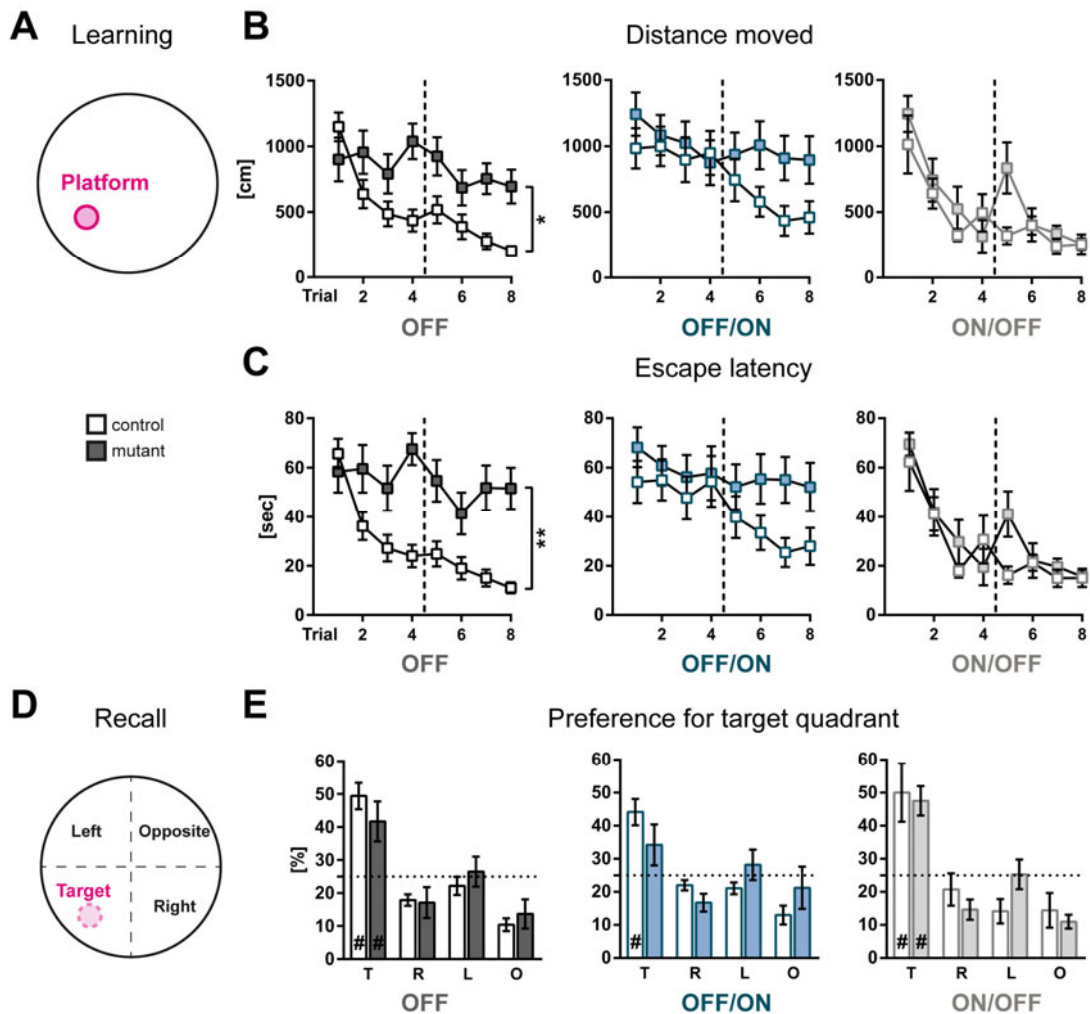


**Figure 3-17: Spatial learning in the water maze is dependent on age of onset of I(h) deficiency.**

**A:** Water maze with the hidden platform for learning trials. **B:** Distance moved to find the platform over 8 trials/two learning days (separated by dotted line) was higher for mutants OFF over trials (left). Control and mutant mice of the OFF/ON group showed similar performance, but note that mutant OFF/ON mice exhibited no decrease over time (middle). Mutant ON/OFF mice were not different from controls (right). **C:** Corresponding escape latencies over trials. **D:** Long-term memory of the platform position was tested in the recall trial without the platform (target, former platform position is indicated by the dotted circle). A preference for the target quadrant (T) over the quadrants left (L), right (R), and opposite (O) is reflected by occupation times higher than expected by chance (25%). **E:** A preference for the target quadrant was observed in control mice of all groups and in mutants of the OFF (left) and ON/OFF (right) groups, but not in mutant OFF/ON mice (middle). Note that mutants OFF and OFF/ON tended to spend less time in the target quadrant. Control OFF  $n = 22$ , mutant OFF  $n = 13$ , control ON/OFF  $n = 8$ , mutant ON/OFF  $n = 11$ , control OFF/ON  $n = 15$ , mutant OFF/ON  $n = 14$ . Data represent mean  $\pm$  S.E.M. \*  $P < 0.05$ , \*\*  $P < 0.01$  after two-way mixed ANOVA for repeated measurements (Group  $\times$  Trial interaction). #  $P < 0.05$  as compared to chance level of 25% with Wilcoxon signed-rank test (Table 6-11, 6-12).

### 3.4.3. Contextual fear conditioning

The contextual fear conditioning protocol tests for learning the association of a foot shock (unconditioned stimulus) applied in a certain environment, i.e. context (conditioned stimulus). It can be assessed by means of increased immobility or freezing behavior of the mouse 24 hours later in the recall trial, when the mouse is exposed to the same environment, in which the shocks were received. For conditioning, mice were placed in the chamber in which they received three foot shocks after a certain delay for recording baseline freezing levels. Mice of all groups and treatment expressed similarly low baseline freezing, which increased after having received the foot shocks (Fig. 3-18 A) (Table 6-13). When being placed into the same arena 24 hours later, mice again showed immobility that increased from the first to the second minute, but then declined in the third minute (Fig. 3-18 B). Only control mice of the OFF/ON group did have similar freezing periods over the whole time in the arena (Fig. 3-18 B middle). However, the overall freezing behavior was not significantly different between control and mutant mice, irrespective of the treatment (Fig. 3-18 C). OFF mutants OFF exhibited more freezing. OFF/ON mutants appeared to freeze less, but the strong variation between individual values does not allow a definite conclusion to be drawn. Contextual fear memory thus appears not to be affected by I(h) deficiency.

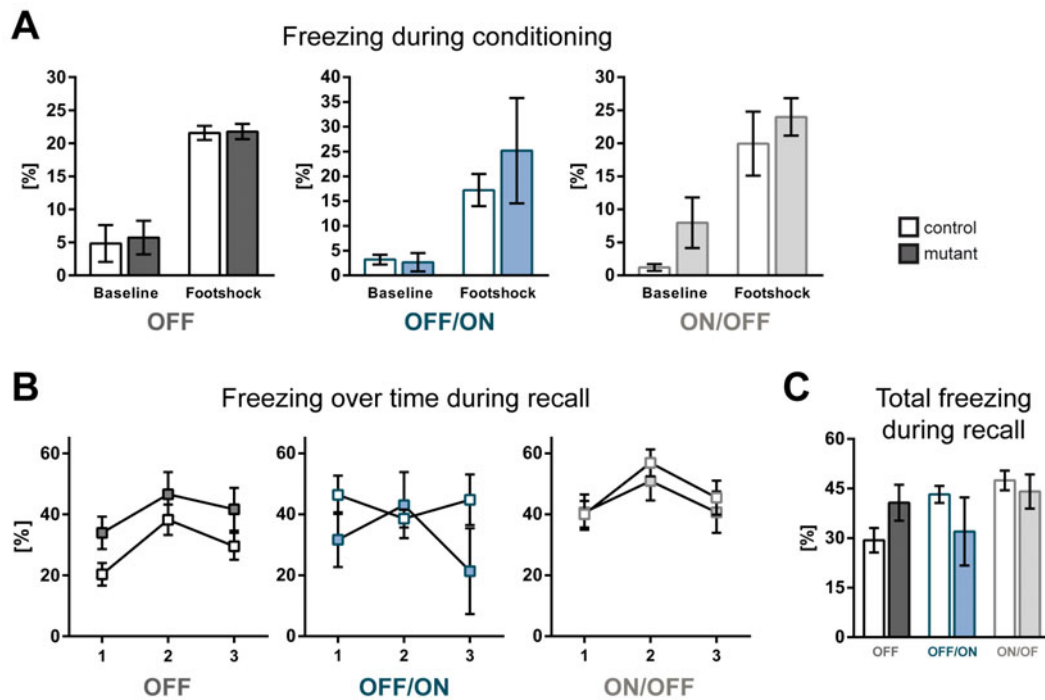


**Figure 3-18: Context-dependent fear memory does not rely on I(h).**

**A:** Freezing behavior, which is expressed as percentage of time spent freezing vs. total time in arena, strongly increased from baseline levels after footshocks were given, and was similar in control and mutant animals of the OFF (left), OFF/ON (middle), and ON/OFF (right) groups. **B:** Recall trial after 24 hours demonstrating that freezing increased within the first two minutes and then declined in the third minute. **C:** Total time freezing during the recall trial tended to be higher in mutants OFF and lower in mutants OFF/ON. Baseline and footshock: Control OFF  $n = 24$ , mutant OFF  $n = 16$ ; Recall: control OFF  $n = 27$ , mutant OFF  $n = 19$ . Control OFF/ON  $n = 6$ , mutant OFF/ON  $n = 5$ . Baseline and footshock: Control ON/OFF  $n = 11$ , mutant ON/OFF  $n = 18$ . Recall: control ON/OFF  $n = 15$ , mutant ON/OFF  $n = 24$ . Data represent mean  $\pm$  S.E.M. (Table 6-13).

### **3.5. I(h) exerts functional roles in motor coordination and motor learning**

#### 3.5.1. Gait abnormalities develop at early postnatal ages

Based on the observation that mutant OFF mice seemed to have abnormal walking patterns, characterization of the gait was performed using the automated gait analysis system Catwalk (Noldus) (Fig. 3-19 A). Control and mutant mice (control OFF n = 6, mutant OFF n = 6, control ON/OFF n = 10, mutant ON/OFF n = 13, control OFF/ON n = 19, mutant OFF/ON n = 14, Table 6-18) were compared for the parameters running speed, stand (duration of paw contact with the glass plate), step cycle (time between two consecutive paw placements on the glass plate), stride length (distance between two consecutive placements of the same paw), base of support (BOS, width between hind or front paws) between the hind paws, regularity index of the step pattern (which expresses the number of normal step sequence patterns relative to the total number of paw placements in percent), and step sequence patterns (alternating and rotating). Irrespective of treatment, control and mutant mice exhibited similar running speeds (Fig. 3-19 B). When compared to their respective controls, mutants OFF and OFF/ON made faster and shorter steps, indicated by a decrease in stand (Fig. 3-19 C) and step cycle duration (Fig. 3-19 D), and a shorter stride length (Fig. 3-19 E). However, the functional relevance of the difference in stand and step cycle in OFF/ON mutants is not clear, as values are still similar to controls in the OFF and ON/OFF group. It rather seems as if control mice in the OFF/ON group had an unusually high stand and step cycle duration when compared to controls OFF and ON/OFF. There was no difference between control and mutant ON/OFF mice (Fig. 3-19 C-E). The BOS between hind paws was increased in mutants OFF and OFF/ON, but not affected in mutants ON/OFF (Fig. 3-19 F). Changes in the temporal relationship between the four paws were further reflected by the regularity index of the step pattern (Fig. 3-19 G), which was reduced in OFF and OFF/ON mutants, but not in mutants of the ON/OFF group. The observed decreased regularity was a consequence of less alternating (Fig. 3-19 H) and more rotating step sequences (Fig. 3-19 I) in OFF and OFF/ON mutants.

In summary, compared to control mice, the gait of mutant OFF and OFF/ON mice was characterized by irregular steps, which were shorter and faster. Mutants ON/OFF did not show altered walking behavior. The gait analysis thus revealed that I(h) deficiency during early postnatal development, but not in adulthood, significantly affects locomotion.

Considering that the HCN-DN transgene is expressed in forebrain motor structures (Fig. 3-3) and in afferents to the cerebellum (Fig. 3-5 D), it was hypothesized that I(h) deficiency also affects motor learning behavior.

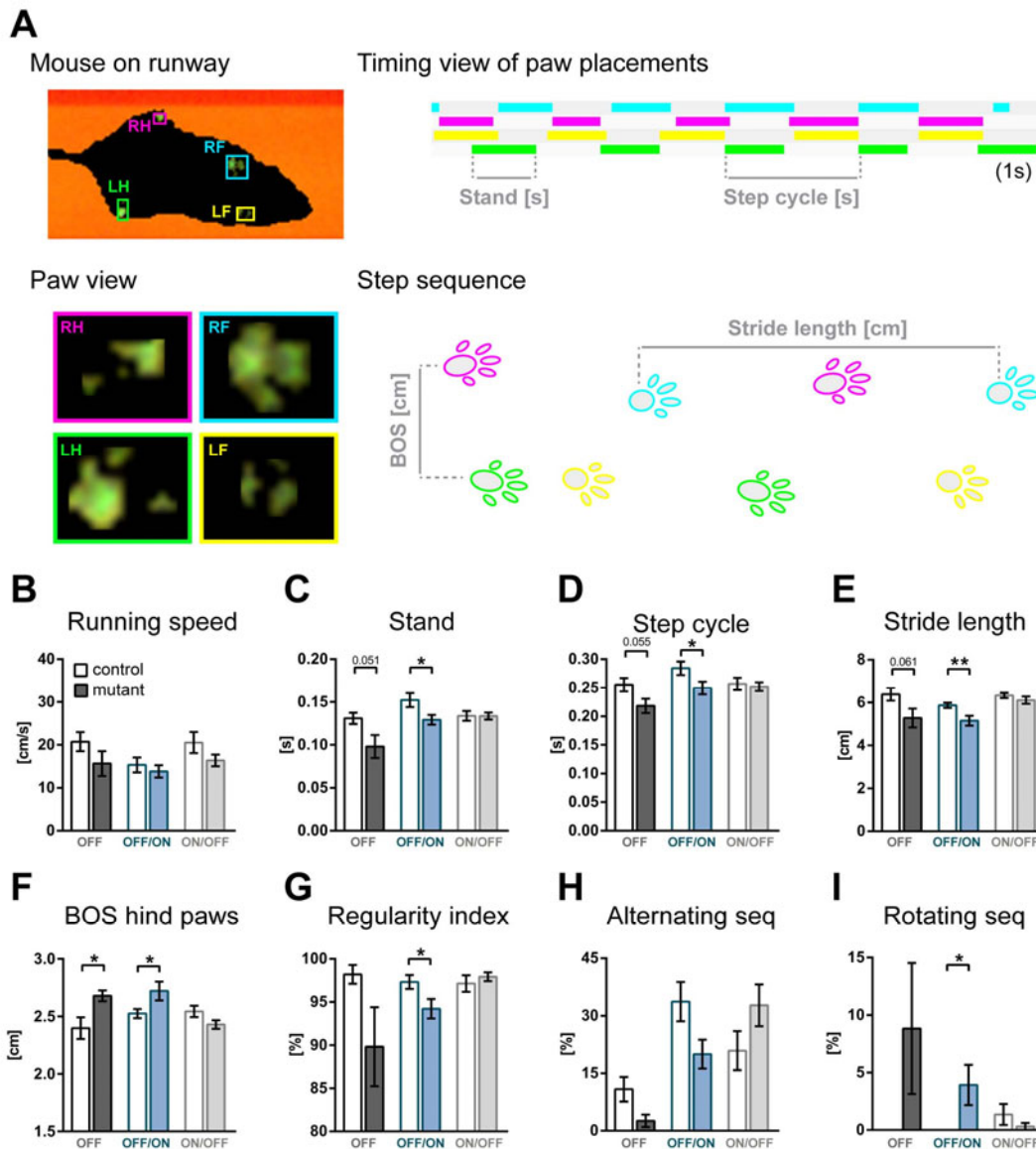


**Figure 3-19: Gait abnormalities upon I(h) deficiency during early development.**

**A:** (Top left) Illustration of a mouse on the runway, (bottom left) expanded view of the paw prints seen above (RH right hind, RF right front, LH left hind, LF left front), (top right) timing view of consecutive paw placements within 1s of a run, demonstrating stand (duration of paw contact with the glass plate) and step cycle (time between two consecutive paw placements on the glass plate), (bottom right) step sequence demonstrating stride length (distance between two consecutive placements of the same paw) and base of support (BOS, width between hind or front paws). **B:** Mean running speed was similar between control and mutant mice of all groups. **C:** Stand and **D:** Step cycle duration, and **E:** Stride length was decreased in mutants OFF and OFF/ON when compared to respective controls. **F:** Base of support (BOS) between hind paws was increased in mutants OFF and OFF/ON. **G:** Regularity in the step patterns of mutants OFF and OFF/ON was decreased due to **H:** Less alternating and **I:** More rotating step sequence patterns. Control, mutant OFF:  $n = 6$ , control ON/OFF:  $n = 10$ , mutant ON/OFF:  $n = 13$ , control OFF/ON:  $n = 19$ , mutant OFF/ON:  $n = 14$ . Data represent mean  $\pm$  S.E.M. **B-G**, \*  $P < 0.05$ , \*\*  $P < 0.01$  with Student's  $t$  test. **H-I**, \*  $P < 0.05$  with Mann-Whitney  $U$  test (Table 6-18).

### 3.5.2. I(h) deficiency during development affects motor learning

The pole, Rotarod, and grip strength tests were used to assess motor coordination, motor learning performance, and forelimb strength (Fig. 3-20) (Table 6-14 to 6-17). The OFF and OFF/ON treatment groups included female and male mice in both genotype groups. There was no gender effect in control OFF mice, the data of which were thus pooled. In mutant OFF mice, female and male littermates were different from each other and were thus presented separately and compared to gender-pooled control OFF littermates. OFF/ON control and mutant mice showed no gender effects and were also pooled. The ON/OFF treatment group only consisted of male littermates.

In the pole test, motor coordination/skill learning over three trials to perform a certain strategy to climb down was tested: (as described (Freitag et al., 2003)): control mice turned the body by 180° and climbed down headfirst with all four paws and with the tail “wrapped” around the pole. While the majority of control OFF mice turned and climbed down the pole, a significantly lower proportion of mutant male OFF mice were able to do so (Fig. 3-20 A left panel) (Table 6-14). Mutant males OFF, irrespective of trial, mostly failed to fully turn their body and were circling down with the body perpendicular to the pole, or falling down. Mutant females OFF performed better than mutant males OFF. However, mutant females OFF did not fully reach the performance of control males OFF, and were significantly different in the second trial (Fig. 3-20 A left). Mutant OFF/ON mice also had difficulties in climbing down the pole over all trials (Fig. 3-20 A middle), and their performance was significantly different from controls in the third trial. In contrast, mutants of the ON/OFF treatment group performed in the same way as their control littermates and had no difficulties in turning and climbing down the pole (Fig. 3-20 A right). Motor learning and coordination was further tested with the Rotarod (Fig. 3-20 B). Results were analyzed with a two-way mixed ANOVA for repeated measurements, having Group as between groups factor and Trial (trials 1-4) as within groups factor (Table 6-15). For mice of the OFF treatment group, an effect of group (control OFF, mutant male OFF, mutant female OFF) on the mean latency to fall over all trials was seen, and Newman-Keuls *post hoc* analysis revealed that mutant males OFF fell faster from the Rotarod as compared to controls OFF, whereas mutant females OFF showed a better performance and were not different from controls (Fig. 3-20 B left panel). In addition, control and mutant females OFF increased their latency to fall over trials, which indicates motor learning over trials. In contrast, mutant males OFF had a similar performance over all trials, suggesting absence of motor learning in male mutants of the OFF group. Mutant OFF/ON animals also had an overall worse performance on the Rotarod as

compared to control OFF/ON littermates (Fig. 3-20 B middle). There was a significant effect of the interaction group and trial, but Newman-Keuls post hoc analysis did not detect any significant difference for single trials between groups. Control and mutant mice of the ON/OFF group did not differ in their performance, and improved their performance over trials (Fig. 3-20 B right). Note that during the course of the study, the performance of control mice on the Rotarod significantly declined (Fig. 3-20 C). Therefore, it was difficult to interpret Rotarod results obtained for OFF/ON and ON/OFF mutant animals (Table 6-16). The grip strength test revealed significantly reduced forelimb strength in mutants of all three treatment groups as compared to control littermates (Table 6-17). However, mutants OFF and OFF/ON seemed to have a more pronounced reduction in forelimb strength than mutants ON/OFF (Fig. 3-20 D).

Taken together, the results indicate that suppression of I(h) in the forebrain during early postnatal development significantly affects gait properties along with motor learning and coordination abilities. The importance of functional HCN channels during development is supported by the observation that normal I(h) function during postnatal development and post-weaning onset of I(h) ablation in mutant ON/OFF mice normalizes motor functions back to control levels, except for the forelimb grip strength.

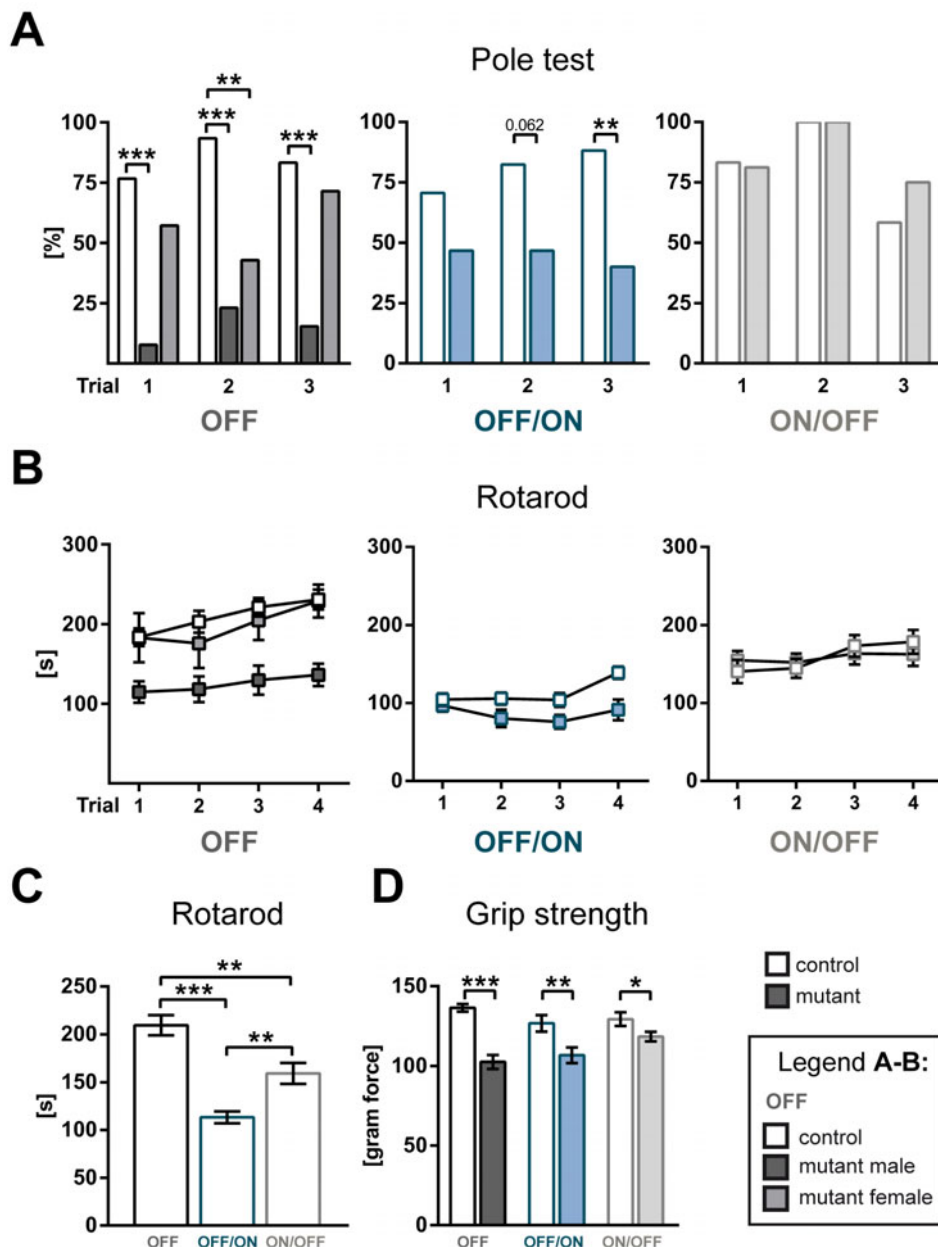


**Figure 3-20: Motor function deficits were partially linked to early developmental I(h) ablation.**

**A:** Pole test showing the percentage of mice successfully climbing down the wooden rod over three consecutive trials. Mutant males OFF (left) and mutant OFF/ON animals (middle) had significant difficulties, whereas mutant ON/OFF mice (right) did not differ from their control littermates. \*\*  $P < 0.01$ , \*\*\*  $P < 0.001$  with Fisher's exact probability test. **B:** Performance on the Rotarod shown as latency to fall over four trials. Male mutant OFF mice showed the strongest difficulties in staying on the rod. **C:** Rotarod performance, shown as the mean of four trials, of control mice declined significantly. \*\*  $P < 0.01$ , \*\*\*  $P < 0.001$  Newman-Keuls *post hoc* comparison after two-way mixed ANOVA. **D:** Forelimb strength measured with the grip test was decreased in mutants, independent of doxycycline treatment. \*  $P < 0.05$ , \*\*  $P < 0.01$ , \*\*\*  $P < 0.001$  with Student's *t* test. Control OFF:  $n = 30$ , mutant male OFF:  $n = 13$ , mutant female OFF:  $n = 7$ , control OFF/ON:  $n = 19$ , mutant OFF/ON:  $n = 14$ . Pole ON/OFF, control:  $n = 12$ , mutant:  $n = 16$ ; Rotarod ON/OFF, control:  $n = 17$ , mutant:  $n = 23$ , grip ON/OFF, control:  $n = 8$ , mutant:  $n = 11$  (Table 6-14 to 6-17).

### 3.5.3. I(h) ablation in cerebellar Purkinje cells does not affect motor behavior

Functional I(h) in cerebellar Purkinje cells has been proposed to be important for motor learning (Nolan et al., 2003; Rinaldi et al., 2013). Considering that the results described above were obtained from mice with forebrain-restricted I(h) deficiency that showed HCN-DN-expressing projections to the cerebellum (Fig. 3-5 D), it cannot be determined whether the effects seen are specific to changes in forebrain motor circuits, or due to altered signaling from forebrain projections to the cerebellum that potentially affect cerebellar processing of motor commands. Therefore, mice with Purkinje cell-restricted I(h) deficiency were generated and analyzed for gait properties and motor learning performance.

Double-transgenic mutant mice expressed the tTA under control of the Purkinje cell protein-2 (PCP2) promoter (Zu, 2004) and the HCN-DN under control of the bidirectional promoter containing TRE (Krestel et al., 2001) to simultaneously express EGFP (Fig. 3-21 A). HCN-DN expression in mutant cerebellar Purkinje cells was confirmed by *in situ* hybridization against an hHCN4-G480S specific probe (Fig. 3-21 B) and western blot detection of HCN-DN by immunolabeling of the attached HA-tag (Fig. 3-21 C). Specificity of transgene expression was further quantified by co-immunostaining with an antibody against PCP2 (EGFP-expressing cells immunostained for PCP2: mutant OFF  $89.23 \pm 1.72\%$  EGFP<sup>+</sup>/PCP2<sup>+</sup> cells, mutant ON/OFF  $86.15 \pm 8.29\%$  EGFP<sup>+</sup>/PCP2<sup>+</sup> cells) (Fig. 3-21 D). *In vitro* patch clamp recordings in brain slices (15-16 days old animals, con: n<sub>Animals</sub> = 3, n<sub>Cells</sub> = 9; mut: n<sub>Animals</sub> = 4, n<sub>Cells</sub> = 9) revealed strong attenuation of I(h) in mutant PCs (Fig. 3-21 E, I(h) at -120 mV: controls  $-879 \pm 64$  pA vs. mutants  $-63 \pm 12$  pA, Students *t* test,  $P < 0.001$ ). Together, the data show successful functional I(h) ablation due to HCN-DN expression in mutant cerebellar PCs. Next the consequences of I(h) ablation in cerebellar Purkinje cells for gait properties, motor learning and motor coordination in control and OFF mutants, and in ON/OFF mutants were analyzed. Mice were tested with the Catwalk gait analysis system, and with pole, accelerating Rotarod, and beam walk tests (control OFF n = 8, mutant OFF n = 9, mutant ON/OFF n = 11, Table 6-19 to 6-21). Gait properties were not different between all three groups (Fig. 3-22 A-G), except for mutants ON/OFF whose gait is characterized by shorter steps as compared to control or mutant OFF littermates (Fig. 3-22 D). Mice of all groups had the same motor learning and coordination performance (Fig. 3-22 H-J), with the exception that mutants ON/OFF had a better initial Rotarod performance on day 1 when compared to control or mutant OFF mice (Fig. 3-22 I).

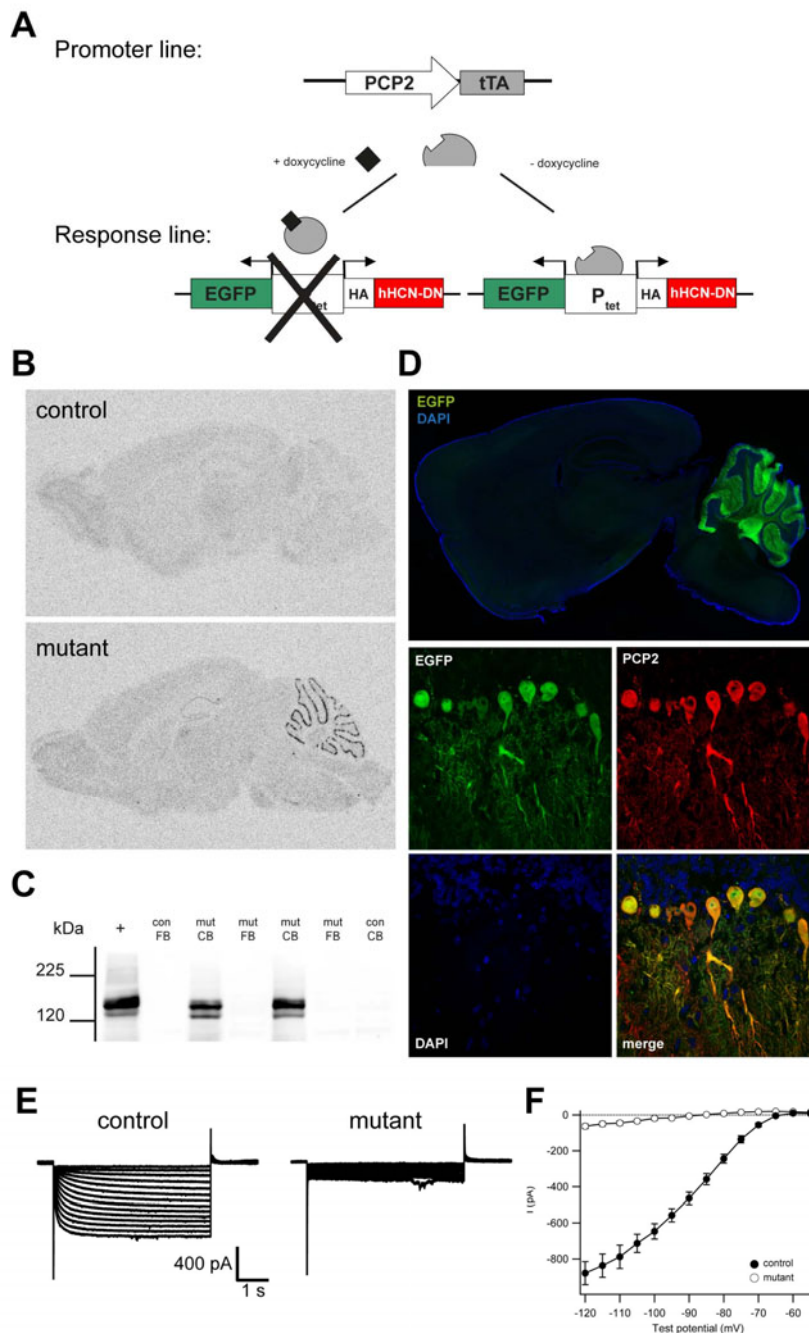


**Figure 3-21: Mice with cerebellar Purkinje cell-specific I(h) ablation.**

**A:** Cerebellar Purkinje cell-restricted HCN-DN expression. The promoter line drives tTA expression in Purkinje cells via the Purkinje cell protein-2 (PCP2) promoter, the response line carries the HCN-DN subunit, tagged with a HA-tag and driven by a bidirectional promoter for simultaneous expression of EGFP. **B:** Detection of HCN-DN mRNA in double-transgenic mutant mice. **C:** Western blot detection of HCN-DN with anti-HA antibody (132 kDa) in control (con) and mutant (mut) forebrain (FB) and cerebellum (CB) membrane fractions (+ refers to positive control). **D:** (Top) Sagittal brain section of a mutant showing EGFP expression in the cerebellum. (Bottom) Co-labeling of EGFP with PCP2 immunostaining demonstrating that EGFP expression was detected in cerebellar Purkinje cell bodies and their dendrites in the molecular layer. **E:** Current traces of control (left) and mutant (right) Purkinje cells in response to hyperpolarizing voltage steps demonstrating the absence of I(h) in mutant cells expressing HCN-DN. **F:** Quantification of I(h) in response to different hyperpolarizing to depolarizing voltage steps. Data are represented as mean  $\pm$  S.E.M. (Whole-cell patch-clamp recordings shown in E-F were performed by PD. Dr. Axel Neu, ZMNH, Hamburg.)

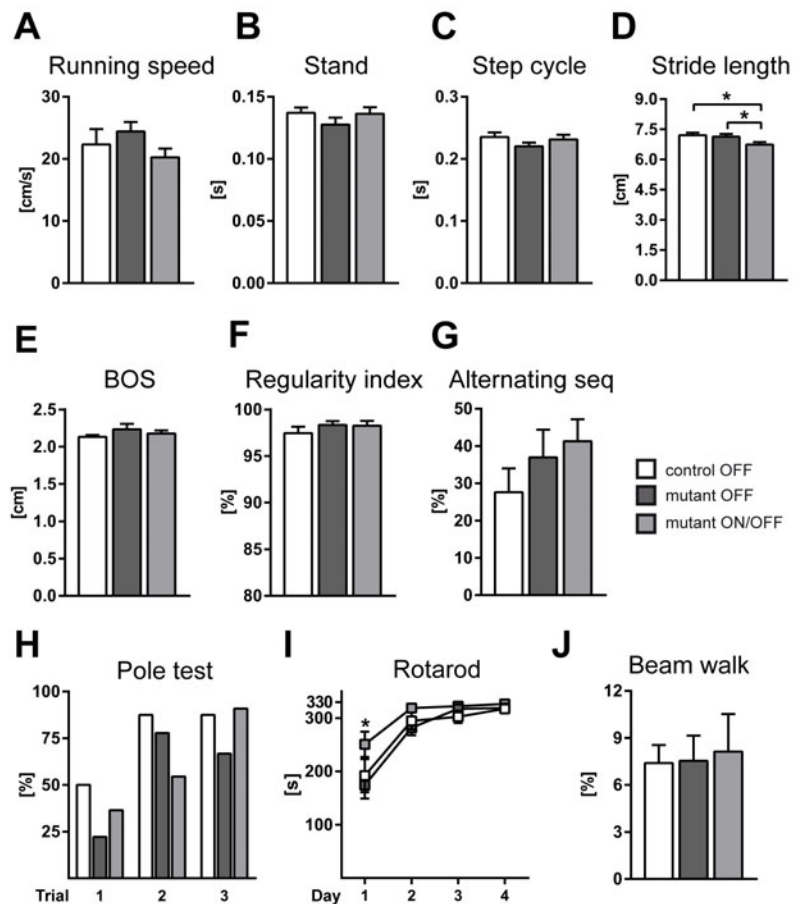


**Figure 3-22: Cerebellar Purkinje cell-specific I(h) ablation does not affect gait properties or motor learning.**

**A-G:** Gait analysis demonstrating **A:** Average running speed, **B:** stand (duration of contact of a paw with the glass plate), **C:** step cycle (time between two consecutive paw placements on the glass plate), **D:** stride length, **E:** base of support (BOS) of the hind limbs, **F:** regularity index, and **G:** percentage of alternating step sequence patterns. **H:** Percentage of mice climbing down the pole over three consecutive trials in the pole test. **I:** Latency to fall on the accelerating Rotarod, shown as the mean of four trials per day over four consecutive days. Mutant ON/OFF animals showed a significantly better performance on day 1 as compared to control and mutant OFF mice. **J:** Beam walk test, showing the percentage of hindlimb slips as proportion of all steps. Data represent mean  $\pm$  S.E.M. Control OFF  $n = 8$ , mutant OFF  $n = 9$ , mutant ON/OFF  $n = 11$ . \*  $P < 0.05$  with **D:** Newman-Keuls post hoc comparison after one-way ANOVA and **I:** two-way mixed ANOVA for repeated measurements (Table 6-19 to 6-21).

Together these findings indicate that I(h) deficiency in cerebellar Purkinje cells, either permanent or starting at later stages, does not affect motor functions.

## 4. Discussion

The main findings of the present study were: 1) I(h) was functionally ablated by HCN-DN expression, which caused neuronal hyperexcitability; 2) Loss of I(h) attenuated neonatal hippocampal and cortical network activity; 3) Functional I(h) deficiency in forebrain projection neurons resulted in strong behavioral hyperactivity and motor function deficits, but only in mild cognitive impairments; 4) Loss of I(h) in cerebellar Purkinje cells did not affect motor functions, independent of age of onset; and 5) Functional I(h) during the early postnatal period is crucial for preventing long-term effects on neuronal network activity and behavior.

### 4.1. Advantages and limitations of functional I(h) ablation by HCN-DN expression

In this study, I(h) was reliably ablated in a subunit-unspecific manner by expressing a dominant-negative human HCN4 (HCN-DN) subunit. The use of specific Tet-Off system promoter mouse lines allowed the for restriction of HCN-DN expression to either forebrain projection neurons (CaMKII $\alpha$  promoter line (Mayford et al., 1996)) or cerebellar Purkinje cells (PCP2 promoter line (Zu, 2004)). As frequently observed in transgenic mouse lines, which were generated by random transgene integration into the mouse genome, which often only contain fragments of the original promoter, the resulting expression pattern was found to overlap with the endogenous protein to varying degrees.

#### 4.1.1. HCN-DN subunit expression functionally ablates endogenous HCN1-4 channel-mediated currents

Commonly used mouse models for studying I(h) are usually targeted to a specific HCN channel subunit, by either a general deletion in all cells or restricting the deletion to a specific brain region using promoter lines that express cre recombinase (Ludwig et al., 2003; Nolan et al., 2003; Stieber et al., 2003; Rinaldi et al., 2013). Given that HCN channels are formed by four different subunits with developmentally regulated variable gene expression, specific activation kinetics and sensitivity to regulation by cyclic nucleotides,

the resulting currents are very diverse. Moreover, in neurons with expression of at least two HCN channel isoforms, such as hippocampal CA1 pyramidal neurons, deletion of only one subunit is not sufficient to study I(h) function in these cells, because residual h-current mediated by the other subunit will remain and might even be increased by homeostatic mechanisms. Another approach to attenuate I(h) is to affect the subcellular localization of HCN channels by deleting the auxiliary subunit TRIP8b (TRIP8b<sup>-/-</sup>), which reduced HCN1 and HCN2 channel surface expression in CA1 pyramidal neurons (Lewis et al., 2011). However, TRIP8b<sup>-/-</sup> mice were still shown to have residual I(h) in distal dendrites of CA1 pyramidal cells that was sensitive to ZD7288. Therefore, a dominant-negative approach is more suitable. The functionality of dominant-negative HCN subunit constructs in suppressing currents mediated by HCN1 and HCN2 channels was previously shown in oocytes; here, the GYG pore motif in *Hcn1* was replaced with alanines (GYG<sub>349-351</sub>AAA), which exerted dominant-negative effects on channel activity *in vitro* (Xue et al., 2002). We previously reported dominant-negative effects of a conditionally expressed *HCN4* mutant construct with deleted cAMP-binding site on I(f), as I(h) is called in the heart (Alig et al., 2009). The data presented in this study show that I(h) was functionally ablated by expression of the HCN-DN construct, in which the pore motif GYG in *HCN4* was changed to GYS. This pore mutation was originally identified in the human KCNQ1 potassium channel subunit and is known to exert dominant-negative effects on Kv7/M-currents (Schroeder et al., 1998). Additionally, a pore mutant construct of the KCNQ2 channel subunit carrying the GYS motif was shown by our laboratory to suppress Kv7/M-currents in CA1 neurons of transgenic mice (Peters et al., 2005). Here, it was demonstrated that this GYS pore mutation ablates HCN channel-mediated currents. The dominant-negative approach thus allowed us to study the role of I(h) in a subunit-unspecific manner. This is supported by the finding that even in neurons with predominant HCN1 and HCN2 subunit expression, such as CA1 pyramidal neurons and cerebellar Purkinje cells, I(h) was strongly attenuated by HCN-DN expression. It also provides further evidence for the potential of HCN1, HCN2, and HCN4 subunits to form heteromeric channels *in vivo*. We previously observed that HCN-DN expression was accompanied by upregulation of endogenous HCN2 protein levels in cortex and striatum of mutant mice (Sandke, 2006). However, the dominant-negative approach should “compensate” for endogenously upregulated HCN channel subunits. Strongly reduced currents obtained by whole-cell patch clamp recordings in hippocampal CA1 and entorhinal cortex layer 3 pyramidal neurons, and cerebellar Purkinje cells demonstrate more effective I(h) attenuation than through genetic deletion of

individual subunits (Ludwig et al., 2003; Nolan et al., 2003, 2005; Lewis et al., 2011). Additional proof was obtained by the complete absence of a response of HCN-DN-expressing neurons to the specific HCN channel blocker ZD7288. HCN-DN expression thus mimicked the effects of ZD7288 seen for control neurons and caused neuronal hyperexcitability, which is in line with what was reported previously (Huang et al., 2009). This demonstrates that I(h) was fully suppressed by the HCN-DN subunit and highlights the advantage of our strategy over single subunit KO models that display compensatory upregulation of other HCN subunits and significant residual I(h) amplitudes (Nolan et al., 2003; Lewis et al., 2011). Striatal medium spiny neurons do not seem to express I(h) (Boyes et al., 2007), and only weak HCN2 and HCN4 expression levels were reported in the striatum (Santoro et al., 2000; Chan et al., 2004). Therefore, CaMKII $\alpha$  promoter-mediated ectopic HCN-DN expression in the striatum is not expected to exert effects on the biophysical properties of medium spiny neurons. Further electrophysiological recordings of HCN-DN-expressing medium spiny neurons would be needed to clarify this possibility.

#### 4.1.2. The transgenic CaMKII $\alpha$ promoter line limits HCN-DN expression to a smaller subset of the endogenously CaMKII $\alpha$ -expressing neuronal population

The CaMKII $\alpha$ -tTA-driven HCN-DN/EGFP expression pattern in cell bodies of presumed principal neurons was found to be restricted to the forebrain, heterogeneous between brain areas, and with distinct laminar distribution within a certain region. Comparison of immunofluorescence labeling of CaMKII-alpha with EGFP-expressing cells in mutant brains revealed a highly mosaic expression pattern, which was generally in line with the description in the original publication (Mayford et al., 1996) showing expression restricted to forebrain regions such as cerebral cortex, hippocampus, and striatum. However, they also reported expression in the amygdala, which was not seen in the present study. Instead, additional labeling of the globus pallidus external segment (GPe) was detected in the present study, which has not been described earlier. Changes in CaMKII $\alpha$  promoter-mediated expression patterns among different double transgenic lines were, however, also reported in the original study, which indicates that potential integration site-dependent effects may account for varying results (Mayford et al., 1996). A more recent study used the same CaMKII $\alpha$  promoter construct to drive GFP expression, with the purpose of characterizing CaMKII $\alpha$  expression (Wang et al., 2013). They reported the most abundant signal in forebrain regions as well, with similar laminar distribution differences in cortical regions as

compared to those seen in the present study, although CaMKII $\alpha$  immunoreactivity was detected in all cortical layers. However, the thalamus, hypothalamus, and Purkinje cells of specific cerebellar lobes were additionally reported to express EGFP (Wang et al., 2013), which was neither seen in the present, nor in the original study (Mayford et al., 1996). Especially the reported distinct expression pattern in the cerebellum indicates integration site-dependent effects in this study. It further supports the assumption that differences mediated by the CaMKII $\alpha$  promoter line are due to effects specific for the transgenic approach, which may be additionally dependent on the transgene whose expression should be driven by the CaMKII $\alpha$  promoter construct. The CaMKII $\alpha$  isoform has been shown to be the predominant subunit in the forebrain, and can be detected in all cortical areas, hippocampus, amygdala, thalamic nuclei, substantia nigra (Erondu and Kennedy, 1985; Miller and Kennedy, 1985). In addition, CaMKII $\alpha$  is known to show a certain laminar intensity distribution in the expression, in that labeling in layer 2/3 and 6 is stronger than in layer 5 pyramidal neurons (Ouimet et al., 1984; Burgin et al., 1990). However, CaMKII $\alpha$  can also be detected in the cerebellar Purkinje cell layer, although at lower levels as compared to the CaMKII $\beta$ , the main subunit in the cerebellum (Miller and Kennedy, 1985; Walaas et al., 1988; Nagasaki et al., 2014). The endogenous expression pattern of the CaMKII $\alpha$  subunit is thus broader than those reported for the CaMKII $\alpha$  promoter construct. Therefore, the presently observed patterns of transgene expression most likely differ due to both the use of a partial fragment of the promoter and to integration site-specific effects (depending on number of copies integrated in a certain region, integration site that influences gene expression, ectopic expression) and thus, must not necessarily be in line with endogenous expression patterns both in terms of regional distribution and amount of expression. To this assumption adds the mosaicism observed in EGFP expression, i.e. cell-to-cell variations in transgene expression within a certain region. This has been observed in the CA1 pyramidal layer, for example, in which deep pyramidal cell bodies but not superficial ones were found to be labeled with EGFP. This phenomenon is a common observation in transgenic mouse lines and thought to be due to incomplete promoter functions (Wang et al., 2013). In our transgenic lines EGFP and HCN-DN expression were driven from the same bidirectional promoter, which was shown to produce a high level of co-expression with low variability between founder lines (Krestel et al., 2001). As co-expressed EGFP and HCN-DN have different subcellular distribution patterns and, most likely, different half-lives, the EGFP labeling intensities were likely not always completely congruent with HCN-DN expression. However, patch-clamp recordings from CA1 (Fig. 3-

2), EC layer 2 (Figs. 3-6 and 3-7) and cerebellar Purkinje cells (Fig. 3-21) in acute brain slices revealed that all EGFP-positive cells did have strongly attenuated  $I(h)$ . Therefore, we are confident that the pattern of EGFP expression reflects the pattern of functional  $I(h)$  suppression by HCN-DN.

## **4.2. HCN-DN-mediated neuronal hyperexcitability affects neonatal and adult network activity**

Studies that were aimed at investigating the role of  $I(h)$  on *in vivo* network patterns have been sparse so far. Here, neonatal and adult network activities in hippocampal and cortical brain regions in mice with  $I(h)$  attenuation were investigated. Although loss of  $I(h)$  caused neuronal hyperexcitability, immature networks containing HCN-DN-expressing neurons displayed hypoexcitable properties. In adult animals hippocampal activity patterns showed specific changes of population activity and communication among layers. Interestingly, no signs of epileptic seizures were detected in any of the acute or chronic recordings from neonatal or adult mice, respectively.

### **4.2.1. $I(h)$ ablation reduces neonatal spontaneous cortical activity**

Hippocampal activity recorded in neonatal (P6-8) mutant mice along the CA1-DG axis was not found to be altered by loss of functional  $I(h)$ . Mutant mice only tended to have slightly lower SPW rates and amplitudes, as well as lower SRO rates. SPWs in the LFP were proposed to represent the *in vivo* correlates of giant depolarizing potentials (GDPs) recorded intracellularly *in vitro* from CA3 neurons in the immature hippocampus (Leinekugel et al., 2002). The current finding that hippocampal activity is unaltered contrasts with contrast to *in vitro* studies that reported a role for  $I(h)$  in the generation and frequency of spontaneously occurring GDPs, because blocking  $I(h)$  reduced GDP frequency and regularity (Strata et al., 1997; Agmon and Wells, 2003; Bender et al., 2005). Over the course of early postnatal development, it has been demonstrated that  $I(h)$  recorded in CA1 and CA3 pyramidal neurons *in vitro* undergoes substantial changes in terms of current amplitude, kinetics, and density; in CA1 pyramidal neurons, especially between P5 and P10,  $I(h)$  amplitude and activation speed were shown to almost double as compared to currents recorded between P1 and P5 (Vasilyev and Barish, 2002). However, it is not clear whether the changes around

P5-10 occur linearly or are rather skewed towards earlier or later ages. It might thus be possible that when recorded at P7, I(h) in the hippocampal formation is still of too low amplitude, kinetics, conductance or density for any potential alteration to be reflected in extracellular LFP patterns at this age. This notion is supported by present findings that adult hippocampal activity in mutant mice was significantly affected by the loss of functional I(h). Besides, another study showed that the generation of GDPs in CA3 was independent of I(h), and GDP frequency was shown to increase rather than decrease upon acute blockade I(h) with Cs<sup>+</sup> or ZD7288 (Sipilä et al., 2006). While the physiological roles and nature of GDPs are still controversial (Bregestovski and Bernard, 2012; Dzhala et al., 2012; Valeeva et al., 2013), data from our laboratory indicate that hippocampal network activity in P7 wild-type mice is mostly driven by EC layer 3 input via the perforant path (Hinsch et al., 2015). The LFP patterns in acute depth-profile recordings with linear silicon probes along the CA1-DG allow a quantification of layer-specific inputs to CA1 to be made. The CSD depth profiles recorded from mouse neonates in this study (Fig. 3-8 B and C) also suggest that SPWs and SROs originated from EC rather than from CA3. Altered maturation of CA3 networks as a result of I(h) attenuation might therefore not be detectable using our preparation. Furthermore, although I(h) is called ‘pacemaker’ current, I(f)-deficient sinus node cells in mice are still able to generate rhythmic activity *in vivo*, which is, however, lower than in controls and better compensated for in sinoatrial node (SAN) cells than in atrioventricular node (AVN) cells (Baruscotti et al., 2011; Mesirca et al., 2014).

Cortical activity in mutant neonates was found to be differentially affected by I(h) ablation. Whereas the activity in somatosensory areas was only mildly and insignificantly changed, the occurrence rates of SATs and SBs in the visual cortex of mutant mice were significantly reduced. Immature early brain activity of neonatal mice during the first two weeks after birth is mostly spontaneously generated and characterized by early network oscillations (ENOs), slow activity transients (SAT), and spindle bursts (SBs, 8-25 Hz) (Garaschuk et al., 2000; Khazipov et al., 2004; Adelsberger et al., 2005; Colonnese and Khazipov, 2010). ENOs have been shown to be driven by cortical Ca<sup>2+</sup> waves (Adelsberger et al., 2005). Two potential mechanisms may underlie the generation of SATs: first, migrating Ca<sup>2+</sup> waves, as demonstrated *in vitro* (Garaschuk et al., 2000; Dupont et al., 2006; Allène et al., 2008), and supported by *in vivo* findings (Adelsberger et al., 2005; Yang et al., 2009), and second, spontaneous peripheral input to the neocortex via e.g., myoclonic twitches or retinal waves (Khazipov et al., 2004; Hanganu et al., 2006; Colonnese and Khazipov, 2010). Independent of the mechanism of generation, a common property of spontaneous activity in cortical

regions is that they are greatly dependent on depolarizing stimuli that are mediated via GABA<sub>A</sub>-, NMDA- and AMPA-receptors (Garaschuk et al., 2000; Minlebaev et al., 2007). So far, I(h) has not been studied in association with spontaneous *in vivo* cortical network activity. The present study is the first to describe the effects of suppressed I(h) on immature network activity in somatosensory and visual cortices, and to show significantly reduced spontaneous events in the visual cortex. As the majority of mutant mice were found to show no visual cortex SAT or SB activity at all, suppression of functional I(h) might have resulted in a hyperpolarizing effect on network excitability that is strong enough to suppress spontaneous events in the visual cortex of neonatal mice. In contrast, since the activity in somatosensory areas has been shown to be predominantly driven by peripheral sensory stimuli, such as spontaneous myoclonic twitches (Khazipov et al., 2004; An et al., 2014), the resulting depolarization in the somatosensory cortex might be strong enough to evoke spontaneous events, and to explain why there was no effect of ablated I(h) on the activity in the somatosensory cortex. Cortical activity is characterized by traveling calcium waves. Due to its depolarizing effect on the membrane potential, I(h) constantly interacts with other voltage-dependent ion channels, such as voltage-gated calcium channels (VGCCs), thereby shaping neonatal and adult network activities. In adult cortical neurons, loss of I(h) decreases steady-state inactivation of VGCCs due to the hyperpolarizing effect on the RMP. Upon depolarization, the larger fraction of available VGCCs may mediate calcium currents eventually triggering action potentials (Huang et al., 2011). In immature neurons, hyperpolarization of the RMP induced by the loss of I(h) may reduce spontaneous activity when excitatory input is not strong enough to depolarize the membrane beyond the action potential threshold. Combined extracellular LFP recordings and calcium imaging studies (Kirmse et al., 2015) in mutant neonatal mice *in vivo* might help to shed light on a potential mechanism by which functional I(h) ablation reduces spontaneously driven intrinsic SATs and SBs in the visual cortex.

#### 4.2.2. I(h) contributes to sharp wave-ripple properties

The most prominent LFP pattern in the hippocampus during states of immobility (e.g. consummatory behaviors) and slow wave sleep is the SPW-R (Buzsáki et al., 1983). SPWs in stratum radiatum reflect the depolarization of CA1 neurons due to synchronous population activity of CA3 pyramidal neurons that is conveyed onto CA1 distal dendrites via Schaffer collaterals (Buzsáki, 1986). In this context, it has been reported that a gradual

buildup of CA3 activity (AP firing, EPSC and IPSC events) precedes the SPW-R (Schlingloff et al., 2014). The depolarization of CA1 distal dendrites in turn induces ripples (140-180 Hz) in the pyramidal layer (Buzsáki et al., 1992), which are generated by the interaction between discharging pyramidal cells and interneurons (Stark et al., 2014). I found that SPW-R properties were strongly affected by attenuated I(h), which was seen as ripples with significantly reduced frequencies and duration, as well as higher SPW-R amplitudes but lower SPW-R occurrence rates in mutant mice. This indicated that I(h) in hippocampal pyramidal neurons contributes to SPW-R *in vivo*. How can suppressed I(h) interfere with SPW-R generation? Since I(h) determines the RMP, input resistance, and the integration of synaptic inputs, I(h) deficiency can cause changes in CA3 activity that could affect the amount of depolarization on stratum radiatum dendrites in CA1. In addition, CA1 neurons deficient in I(h) will respond differently to incoming excitatory stimuli. Indeed, mutant mice had SPWs of greater amplitude, which is indicative of either increased depolarization by CA3 Schaffer collaterals, or increased summation of excitatory stimuli at the dendrites of CA1 pyramidal neurons. The latter would be in line with our *in vitro* findings demonstrating increased summation of incoming excitatory potentials upon HCN-DN expression and concomitant I(h) ablation, which likely resulted in higher amplitude SPWs *in vivo*. This notion is also supported by findings demonstrating that blocking HCN channels with ZD7288 *in vitro* led to increased SPW amplitudes (Kranig et al., 2013). The intra-ripple frequency was reported to correlate with the magnitude of the SPW, in that high amplitude SPWs generate ripples of higher mean peak frequency (Sullivan et al., 2011; Patel et al., 2013). However, I(h) deficiency in mutant mice caused a reduction in ripple frequency, similar to what was observed upon Tetanustoxin-dependent block of the CA3 output *in vivo* (Nakashiba et al., 2009). It thus seems as if HCN-DN expression differentially affected SPWs and ripple, in that a change in either depolarizing CA3 input to CA1, or changed CA1 pyramidal cell responses to EPSCs, was not necessarily reflected by the concomitant ripple oscillation. There are several sources known to contribute to the extracellular field ripple (Buzsáki, 2015). Spiking activity of depolarized CA1 pyramidal neurons and simultaneously activated interneurons is phase-locked to ripple frequency oscillations and has been reported to substantially contribute to the LFP ripple (Ylinen et al., 1995; Schomburg et al., 2012; Schlingloff et al., 2014). Pyramidal neuron APs preferentially occur at the negative trough of the ripple, followed by interneuron spiking after a certain delay (Stark et al., 2014), whereas the peak of the ripple oscillations is generated by somatic IPSCs (Ylinen et al., 1995). The ripple in LFP recordings thus reflects the interplay of CA1

pyramidal neuron and interneuron responses to the depolarization by CA3 Schaffer collaterals. Both, optogenetic silencing of pyramidal neurons and optogenetic activation of interneurons have been shown to block ripple oscillations *in vivo* (Stark et al., 2014). We restricted HCN-DN expression to pyramidal neurons, whereas interneurons were not affected. It therefore seems unlikely that interneuron activity was directly affected by suppressed I(h). However, one possibility that might account for reduced frequencies might be altered responses of mutant CA1 pyramidal neurons to rhythmic somatic IPSCs generated by interneurons during the ripple. Functional I(h) would activate and counteract the hyperpolarization of the membrane brought about by IPSCs, thereby contributing to the generation of the next cycle in the oscillation. Without I(h), repolarization of the membrane might take longer, which could result in lower frequency ripples. It was indeed shown that blocking I(h) especially affects the IPSC component of an EPSC-IPSC sequence elicited in CA1 pyramidal neurons upon Schaffer collateral stimulation (Pavlov et al., 2011). Another contributor to lower-frequency ripples might be a change in the spiking behavior of the pyramidal neurons during the ripple, especially since LFP ripples correlate and are coherent with the membrane potential oscillations of a pyramidal neuron during the ripple (English et al., 2014). Further combined recordings of the LFP and firing activity would help to clarify whether suppressed I(h) alters the electrical behavior of pyramidal neurons during a ripple in the intact brain. In addition, recordings of interneuron-pyramidal neuron pairs in brain slices of mutant mice could help elucidate the effects of HCN-DN expression on the integration of interneuron-mediated IPSCs by pyramidal neurons at the soma. It was also observed that the occurrence rate of SPW-R was lower in mutant mice. The termination of SPW-R was reported to be mediated by an afterhyperpolarization of the membrane and implied to create a refractoriness (English et al., 2014). I(h) deficiency might prolong the afterhyperpolarization and thus account for lower SPW-R rates. A different explanation proposed that reduced SPW-R rates obtained upon ZD7288-mediated HCN channel block is due to a hyperpolarized CA3 recurrent network (Kranig et al., 2013). Increased SPW amplitudes in mutant mice rather argue against that explanation (but could also be due to increased EPSP summation).

#### 4.2.3. I(h) contributes to theta frequency oscillations

Several studies have shown that I(h) contributes to theta resonance in neurons and theta oscillations of neuronal networks in the hippocampus and entorhinal cortex. For example,

neurons in medial entorhinal cortex exhibit intrinsic membrane potential oscillations in theta frequency, which decreases along the dorsal to ventral axis (Giocomo et al., 2007; Garden et al., 2008; Giocomo and Hasselmo, 2008). This dorsal-ventral theta frequency gradient is mediated by HCN channel-mediated currents, and was shown to be disrupted upon deletion of HCN1 channels in HCN1<sup>-/-</sup> mice (Giocomo and Hasselmo, 2009). The change in the frequency of membrane potential oscillations from theta to lower subthreshold frequencies thereby has been shown to be due to reduced HCN1 channel-mediated currents (Nolan et al., 2007). Likewise, in hippocampal pyramidal neurons, which are endowed with theta resonance mediated by h-currents at subthreshold levels (Hu et al., 2002, 2009), recordings from CA1 pyramidal neurons along the somatodendritic axis and combined computational models demonstrate the dependence of intrinsic resonant frequency on I(h) density (Narayanan and Johnston, 2007, 2008; Vaidya and Johnston, 2013). Here, LFP peak theta frequencies were found to be decreased in mice deficient in I(h). Furthermore, in control mice the theta frequency shifted to higher values from pyramidal layer to lacunosum moleculare, consistent with the somatodendritic gradient of I(h) (Magee, 1999; Lörincz et al., 2002), whereas mutant mice exhibited similar frequencies in all layers of CA1. These data indicate that I(h) deficiency decreases the frequency of network theta oscillations and eliminates the theta gradient in CA1 pyramidal neurons along the somatodendritic axis, consistent with previous findings. However, forebrain-restricted HCN1 channel deletions in HCN1<sup>f/f,cre</sup> mice have also demonstrated increased power in theta oscillations (Nolan et al., 2005; Giocomo et al., 2011; Hussaini et al., 2011), whereas functional I(h) deficiency in mutant mice was previously found to decrease the power of network oscillations (Merseburg et al., 2012). It thus seems as if a more complete ablation of I(h) rather leads to reduced oscillatory power. In support of this notion are findings reported for rat models of temporal lobe epilepsy (Marcelin et al., 2009; Laurent et al., 2015). Kainate- or pilocarpine-induced status epilepticus is known to cause an HCN channelopathy in the hippocampus and entorhinal cortex, which is characterized by a reduction in I(h) due to deregulation and mislocalization of HCN1 and HCN2 channels (Shah et al., 2004; Jung et al., 2007; Shin et al., 2009). A reduction of available HCN channels was thereby shown to reduce both, theta oscillation frequency and power in epileptic rats (Marcelin et al., 2009). Furthermore, rats with temporal lobe epilepsy were found to have coherence differences in theta and gamma oscillations along the CA1-DG axis, although different to what has been observed in the present study, coherence was reduced rather than increased (Laurent et al., 2015). Although temporal lobe epilepsy is known to be accompanied by hippocampal sclerosis that might in

part account for changes in theta oscillations (Laurent et al., 2015), these data still support the assumption that functional I(h) deficiency causes deficits in oscillatory frequency and power.

### **4.3. Implications for the role of I(h) in learning and memory**

I(h) has been proposed to constrain learning and memory processes by mechanisms differing depending on brain regions and underlying involved cognitive processes. Working memory performance was shown to be enhanced upon block of HCN channels due to  $\alpha$ 2A adrenoceptor-mediated cAMP inhibition (Wang et al., 2007; Barth et al., 2008). However, other results propose the opposite by demonstrating that the presence of HCN1-mediated currents promotes intrinsic persistent firing activity of L5 pyramidal neurons in medial prefrontal cortex, and forebrain HCN1 deletion reduces working memory performance (Thuault et al., 2013). In the present study, functional loss of I(h) in the forebrain was found to exert only mild effects on working memory. An interesting finding is that the tendency towards a reduced performance was independent of the age of onset of I(h) deficiency. This would point towards a role for I(h) in contributing to persistent activity in the prefrontal cortex to execute working memory (Thuault et al., 2013), rather than to constrain working memory-related prefrontal cortex activity (Wang et al., 2007).

Enhanced hippocampus-dependent spatial learning and memory in mice with forebrain HCN1 deletion was shown to result from LTP induction (Nolan et al., 2005; Tsay et al., 2007). Two opposing studies, however, report either enhancing effects of presynaptic I(h) on LTP in mossy fibers that synapse on CA3 (Mellor et al., 2002), or no contribution of I(h) (Chevalleyre and Castillo, 2002). In contrast to what has been observed in mice with forebrain-restricted HCN1-channel deficiency (Nolan et al., 2005), enhanced spatial learning performance in the water maze task was not seen for mutant mice in the present study. On the contrary, mutant mice seemed to have difficulties in learning the platform position and tended to exhibit a lower performance in recalling the platform position. Impaired learning was reflected by increased distances the mutant mice had to swim and, concomitantly, increased escape latencies. Since, however, suppressed I(h) caused motor function deficits in mutant mice, these results can additionally be influenced by reduced swimming abilities. To account for such possibilities, the mice were previously tested using a visible platform and exhibited a reduced performance (Merseburg, 2011). Therefore,

impaired learning performance in the invisible platform water maze task is likely to be influenced in part by motor dysfunctions in mutant mice. Consistent with this notion are other results showing that mice with a general deletion in *Hcn1*, which are also reported to have sensorimotor function deficits, exhibit slightly impaired performance in the visible platform task (Nolan et al., 2003). The probe trial is designed for a preferential search in the target quadrant and might be a measurement that is more independent of swimming performance. Since mutant mice exhibited a lower performance in the probe trial, it can be proposed that functional I(h) ablation caused deficits in hippocampus-dependent learning. Contextual fear learning was unaffected by I(h) deficiency, a finding that is in line with results reported for *TRIP8b*<sup>-/-</sup> mice (Lewis et al., 2011). Together the data suggest that functional loss of I(h) in the forebrain did not affect, or only moderately affected the cognitive performance in mice.

At the network level, this might be associated with the alterations observed in the SPW-R properties of adult mutant mice, as discussed earlier. SPW-R activity is known to promote replay of previous experience and, thus, contributes to memory consolidation (Lee and Wilson, 2002; Ji and Wilson, 2007; Nakashiba et al., 2009). In the rodent hippocampus, the activity of place cells in CA1 pyramidal layer recurs in a time-compressed manner during SPW-R, and suppression SPW-R has been shown to impair learning and memory (Girardeau et al., 2009, 2014; Girardeau and Zugaro, 2011). Besides, place cell properties are influenced by HCN1 channel-mediated currents (Hussaini et al., 2011). I(h) attenuation could thus contribute in several ways. However, since the present results revealed only mild effects of forebrain I(h) deficiency on cognitive performance, despite the pronounced effects on SPW-R properties and occurrence rates, this might not have a strong influence on overall behavior in the present study.

#### **4.4. Motor function deficits and hyperactivity suggest roles of I(h) in cortico-basal ganglia communication**

I(h) is known to play a role in the execution of motor functions and learning of coordinated movements (Nolan et al., 2003; Chung et al., 2009; Lewis et al., 2011). Mice with a spontaneous loss-of-function mutation in *Hcn2* (*HCN2*<sup>ap/ap</sup>) were shown to be severely impaired in the accelerating Rotarod and had an abnormal gait (Chung et al., 2009). Mice with a general deletion in *Hcn1* had learning deficits on the Rotarod as well, although much

less pronounced than compared to those observed in HCN2<sup>ap/ap</sup> mice. Recordings in cerebellar Purkinje neurons of HCN1<sup>-/-</sup> mice revealed changes in the integrative properties due to prolonged hyperpolarization upon inhibitory input. In contrast, when loss of HCN1 channel-mediated I(h) was restricted to the forebrain using the CaMKII $\alpha$  promoter (HCN1<sup>ff,cre</sup>), mice had normal motor functions. Thus, the authors concluded that HCN1 channels in cerebellar Purkinje neurons are needed for learning of coordinated movements (Nolan et al., 2003). The present study demonstrates that a forebrain-restricted subunit-unspecific I(h) deficiency causes deficits on the accelerating Rotarod and in the pole test, both of which require learning and execution of coordinated movements. Furthermore, gait analysis revealed significant changes in mutant mice, seen in shorter stand and stride length, an increase in the width between the hind limbs (base of support) and irregular step sequences. These results indicate that I(h) in forebrain structures does contribute to motor functions. Moreover, because mice with cerebellar Purkinje neuron-restricted I(h) deficiency performed well on the Rotarod and exhibited normal gait properties, it seems unlikely that loss of I(h) in cerebellar Purkinje neurons *per se* is responsible for the observed deficits, contrary to what has been proposed upon earlier findings.

In HCN1<sup>ff,cre</sup> mice the deletion is also restricted to CaMKII $\alpha$ -expressing neurons, as HCN-DN expression in the present study is CaMKII $\alpha$ -dependent. However, our approach is subunit unspecific, whereas the former only targets HCN1 channels, leaving residual I(h) mediated by HCN2-4 channels. Additionally, it is likely that knockout of only one subunit induces compensatory mechanisms to account for the loss in HCN1 channel-mediated currents, potentially by increased expression of endogenous subunits or other homeostatic mechanisms (Chen et al., 2010). Consistently, the authors demonstrated increased HCN3 protein in all areas of the brain upon deletion of *Hcn1* (Nolan et al., 2003). The authors claimed that HCN3 protein overexpression might not be functionally relevant because HCN3 channels have so far not been found to express currents in heterologous systems. However, HCN3 channels have later been demonstrated to conduct I(h) in heterologous systems (Stieber et al., 2005), indicating that an increase in HCN3-channel expression might indeed exert compensatory effects on the overall current. In contrast, in the present approach overexpression of the HCN-DN subunit can compensate for the compensatory upregulation of endogenous HCN channel subunits (as seen for HCN2 and HCN4 protein (Sandke, 2006)), which might explain why mutant mice lacking I(h) mediated by all four subunits in the forebrain show a more pronounced motor deficits than mice with a forebrain-

restricted deletion of I(h) mediated by HCN1 channels. This highlights the limitations of the use of subunit-specific deletions of HCN channels in interpreting the function of I(h).

In a follow up study, it was shown that mice with Purkinje cell-restricted deletion of *Hcn1* (HCN1<sup>ff,L7Cre</sup>) were initially, i.e. at the first day of learning to balance on the accelerating Rotarod, not different from control animals, but had deficits in later stages of learning, supporting the earlier claim for the role of HCN1 channels in Purkinje neurons. In comparison, HCN1<sup>-/-</sup> mice were tested again in this study, and had an overall worse performance (Rinaldi et al., 2013). Contrasting results obtained for HCN1<sup>ff,L7Cre</sup> mice versus mice with complete I(h) deficiency in Purkinje neurons are more difficult to interpret. *In situ* hybridization studies revealed HCN1 mRNA in the molecular layer and Purkinje cell layer, whereas HCN2 mRNA was shown to be present in the Purkinje cell layer and granular layer of the cerebellum (Moosmang et al., 1999); together with data demonstrating immunoreactivity for HCN2 in the molecular layer of the cerebellum, it shows that Purkinje neurons also express HCN2 channels (Notomi and Shigemoto, 2004). Therefore, HCN1-specific I(h) deficiency in cerebellar Purkinje neurons might not completely ablate all I(h) in these cells. However, the worse performance of HCN1<sup>ff,L7Cre</sup> mice on the Rotarod (Rinaldi et al., 2013) as compared to mice tested in the present study seems striking, as one would have predicted the opposite finding due to a more complete I(h) deficiency. Furthermore, it is worth mentioning that HCN1<sup>ff,L7Cre</sup> mice performed initially as good as control mice and, whereas control mice maintained the initial performance, the mutant mice exhibited a decrease during the following learning trials (Rinaldi et al., 2013). It thus seems as if the observed differences are not necessarily due to differences in motor learning, but potentially due to differences in motivation to stay on the Rotarod. The current data showed that mutant mice steadily increased their performance over trials and maintained maximal performance during the following trials. Independent of inconsistencies between studies, the data still indicate that changes in the activity of cerebellar Purkinje neurons upon I(h) deficiency, targeted to one subunit or subunit-unspecific, exerts a functionally less pronounced role as has been suggested so far.

The organization of movement in the brain, i.e. planning, initiation, execution, and termination, as well as error correction, is performed by tightly interconnected circuits, involving primary motor and premotor areas of the cortex, the basal ganglia, and the cerebellum. The highest level of motor control is performed by primary cortical motor and premotor areas, specifically by the corticospinal tract formed by layer 5 pyramidal neurons

that project directly to the spinal cord. The basal ganglia and cerebellum can be considered as feedback loops, which integrate sensory information from cortical areas and peripheral sensory input to fine tune corticospinal motor commands. In the following, it should be discussed in how far subcortical motor control structures could be affected by I(h) deficiency that potentially leads to the observed motor function abnormalities seen in mutant mice.

#### 4.4.1. Role of I(h) in the cortico-basal ganglia-thalamocortical loop

The basal ganglia are comprised of four nuclei, including the striatum, globus pallidus (external and internal segment; GPe and GPi, respectively), substantia nigra pars reticulata (SNr) and pars compacta (SNc), and the subthalamic nucleus (STN). The striatum, with its major cell type being GABAergic medium spiny neurons, is the main input compartment of the basal ganglia and receives extensive cortical information via corticostriatal projections. Corticostriatal projections are formed by pyramidal neurons in layer 5 of the cortex, which are locally interconnected with layer 2/3 pyramidal neurons (Shepherd, 2013). Layer 2/3 neurons express I(h) mediated by HCN2 channel isoforms (Santoro et al., 2000; Notomi and Shigemoto, 2004). In the present study it has been shown that presumptive layer 2/3 pyramidal neurons express HCN-DN. Suppressed I(h) in these neurons might therefore affect the information that is conveyed onto layer 5 pyramidal neurons and subsequently onto the striatum via corticostriatal projections, and thus contribute to altered inputs to the basal ganglia. In contrast, HCN1 channel-mediated currents that are predominantly expressed by layer 5 pyramidal neurons might contribute to a much lesser extent to motor control. First of all, layer 5 pyramidal neurons in primary motor cortex were not found to express HCN-DN and should thus have functional I(h), yet mutant mice display profound motor deficits. This assumption is further supported by the finding that knockout of HCN1 channels restricted to forebrain projection neurons were not found to result in a motor phenotype (Nolan et al., 2003), whereas loss-of-function mutations in *Hcn2* contributes to severe deficits (Chung et al., 2009). Besides, pyramidal neurons in layers 2 and 3 of the neocortex have been shown to directly project to the striatum matrix (Gerfen, 1989). Together, the data indicate a potential deregulation already on the level of cortical motor command circuits induced by HCN-DN expression. Although strong EGFP fluorescence was detected in the striatum, which is indicative of HCN-DN expression in medium spiny neurons, it is not expected to influence their activity, as medium spiny neurons have not

been reported to express I(h) (Boyes et al., 2007). Corticostriatal input to the basal ganglia is next conveyed either via the direct pathway formed by GABAergic striatonigral projections to the STN, or the indirect pathway that first passes the GPe via inhibitory striatopallidal projections before synapsing onto the STN with inhibitory pallidal-subthalamic projections. The direct and indirect pathways thereby exert control over inhibition of the motor thalamus, which is the target structure of basal ganglia output, and which projects excitatory thalamocortical projections back to cortical motor areas. Activation of the direct pathway via dopamine and D1 receptors facilitates cortically initiated movements by disinhibiting the thalamus, whereas the indirect pathway, which is inhibited by dopamine acting on D2 receptors, signals movement inhibition by increased inhibitory signaling to the thalamus (Alexander and Crutcher, 1990; Tepper et al., 2004). In addition, the hyperdirect pathway conveying direct cortical projections to the STN (Watabe-Uchida et al., 2012) represents another possibility for I(h) deficiency-mediated impairment of cortico-basal ganglia communication (Nambu et al., 2002). As basal ganglia dysfunction has been linked to several movement disorders, including Parkinson's disease and Huntington's disease, and also with cognitive and motivational disorders such as attention-deficit-hyperactivity disorder (ADHD) (Björklund and Dunnett, 2007), it is tempting to speculate that I(h) deficiency in basal ganglia nuclei contributes to movement disorders. Indeed, mutant mice exhibited strong hyperactive and stereotyped circling behavior, which could result from HCN-DN-induced deregulation of the direct or indirect pathway, leading to decreased thalamic inhibition and consequently elevated signaling of movement initiation. EGFP fluorescence was detected in the GPe in mutant mice, which points towards potential changes in the activity of the pathways responsible for conveying movement initiation signals back to the cortex. The severe motor phenotype observed in mice with deletions of *Hcn2* supports this idea. Likewise, studies demonstrated that autonomous pacemaking activity in GPe neurons relies on HCN1 and HCN2 channel-mediated conductances, and that those neurons develop an HCN2 channelopathy upon induction of the parkinsonian state in mouse models of Parkinson's disease (Chan et al., 2004, 2011). Behaviorally, those mice were also reported to show motor function deficits in the pole test and gait abnormalities, such as a shorter stride length, similar to what has been observed in the present study (Chan et al., 2011).

#### 4.4.2. Role of I(h) in cerebellar motor control

Although the integrative properties of cerebellar Purkinje neurons are compromised upon I(h) deficiency *in vitro*, which was reflected in prolonged hyperpolarization of the membrane potential in response to negative currents and concomitant pauses between tonic firing modes (Williams et al., 2002; Nolan et al., 2003), these changes are not necessarily reflected in the behaving animal, as was demonstrated in the present study for mice with Purkinje neuron-targeted I(h) deficiency. However, the finding that I(h) deficiency in the forebrain causes gait abnormalities and motor learning deficits in mutant mice still suggest a role for I(h) in information processing by the cerebellar motor feedback loop. Purkinje neurons provide the sole output of the cerebellar cortex, but receive excitatory input from afferent climbing and mossy fibers that provide central and peripheral sensory information, respectively. Climbing fibers convey sensory information from cortical areas, including somatosensory and visual cortices, and synapse on Purkinje cell dendrites in the molecular layer of the cerebellum. As discussed above, the cortico-basal ganglia-thalamocortical loop might be influenced by the lack of I(h), which in turn can have consequences for the activity that reaches Purkinje neurons via climbing fibers, and hence influence motor control mediated by the cerebellar circuits. Mossy fibers originate in the spinal cord and brainstem, and signal information from the periphery. Mossy fibers synapse onto granule cells of the cerebellar granular layer. Granule cells then form excitatory parallel fibers that target Purkinje neuron dendrites in the molecular layer. Analysis of the distribution of HCN-DN expression in brains of mutant mice with forebrain-restricted I(h) deficiency revealed EGFP-expressing fibers in the granular layer, which are presumably afferent mossy fibers. Preliminary data, which were not included in the present results, revealed EGFP-positive projections, potentially ectopic expression, in the spinal cord, seemingly located in regions that send projections to the brain. Therefore, it is likely that the observed motor phenotype is partially influenced by altered signaling coming from the periphery. In support of this notion is the present finding that mutant mice, independent of age of onset of I(h) deficiency, have a weaker grip strength. Spinocerebellar pathways are known to contribute to muscle weakness when impaired in their normal activity. In addition, it might explain the severe sensorimotor reflex development observed in neonatal mutant mice in my earlier study (Merseburg, 2011). However, the data is still preliminary and a thorough analysis of the morphology of EGFP-expressing projections would be needed for a definite conclusion to be drawn.

#### 4.5. I(h) is necessary during early postnatal development

There is growing body of evidence that implies I(h) to play a significant role in development. However, no models are available yet that are designed to restrict I(h) deficiency to specific developmental stages (Rocha et al., 2006; Bender and Baram, 2008). The present study is the first to describe a conditional doxycycline-dependent system for suppression of HCN channel-mediated currents. Our previous findings showed that mice deficient in I(h) from birth display behavioral abnormalities that become apparent as early as P6 and are reflected in impaired sensorimotor reflex development. Adult mutant mice display behavioral hyperactivity and reduced anxiety-like traits, gait abnormalities, motor learning deficits, and mild cognitive impairments (Sandke, 2006; Merseburg, 2011). The present study was aimed at investigating whether the abnormalities mentioned before were consequences of early postnatal I(h) deficiency, or mediated by effects of I(h) ablation on physiological functions, or a combination of both. Thus, a comparison was made between mice with I(h) deficiency from birth throughout life and mice with I(h) deficiency restricted to the early postnatal developmental period (OFF vs. OFF/ON) in order to address the developmental question. However, as I(h) has a wide range of different homeostatic effects on the adult brain that are independent of the early postnatal development, mice with late-onset I(h) deficiency starting at juvenile ages were added to the comparison (OFF vs OFF/ON vs ON/OFF). Overall, it was found that mice with early postnatal I(h) ablation, i.e. OFF and OFF/ON mutant mice, showed a similar behavioral phenotype, whereas in most cases mutant mice with late-onset I(h) deficiency, i.e. ON/OFF mutants, were not distinguishable from control littermates. These data strongly indicate that functional I(h) during early postnatal development critically influences CNS maturation.

In the present results, whole-cell recordings in acute hippocampal slices revealed strongly attenuated I(h) in CA1 pyramidal neurons of P7 neonatal mutants. Although I(h) in the hippocampus has been shown to be substantially regulated during development (Bender et al., 2001, 2005; Brewster et al., 2002, 2005, 2007; Vasilyev and Barish, 2002; Bender and Baram, 2008), early *in vivo* hippocampal activity was not found to be affected by functionally suppressed HCN channel-mediated currents in the current study (but see 4.2.1 for discussion). Of note, some reports of HCN channel-deregulation during development were based on findings upon early developmental seizure-induction, and thus likely include homeostatic or maladaptive pathological changes that constrains an I(h)-specific

interpretation of the results (Brewster et al., 2002, 2005). In contrast to findings in the hippocampus, spontaneous cortical events in sensory areas were significantly attenuated by suppressed  $I(h)$  in neonatal mutant mice. As spontaneous activity in immature networks is crucial for proper maturation of functional connections, it can be assumed that a decrease in spontaneous cortical events upon  $I(h)$  deficiency causes persistent alterations in the adult network, and concomitantly in adult behavior. Consistent with this notion, adult hippocampal network activity was found to be significantly affected by permanent  $I(h)$  suppression in mutant mice. The strong reduction in intra-ripple frequency together with increased SPW amplitudes were not observed in mice with late-onset  $I(h)$  ablation. This is a strong indicator that a lack of functional h-currents during the development negatively influenced the maturation of functional connectivity within the hippocampus and between hippocampus and entorhinal cortex. The entorhinal cortex perforant path input to CA1 and dentate gyrus has been shown to have a development-dependent  $I(h)$  regulation (Bender et al., 2001, 2007; Bender and Baram, 2008). In addition, entorhinal cortex L3 pyramidal neurons exhibited strongly attenuated  $I(h)$  upon HCN-DN expression in the present study. Peak theta frequencies and interlaminar coherence differences were found to be affected by  $I(h)$  deficiency in both OFF and ON/OFF mutants during REM sleep. As resonance relies on active conductances and is mediated by  $I(h)$  at hyperpolarized subthreshold levels in CA1 pyramidal neurons (Hu et al., 2002; Narayanan and Johnston, 2007), this finding most likely reflects homeostatic physiological functions of  $I(h)$ . Yet, differences in peak theta frequencies were differentially expressed and lower in OFF than ON/OFF mutants, which points to an additional developmental component.

Sleep is important for memory consolidation, and changes in hippocampal network activity during slow wave sleep or REM sleep can have consequences for cognition (see 4.3 Discussion) (Diekelmann and Born, 2010). Furthermore, pre- and postsynaptic HCN1 channels within the hippocampal-entorhinal cortex network were reported to influence synaptic transmission and long-term potentiation underlying memory formation processes (Nolan et al., 2005; Tsay et al., 2007; Huang et al., 2011). Yet, the cognitive performance in mutant mice deficient in  $I(h)$  were only mildly affected, and in contrast to previous reports,  $I(h)$  deficiency tended to impair learning and memory rather than enhancing it (Nolan et al., 2005; Wang et al., 2007). Interestingly, the tendency of mutant mice to have deficits in working memory was independent of the doxycycline regime, thus highlighting the importance of  $I(h)$  in executive functions in the prefrontal cortex (Thuault et al., 2013).

Gait abnormalities and motor learning deficits only developed early in life, because only ON/OFF mutants with late-onset I(h) deficiency were indistinguishable from control mice, whereas OFF and OFF/ON mutants had an irregular gait and motor skill learning deficits in the Pole test. The interpretation of results obtained for motor learning abilities on the accelerating Rotarod is hampered at the moment due to the unusually low performance of control mice in the OFF/ON and ON/OFF doxycycline treatment groups. Testing of another cohort of control mice revealed that with additional training, mice were able to reach higher latencies to fall on the Rotarod (data not shown). Therefore, extending the protocol to include additional learning trials would help to improve the performance and potentially reveal differences between control and mutant mice in the OFF/ON group, because OFF/ON mutant mice were similarly impaired in the Pole test as OFF mutant animals. Functional I(h) ablation caused a reduction in forelimb grip strength that was independent of the age of onset.

Lastly, I(h) deficiency contributed to stereotyped hyperactive circling behavior in mutant mice. The open field test allowed an assessment of exploratory behavior to be made and demonstrated that hyperactivity (i.e., increased distance moved, increasing locomotion with time in the arena) and reduced anxiety-like traits (i.e., increased time spent in center square vs. less time spent in border area) were due to developmental I(h) deficiency in OFF and OFF/ON mutants, whereas ON/OFF mutants were normal when compared to control mice. However, it has been reported that lentivirus-mediated knockdown of HCN1 channels in the dorsal hippocampus in adult rats causes similar anxiolytic effects as seen in the present study (Kim et al., 2012).

In summary, the present data demonstrate that our model for conditionally suppressing I(h) independently of subunit composition is suitable for discrimination between development-dependent and homeostatic physiological functions of I(h), and to confirm the notion of essential roles of I(h) in postnatal maturation of the brain.

## 5. References

- Accili EA, Proenza C, Baruscotti M, DiFrancesco D (2002) From funny current to HCN channels: 20 years of excitement. *News Physiol Sci* 17:32–37.
- Adelsberger H, Garaschuk O, Konnerth A (2005) Cortical calcium waves in resting newborn mice. *Nat Neurosci* 8:988–990.
- Agmon A, Wells JE (2003) The role of the hyperpolarization-activated cationic current I(h) in the timing of interictal bursts in the neonatal hippocampus. *J Neurosci* 23:3658–3668.
- Alexander GE, Crutcher MD (1990) Functional architecture of basal ganglia circuits: neural substrates of parallel processing. *Trends Neurosci* 13:266–271.
- Alig J, Marger L, Mesirca P, Ehmke H, Mangoni MEME, Isbrandt D (2009) Control of heart rate by cAMP sensitivity of HCN channels. *Proc Natl Acad Sci* 106:12189–12194.
- Allène C, Cattani A, Ackman JB, Bonifazi P, Aniksztejn L, Ben-Ari Y, Cossart R (2008) Sequential generation of two distinct synapse-driven network patterns in developing neocortex. *J Neurosci* 28:12851–12863.
- Altomare C, Bucchi a, Camatini E, Baruscotti M, Viscomi C, Moroni a, DiFrancesco D (2001) Integrated allosteric model of voltage gating of HCN channels. *J Gen Physiol* 117:519–532.
- An S, Kilb W, Luhmann HJ (2014) Sensory-Evoked and Spontaneous Gamma and Spindle Bursts in Neonatal Rat Motor Cortex. *J Neurosci* 34:10870–10883.
- Aponte Y, Lien C-C, Reisinger E, Jonas P (2006) Hyperpolarization-activated cation channels in fast-spiking interneurons of rat hippocampus. *J Physiol* 574:229–243.
- Araki T, Ito M, Oshima T (1961) Potential changes produced by application of current steps in motoneurons. *Nature* 191:1104–1105.
- Aylward RLM (2008) Epilepsy: a review of reports, guidelines, recommendations and models for the provision of care for patients with epilepsy. *Clin Med* 8:433–438.
- Bader CR, Macleish PR, Schwartz EA (1979) A voltage-clamp study of the light response in solitary rods of the tiger salamander. *J Physiol* 296:1–26.
- Bal T, McCormick D a (1997) Synchronized oscillations in the inferior olive are controlled by the hyperpolarization-activated cation current I(h). *J Neurophysiol* 77:3145–3156.
- Barbuti A, Baruscotti M, DiFrancesco D (2007) The pacemaker current: From basics to the clinics. *J Cardiovasc Electrophysiol* 18:342–347.
- Barth AMI, Vizi ES, Zelles T, Lendvai B (2008) Alpha2-adrenergic receptors modify dendritic spike generation via HCN channels in the prefrontal cortex. *J Neurophysiol* 99:394–401.
- Baruscotti M, Bucchi A, Viscomi C, Mandelli G, Consalez G, Gnecci-Rusconi T, Montano N, Casali KR, Micheloni S, Barbuti A, DiFrancesco D (2011) Deep

## REFERENCES

- bradycardia and heart block caused by inducible cardiac-specific knockout of the pacemaker channel gene *Hcn4*. *Proc Natl Acad Sci U S A* 108:1705–1710.
- Ben-Ari Y (2001) Developing networks play a similar melody. *Trends Neurosci* 24:353–360.
- Ben-Ari Y, Cherubini E, Corradetti R, Gaiarsa J-LL (1989) Giant synaptic potentials in immature rat CA3 hippocampal neurones. *J Physiol* 416:303–325.
- Ben-Ari Y, Holmes GL (2006) Effects of seizures on developmental processes in the immature brain. *Lancet Neurol* 5:1055–1063.
- Bender R a, Soleymani S V, Brewster AL, Nguyen ST, Beck H, Mathern GW, Baram TZ (2003) Enhanced expression of a specific hyperpolarization-activated cyclic nucleotide-gated cation channel (HCN) in surviving dentate gyrus granule cells of human and experimental epileptic hippocampus. *J Neurosci* 23:6826–6836.
- Bender RA, Baram TZ (2008) Hyperpolarization activated cyclic-nucleotide gated (HCN) channels in developing neuronal networks. *Prog Neurobiol* 86:129–140.
- Bender RA, Brewster A, Santoro B, Ludwig A, Hofmann F, Biel M, Baram TZ (2001) Differential and age-dependent expression of hyperpolarization-activated, cyclic nucleotide-gated cation channel isoforms 1-4 suggests evolving roles in the developing rat hippocampus. *Neuroscience* 106:689–698.
- Bender RA, Galindo R, Mameli M, Gonzalez-vega R, Valenzuela F, Baram TZ, Valenzuela CF, Baram TZ (2005) Synchronized network activity in developing rat hippocampus involves regional hyperpolarization-activated cyclic nucleotide-gated (HCN) channel function. *Eur J Neurosci* 22:2669–2674.
- Bender RA, Kirschstein T, Kretz O, Brewster AL, Richichi C, Rüschemschmidt C, Shigemoto R, Beck H, Frotscher M, Baram TZ (2007) Localization of HCN1 channels to presynaptic compartments: novel plasticity that may contribute to hippocampal maturation. *J Neurosci* 27:4697–4706.
- Biel M, Wahl-schott C, Michalakis S, Zong X (2009) Hyperpolarization-Activated Cation Channels : From Genes to Function. :847–885.
- Björklund A, Dunnett SB (2007) Fifty years of dopamine research. *Trends Neurosci* 30:185–187.
- Blumenfeld H, Klein JP, Schridde U, Vestal M, Rice T, Khera DS, Bashyal C, Giblin K, Paul-Laughinghouse C, Wang F, Phadke A, Mission J, Agarwal RK, Englot DJ, Motelow J, Nersesyan H, Waxman SG, Levin AR (2008) Early treatment suppresses the development of spike-wave epilepsy in a rat model. *Epilepsia* 49:400–409.
- Bois P, Bescond J, Renaudon B, Lenfant J (1996) Mode of action of bradycardic agent, S 16257, on ionic currents of rabbit sinoatrial node cells. *Br J Pharmacol* 118:1051–1057.
- Boyes J, Bolam JP, Shigemoto R, Stanford IM (2007) Functional presynaptic HCN channels in the rat globus pallidus. *Eur J Neurosci* 25:2081–2092.
- Bregestovski P, Bernard C (2012) Excitatory GABA: How a Correct Observation May Turn Out to be an Experimental Artifact. *Front Pharmacol* 3:65.
- Brewster A, Bender RA, Chen Y, Dube C, Eghbal-Ahmadi M, Baram TZ (2002)

## REFERENCES

- Developmental febrile seizures modulate hippocampal gene expression of hyperpolarization-activated channels in an isoform-and cell-specific manner. *J Neurosci* 22:4591.
- Brewster AL, Bernard J a, Gall CM, Baram TZ (2005) Formation of heteromeric hyperpolarization-activated cyclic nucleotide-gated (HCN) channels in the hippocampus is regulated by developmental seizures. *Neurobiol Dis* 19:200–207.
- Brewster AL, Chen Y, Bender R a, Shigemoto R, Baram TZ, Yeh A (2007) Quantitative analysis and subcellular distribution of mRNA and protein expression of the hyperpolarization-activated cyclic nucleotide-gated channels throughout development in rat hippocampus. *Cereb Cortex* 17:702–712.
- Burgin KE, Waxham MN, Rickling S, Westgate S a, Mobley WC, Kelly PT (1990) In situ hybridization histochemistry of Ca<sup>2+</sup>/calmodulin-dependent protein kinase in developing rat brain. *J Neurosci* 10:1788–1798.
- Buzsáki G (1986) Hippocampal sharp waves: their origin and significance. *Brain Res* 398:242–252.
- Buzsáki G (2002) Theta Oscillations in the Hippocampus. *Neuron* 33:325–340.
- Buzsáki G (2005) Theta rhythm of navigation: Link between path integration and landmark navigation, episodic and semantic memory. *Hippocampus* 15:827–840.
- Buzsáki G (2015) Hippocampal sharp wave-ripple: A cognitive biomarker for episodic memory and planning. *Hippocampus* 1188:n/a – n/a.
- Buzsáki G, Buhl DL, Harris KD, Csicsvari J, Czéh B, Morozov A (2003) Hippocampal network patterns of activity in the mouse. *Neuroscience* 116:201–211.
- Buzsáki G, Draguhn A (2004) Neuronal oscillations in cortical networks. *Science* 304:1926–1929.
- Buzsáki G, Horváth Z, Urioste R, Hetke J, Wise K (1992) High-frequency network oscillation in the hippocampus. *Science* 256:1025–1027.
- Buzsáki G, Leung LW, Vanderwolf CH (1983) Cellular bases of hippocampal EEG in the behaving rat. *Brain Res* 287:139–171.
- Buzsáki G, Moser EI (2013) Memory, navigation and theta rhythm in the hippocampal-entorhinal system. *Nat Neurosci* 16:130–138.
- Chan CS, Glajch KE, Gertler TS, Guzman JN, Mercer JN, Lewis AS, Goldberg AB, Tkatch T, Shigemoto R, Fleming SM, Chetkovich DM, Osten P, Kita H, Surmeier DJ (2011) HCN channelopathy in external globus pallidus neurons in models of Parkinson's disease. *Nat Neurosci* 14:85–92.
- Chan CS, Shigemoto R, Mercer JN, Surmeier DJ (2004) HCN2 and HCN1 channels govern the regularity of autonomous pacemaking and synaptic resetting in globus pallidus neurons. *J Neurosci* 24:9921–9932.
- Chapman CA, Lacaille JC (1999) Intrinsic theta-frequency membrane potential oscillations in hippocampal CA1 interneurons of stratum lacunosum-moleculare. *J Neurophysiol* 81:1296–1307.
- Chen S, Wang J, Siegelbaum S a (2001) Properties of hyperpolarization-activated pacemaker current defined by coassembly of HCN1 and HCN2 subunits and basal

## REFERENCES

- modulation by cyclic nucleotide. *J Gen Physiol* 117:491–504.
- Chen X, Shu S, Bayliss DA (2005a) Suppression of  $I_h$  contributes to propofol-induced inhibition of mouse cortical pyramidal neurons. *J Neurophysiol* 94:3872–3883.
- Chen X, Shu S, Schwartz L, Sun C, Kapur J, Bayliss DA (2010) Homeostatic Regulation of Synaptic Excitability: Tonic GABAA Receptor Currents Replace  $I_h$  in Cortical Pyramidal Neurons of HCN1 Knock-Out Mice. *J Neurosci* 30:2611.
- Chen X, Sirois JE, Lei Q, Talley EM, Lynch C, Bayliss DA (2005b) HCN subunit-specific and cAMP-modulated effects of anesthetics on neuronal pacemaker currents. *J Neurosci* 25:5803–5814.
- Chevalyere V, Castillo PE (2002) Assessing the role of  $I_h$  channels in synaptic transmission and mossy fiber LTP. *Proc Natl Acad Sci U S A* 99:9538–9543.
- Chrobak JJ (2000) Physiological Patterns in the Hippocampo-Entorhinal Cortex System. 465:457–465.
- Chung WK et al. (2009) Absence epilepsy in apathetic, a spontaneous mutant mouse lacking the  $h$  channel subunit, HCN2. *Neurobiol Dis* 33:499–508.
- Colonnese MT, Khazipov R (2010) “Slow activity transients” in infant rat visual cortex: a spreading synchronous oscillation patterned by retinal waves. *J Neurosci* 30:4325–4337.
- Dibbens LM, Reid CA, Hodgson B, Thomas EA, Phillips AM, Gazina E, Cromer BA, Clarke AL, Baram TZ, Scheffer IE, Berkovic SF, Petrou S (2010) Augmented currents of an HCN2 variant in patients with febrile seizure syndromes. *Ann Neurol* 67:542–546.
- Diekelmann S, Born J (2010) The memory function of sleep. *Nat Rev Neurosci* 11:114–126.
- DiFrancesco D (1994) Some properties of the UL-FS 49 block of the hyperpolarization-activated current ( $i(f)$ ) in sino-atrial node myocytes. *Pflügers Arch Eur J Physiol* 427:64–70.
- Difrancesco JC, Barbuti A, Milanese R, Coco S, Bucchi A, Bottelli G, Ferrarese C, Franceschetti S, Terragni B, Baruscotti M, Difrancesco D (2011) Recessive Loss-of-Function Mutation in the Pacemaker HCN2 Channel Causing Increased Neuronal Excitability in a Patient with Idiopathic Generalized Epilepsy. *J Neurosci* 31:17327–17337.
- DiFrancesco JC, DiFrancesco D (2015) Dysfunctional HCN ion channels in neurological diseases. *Front Cell Neurosci* 6:1–10.
- Dube C, Chen K, Eghbal-Ahmadi M, Brunson K, Soltesz I, Baram TZ (2000) Prolonged febrile seizures in the immature rat model enhance hippocampal excitability long term. *Ann Neurol* 47:336–344.
- Dupont E, Hanganu IL, Kilb W, Hirsch S, Luhmann HJ (2006) Rapid developmental switch in the mechanisms driving early cortical columnar networks. *Nature* 439:79–83.
- Dyhrfeld-Johnsen J, Morgan RJ, Földy C, Soltesz I (2008) Upregulated H-current in hyperexcitable CA1 dendrites after febrile seizures. *Front Cell Neurosci* 2:2.

## REFERENCES

- Dzhala V, Valeeva G, Glykys J, Khazipov R, Staley K (2012) Traumatic Alterations in GABA Signaling Disrupt Hippocampal Network Activity in the Developing Brain. *J Neurosci* 32:4017–4031.
- English DF, Peyrache a., Stark E, Roux L, Vallentin D, Long M a., Buzsaki G (2014) Excitation and Inhibition Compete to Control Spiking during Hippocampal Ripples: Intracellular Study in Behaving Mice. *J Neurosci* 34:16509–16517.
- Erondu NE, Kennedy MB (1985) Regional Distribution Kinase in Rat Brain ' of Type II Ca \* + / Calmodulin-dependent. *J Neurosci* 5:3270–3277.
- Fehr S, Ivell R, Koll R, Schams D, Fields M, Richter D (1987) Expression of the oxytocin gene in the large cells of the bovine corpus luteum. *FEBS Lett* 210:45–50.
- Franklin KBJ, Paxinos G (2007) *The Mouse Brain in Stereotaxic Coordinates*, 3rd ed. Academic Press.
- Franz O, Liss B, Neu A, Roeper J (2000) Single-cell mRNA expression of HCN1 correlates with a fast gating phenotype of hyperpolarization-activated cyclic nucleotide-gated ion channels (I<sub>h</sub>) in central neurons. *Eur J Neurosci* 12:2685–2693.
- Freitag S, Schachner M, Morellini F (2003) Behavioral alterations in mice deficient for the extracellular matrix glycoprotein tenascin-R. *Behav Brain Res* 145:189–207.
- Garaschuk O, Hanse E, Konnerth A (1998) Developmental profile and synaptic origin of early network oscillations in the CA1 region of rat neonatal hippocampus. *J Physiol* 507 ( Pt 1:219–236.
- Garaschuk O, Linn J, Eilers J, Konnerth A (2000) Large-scale oscillatory calcium waves in the immature cortex. *Nat Neurosci* 3:452–459.
- Garden DLF, Dodson PD, O'Donnell C, White MD, Nolan MF (2008) Tuning of synaptic integration in the medial entorhinal cortex to the organization of grid cell firing fields. *Neuron* 60:875–889.
- Gasparini S, DiFrancesco D (1997) Action of the hyperpolarization-activated current (I<sub>h</sub>) blocker ZD 7288 in hippocampal CA1 neurons. *Pflugers Arch Eur J Physiol* 435:99–106.
- Gerfen CR (1989) The neostriatal mosaic: striatal patch-matrix organization is related to cortical lamination. *Science* 246:385–388.
- Giocomo LM, Hasselmo ME (2008) Time Constants of h Current in Layer II Stellate Cells Differ along the Dorsal to Ventral Axis of Medial Entorhinal Cortex. *J Neurosci* 28:9414–9425.
- Giocomo LM, Hasselmo ME (2009) Knock-out of HCN1 subunit flattens dorsal-ventral frequency gradient of medial entorhinal neurons in adult mice. *J Neurosci* 29:7625–7630.
- Giocomo LM, Hussaini SA, Zheng F, Kandel ER, Moser M-B, Moser EI (2011) Grid Cells Use HCN1 Channels for Spatial Scaling. *Cell* 147:1159–1170.
- Giocomo LM, Zilli EA, Fransén E, Hasselmo ME (2007) Temporal frequency of subthreshold oscillations scales with entorhinal grid cell field spacing. *Science* 315:1719–1722.

## REFERENCES

- Girardeau G, Benchenane K, Wiener SI, Buzsáki G, Zugaro MB (2009) Selective suppression of hippocampal ripples impairs spatial memory. *Nat Neurosci* 12:1222–1223.
- Girardeau G, Cei A, Zugaro M (2014) Learning-Induced Plasticity Regulates Hippocampal Sharp Wave-Ripple Drive. *J Neurosci* 34:5176–5183.
- Girardeau G, Zugaro M (2011) Hippocampal ripples and memory consolidation. *Curr Opin Neurobiol* 21:452–459.
- Halliwel J V., Adams PR (1982) Voltage-clamp analysis of muscarinic excitation in hippocampal neurons. *Brain Res* 250:71–92.
- Hanganu IL, Ben-Ari Y, Khazipov R (2006) Retinal waves trigger spindle bursts in the neonatal rat visual cortex. *J Neurosci* 26:6728–6736.
- He C, Chen F, Li B, Hu Z (2014) Neurophysiology of HCN channels: from cellular functions to multiple regulations. *Prog Neurobiol* 112:1–23.
- Hinsch R, Marguet S, Sirota A, Fazeli AW, Isbrandt D (2015) Development of hippocampal network activity patterns in mice during the first two weeks of life. In: *Neuroscience Meeting Planner*. Chicago, IL: Society for Neuroscience, 2015. Online, pp Program #257.20.
- Hu H, Vervaeke K, Graham LJ, Storm JF (2009) Complementary theta resonance filtering by two spatially segregated mechanisms in CA1 hippocampal pyramidal neurons. *J Neurosci* 29:14472–14483.
- Hu H, Vervaeke K, Storm JF (2002) Two forms of electrical resonance at theta frequencies, generated by M-current, h-current and persistent Na<sup>+</sup> current in rat hippocampal pyramidal cells. *J Physiol* 545:783–805.
- Huang Z, Lujan R, Kadurin I, Uebele VN, Renger JJ, Dolphin AC, Shah MM (2011) Presynaptic HCN1 channels regulate Cav3.2 activity and neurotransmission at select cortical synapses. *Nat Neurosci* 14:478–486.
- Huang Z, Lujan R, Martinez-Hernandez J, Lewis AS, Chetkovich DM, Shah MM (2012) TRIP8b-independent trafficking and plasticity of adult cortical presynaptic HCN1 channels. *J Neurosci* 32:14835–14848.
- Huang Z, Walker MC, Shah MM (2009) Loss of Dendritic HCN1 Subunits Enhances Cortical Excitability and Epileptogenesis. *J Neurosci* 29:10979–10988.
- Hussaini SA a., Kempadoo KA a., Thuault SJJ, Siegelbaum SA a., Kandel ERR (2011) Increased Size and Stability of CA1 and CA3 Place Fields in HCN1 Knockout Mice. *Neuron* 72:643–653.
- Ito M, Oshima T (1965) Electrical behaviour of the motoneurone membrane during intracellularly applied current steps. *J Physiol* 180:607–635.
- Ji D, Wilson M a (2007) Coordinated memory replay in the visual cortex and hippocampus during sleep. *Nat Neurosci* 10:100–107.
- Jung S, Jones TD, Lugo JN, Sheerin AH, Miller JW, D'Ambrosio R, Anderson AE, Poolos NP (2007) Progressive dendritic HCN channelopathy during epileptogenesis in the rat pilocarpine model of epilepsy. *J Neurosci* 27:13012–13021.
- Khazipov R, Khalilov I (2004) Developmental changes in GABAergic actions and

## REFERENCES

- seizure susceptibility in the rat hippocampus. *Eur J ...* 19:590–600.
- Khazipov R, Luhmann HJ (2006) Early patterns of electrical activity in the developing cerebral cortex of humans and rodents. *Trends Neurosci* 29:414–418.
- Khazipov R, Sirota A, Leinekugel X, Holmes GL, Ben-Ari Y, Buzsáki G (2004) Early motor activity drives spindle bursts in the developing somatosensory cortex. *Nature* 432:758–761.
- Kim CS, Chang PY, Johnston D (2012) Enhancement of dorsal hippocampal activity by knockdown of HCN1 channels leads to anxiolytic- and antidepressant-like behaviors. *Neuron* 75:503–516.
- Kirmse K, Kummer M, Kovalchuk Y, Witte OW, Garaschuk O, Holthoff K (2015) GABA depolarizes immature neurons and inhibits network activity in the neonatal neocortex in vivo. *Nat Commun* 6:7750.
- Kranig S a. A, Duhme N, Waldeck C, Draguhn A, Reichinnek S, Both M (2013) Different functions of hyperpolarization-activated cation channels for hippocampal sharp waves and ripples in vitro. *Neuroscience* 228:325–333.
- Krestel HE, Mayford MR, Seeburg PH, Sprengel R (2001) A GFP-equipped bidirectional expression module well suited for monitoring tetracycline-regulated gene expression in mouse. *Nucleic Acids Res* 29:E39.
- Laurent F, Brotons-mas JR, Cid E, Lopez-pigozzi D, Valero M, Gal B, de la Prida LM, Menendez XL, Prida D (2015) Proximodistal Structure of Theta Coordination in the Dorsal Hippocampus of Epileptic Rats. *Franc. J Neurosci* 35:1–17.
- Lee AK, Wilson M a (2002) Memory of sequential experience in the hippocampus during slow wave sleep. *Neuron* 36:1183–1194.
- Leinekugel X, Khazipov R, Cannon R (2002) Correlated Bursts of Activity in the Neonatal Hippocampus in Vivo. *Science (80- )* 296:2049–2052.
- Lewis AS, Schwartz E, Chan CS, Noam Y, Shin M, Wadman WJ, Surmeier DJ, Baram TZ, Macdonald RL, Chetkovich DM (2009) Alternatively spliced isoforms of TRIP8b differentially control h channel trafficking and function. *J Neurosci* 29:6250–6265.
- Lewis AS, Vaidya SP, Blaiss CA, Liu Z, Stoub TR, Brager DH, Chen X, Bender R a., Estep CM, Popov AB, Kang CE, Van Veldhoven PP, Bayliss D a., Nicholson D a., Powell CM, Johnston D, Chetkovich DM (2011) Deletion of the hyperpolarization-activated cyclic nucleotide-gated channel auxiliary subunit TRIP8b impairs hippocampal Ih localization and function and promotes antidepressant behavior in mice. *J Neurosci* 31:7424–7440.
- Liss B, Haeckel O, Wildmann J, Miki T, Seino S, Roeper J (2005) K-ATP channels promote the differential degeneration of dopaminergic midbrain neurons. *Nat Neurosci* 8:1742–1751.
- Lörincz A, Notomi T, Tamás G, Shigemoto R, Nusser Z (2002) Polarized and compartment-dependent distribution of HCN1 in pyramidal cell dendrites. *Nat Neurosci* 5:1185–1193.
- Ludwig a, Zong X, Stieber J, Hullin R, Hofmann F, Biel M (1999) Two pacemaker channels from human heart with profoundly different activation kinetics. *EMBO J* 18:2323–2329.

## REFERENCES

- Ludwig A, Budde T, Stieber J, Moosmang S, Wahl C, Holthoff K, Langebartels A, Wotjak C, Munsch T, Zong X, Feil S, Feil R, Lancel M, Chien KR, Konnerth A, Pape H, Biel M, Hofmann F, others (2003) Absence epilepsy and sinus dysrhythmia in mice lacking the pacemaker channel HCN2. *EMBO J* 22:216–224.
- Ludwig A, Zong X, Jeglitsch M, Hofmann F, Biel M (1998) A family of hyperpolarization-activated mammalian cation channels. *Nature* 393:587–591.
- Luján R, Albasanz JL, Shigemoto R, Juiz JM (2005) Preferential localization of the hyperpolarization-activated cyclic nucleotide-gated cation channel subunit HCN1 in basket cell terminals of the rat cerebellum. *Eur J Neurosci* 21:2073–2082.
- Maccaferri G, McBain CJ (1996) The hyperpolarization-activated current (I<sub>h</sub>) and its contribution to pacemaker activity in rat CA1 hippocampal stratum oriens-alveus interneurons. *J Physiol* 497 ( Pt 1):119–130.
- Macri V, Angoli D, Accili E a (2012) Architecture of the HCN selectivity filter and control of cation permeation. *Sci Rep* 2:894.
- Magee J (1999) Dendritic I<sub>h</sub> normalizes temporal summation in hippocampal CA1 neurons. *Nat Neurosci* 2:848.
- Magee JCC (1998) Dendritic hyperpolarization-activated currents modify the integrative properties of hippocampal CA1 pyramidal neurons. *J Neurosci* 18:7613.
- Marcelin B, Chauvière L, Becker A, Migliore M, Esclapez M, Bernard C (2009) H Channel-Dependent Deficit of Theta Oscillation Resonance and Phase Shift in Temporal Lobe Epilepsy. *Neurobiol Dis* 33:436–447.
- Marguet SL, Le-Schulte VTQ, Merseburg A, Neu A, Eichler R, Jakovcevski I, Ivanov A, Hanganu-Opatz IL, Bernard C, Morellini F, Isbrandt D (2015) Treatment during a vulnerable developmental period rescues a genetic epilepsy. *Nat Med* 21:1–12.
- Mayford M, Bach ME, Huang YY, Wang L, Hawkins RD, Kandel ER (1996) Control of memory formation through regulated expression of a CaMKII transgene. *Science* 274:1678–1683.
- McCormick DA, Pape HC (1990) Properties of a hyperpolarization-activated cation current and its role in rhythmic oscillation in thalamic relay neurones. *J Physiol* 431:291–318.
- Mellor J, Nicoll R a, Schmitz D (2002) Mediation of hippocampal mossy fiber long-term potentiation by presynaptic I<sub>h</sub> channels. *Science* 295:143–147.
- Merseburg A (2011) Phenotypic Characterization and Pharmacological Treatment of Transgenic Mice with Conditional Suppression of HCN Channel Activity in Forebrain Neurons.
- Merseburg A, Schlusche AK, Marguet S, Grendel J, Morellini F, Isbrandt D, Merseburg A, Schlusche AK, Marguet S, Grendel J, Morellini F, Isbrandt D (2012) Suppression of HCN channel mediated I<sub>h</sub> in forebrain neurons impairs early postnatal development and alters hippocampal network activity in vivo. In: *Neuroscience Meeting Planner*. New Orleans, LA: Society for Neuroscience, 2012. Online, pp Program No. 647.05. New Orleans, LA, USA.
- Mesirca P et al. (2014) Cardiac arrhythmia induced by genetic silencing of “funny” (f) channels is rescued by GIRK4 inactivation. *Nat Commun* 5:4664.

## REFERENCES

- Milanesi R, Baruscotti M, Gneccchi-Ruscione T, DiFrancesco D (2006) Familial Sinus Bradycardia Associated with a Mutation in the Cardiac Pacemaker Channel. *N Engl J Med* 354:151–157.
- Miller SG, Kennedy MB (1985) Distinct forebrain and cerebellar isozymes of type II Ca<sup>2+</sup>/calmodulin-dependent protein kinase associate differently with the postsynaptic density fraction. *J Biol Chem* 260:9039–9046.
- Milligan CJ, Edwards IJ, Deuchars J (2006) HCN1 ion channel immunoreactivity in spinal cord and medulla oblongata. *Brain Res* 1081:79–91.
- Minlebaev M, Ben-Ari Y, Khazipov R (2007) Network mechanisms of spindle-burst oscillations in the neonatal rat barrel cortex in vivo. *J Neurophysiol* 97:692–700.
- Mohns EJ, Blumberg MS (2008) Synchronous bursts of neuronal activity in the developing hippocampus: modulation by active sleep and association with emerging gamma and theta rhythms. *J Neurosci* 28:10134–10144.
- Moosmang S, Biel M, Hofmann F, Ludwig A (1999) Differential distribution of four hyperpolarization-activated cation channels in mouse brain. *Biol Chem* 380:975–980.
- Moosmang S, Stieber J, Zong X, Biel M, Hofmann F, Ludwig A (2001) Cellular expression and functional characterization of four hyperpolarization-activated pacemaker channels in cardiac and neuronal tissues. *Eur J Biochem* 268:1646–1652.
- Morellini F (2013) Spatial memory tasks in rodents: What do they model? *Cell Tissue Res* 354:273–286.
- Morellini F, Schachner M (2006) Enhanced novelty-induced activity, reduced anxiety, delayed resynchronization to daylight reversal and weaker muscle strength in tenascin-C-deficient mice. *Eur J Neurosci* 23:1255–1268.
- Much B, Wahl-Schott C, Zong X, Schneider A, Baumann L, Moosmang S, Ludwig A, Biel M (2003) Role of Subunit Heteromerization and N-Linked Glycosylation in the Formation of Functional Hyperpolarization-activated Cyclic Nucleotide-gated Channels. *J Biol Chem* 278:43781–43786.
- Nagasaki N, Hirano T, Kawaguchi S (2014) Opposite regulation of inhibitory synaptic plasticity by  $\alpha$  and  $\beta$  subunits of Ca<sup>2+</sup>/calmodulin-dependent protein kinase II. *J Physiol* 592.22:4891–4909.
- Nakashiba T, Buhl DL, McHugh TJ, Tonegawa S (2009) Hippocampal CA3 output is crucial for ripple-associated reactivation and consolidation of memory. *Neuron* 62:781–787.
- Nambu A, Tokuno H, Takada M (2002) Functional significance of the cortico-subthalamo-pallidal “hyperdirect” pathway. *Neurosci Res* 43:111–117.
- Narayanan R, Johnston D (2007) Long-term potentiation in rat hippocampal neurons is accompanied by spatially widespread changes in intrinsic oscillatory dynamics and excitability. *Neuron* 56:1061–1075.
- Narayanan R, Johnston D (2008) The h Channel Mediated Location Dependence and Plasticity of Intrinsic Phase Response in Rat Hippocampal Neurons. *J Neurosci* 28:5846–5860.

## REFERENCES

- Nava C et al. (2014a) De novo mutations in HCN1 cause early infantile epileptic encephalopathy. *Nat Genet* 46:640–645.
- Nava C et al. (2014b) Prospective diagnostic analysis of copy number variants using SNP microarrays in individuals with autism spectrum disorders. *Eur J Hum Genet* 22:71–78.
- Neuhoff H, Neu A, Liss B, Roeper J (2002) I(h) channels contribute to the different functional properties of identified dopaminergic subpopulations in the midbrain. *J Neurosci* 22:1290–1302.
- Nolan M, Malleret G, Dudman J, Buhl D, Santoro B, Gibbs E, Vronskaya S, Buzsaki G, Siegelbaum S, Kandel E (2005) A Behavioral Role for Dendritic Integration HCN1 Channels Constrain Spatial Memory and Plasticity at Inputs to Dendrites of CA1 Pyramidal Neurons. *Cell* 120:151–152.
- Nolan MF, Dudman JT, Dodson PD, Santoro B (2007) HCN1 Channels Control Resting and Active Integrative Properties of Stellate Cells from Layer II of the Entorhinal Cortex. *J Neurosci* 27:12440–12451.
- Nolan MFF, Malleret G, Lee KHH, Gibbs E, Dudman JTT, Santoro B, Yin D, Thompson RFF, Siegelbaum SAA, Kandel ER, others, Morozov A (2003) The hyperpolarization-activated HCN1 channel is important for motor learning and neuronal integration by cerebellar Purkinje cells. *Cell* 115:551–564.
- Noma A, Irisawa H (1976) Membrane currents in the rabbit sinoatrial node cell as studied by the double microelectrode method. *Pflügers Arch Eur J Physiol* 364:45–52.
- Notomi T, Shigemoto R (2004) Immunohistochemical localization of Ih channel subunits, HCN1-4, in the rat brain. *J Comp Neurol* 471:241–276.
- Ouimet CC, McGuinness TL, Greengard P (1984) Immunocytochemical localization of calcium/calmodulin-dependent protein kinase II in rat brain. *Proc Natl Acad Sci U S A* 81:5604–5608.
- Pape HC (1996) Queer current and pacemaker: the hyperpolarization-activated cation current in neurons. *Annu Rev Physiol* 58:299–327.
- Patel J, Schomburg EW, Berényi A, Fujisawa S, Buzsáki G (2013) Local generation and propagation of ripples along the septotemporal axis of the hippocampus. *J Neurosci* 33:17029–17041.
- Pavlov I, Scimemi A, Savtchenko L, Kullmann DM, Walker MC (2011) Ih-mediated depolarization enhances the temporal precision of neuronal integration. *Nat Commun* 2:199.
- Paxinos, G., Hallyday, G., Watson, C., Koutcherov, Y. & Wang H (2007) Atlas of the Developing Mouse Brain at E17.5, P0 and P6. Academic Press.
- Peters HC, Hu H, Pongs O, Storm JF, Isbrandt D (2005) Conditional transgenic suppression of M channels in mouse brain reveals functions in neuronal excitability, resonance and behavior. *Nat Neurosci* 8:51–60.
- Pike FG, Goddard RS, Suckling JM, Ganter P, Kasthuri N, Paulsen O (2000) Distinct frequency preferences of different types of rat hippocampal neurones in response to oscillatory input currents. *J Physiol* 529 Pt 1:205–213.

## REFERENCES

- Ponomarenko AA, Korotkova TM, Sergeeva OA, Haas HL (2004) Multiple GABAA receptor subtypes regulate hippocampal ripple oscillations. *Eur J Neurosci* 20:2141–2148.
- Poolos NP, Migliore M, Johnston D (2002) Pharmacological upregulation of h-channels reduces the excitability of pyramidal neuron dendrites. *Nat Neurosci* 5:767–774.
- Raman IM, Bean BP (1999) Ionic currents underlying spontaneous action potentials in isolated cerebellar Purkinje neurons. *J Neurosci* 19:1663–1674.
- Richichi C, Brewster AL, Bender RA, Simeone TA, Zha Q, Yin HZ, Weiss JH, Baram TZ (2008) Mechanisms of seizure-induced “transcriptional channelopathy” of hyperpolarization-activated cyclic nucleotide gated (HCN) channels. *Neurobiol Dis* 29:297–305.
- Rinaldi A, Defterali C, Mialot A, Garden DLF, Beraneck M, Nolan MF (2013) HCN1 channels in cerebellar Purkinje cells promote late stages of learning and constrain synaptic inhibition. *J Physiol* 591:5691–5709.
- Rivlin-Etzion M, Marmor O, Heimer G, Raz A, Nini A, Bergman H (2006) Basal ganglia oscillations and pathophysiology of movement disorders. *Curr Opin Neurobiol* 16:629–637.
- Robinson RB, Siegelbaum SA (2003) Hyperpolarization-activated cation currents: from molecules to physiological function. *Annu Rev Physiol* 65:453–480.
- Rocha N, Rolfs A, Strauss U (2006) Ih is maturing: implications for neuronal development. *Neurodegener Dis* 3:27–31.
- Russell MW, Dick M, Collins FS, Brody LC (1996) KVLQT1 mutations in three families with familial or sporadic long QT syndrome. *Hum Mol Genet* 5:1319–1324.
- Sandke S (2006) Untersuchungen neuronaler H-Kanal Aktivität mit Hilfe transgener Mäuse (*Mus musculus*). Dissertation, Universität Hamburg.
- Santoro B, Chen S, Luthi A, Pavlidis P, Shumyatsky GP, Tibbs GR, Siegelbaum SA (2000) Molecular and functional heterogeneity of hyperpolarization-activated pacemaker channels in the mouse CNS. *J Neurosci* 20:5264–5275.
- Santoro B, Grant SG, Bartsch D, Kandel ER (1997) Interactive cloning with the SH3 domain of N-src identifies a new brain specific ion channel protein, with homology to eag and cyclic nucleotide-gated channels. *Proc Natl Acad Sci U S A* 94:14815–14820.
- Santoro B, Lee JY, Englot DJ, Gildersleeve S, Piskorowski R a., Siegelbaum S a., Winawer MR, Blumenfeld H (2010) Increased seizure severity and seizure-related death in mice lacking HCN1 channels. *Epilepsia* 51:1624–1627.
- Santoro B, Liu DT, Yao H, Bartsch D, Kandel ER, Siegelbaum SA, Tibbs GR (1998) Identification of a gene encoding a hyperpolarization-activated pacemaker channel of brain. *Cell* 93:717–729.
- Santoro B, Piskorowski RA, Pian P, Hu L, Liu H, Siegelbaum SA (2009) TRIP8b Splice Variants Form a Family of Auxiliary Subunits that Regulate Gating and Trafficking of HCN Channels in the Brain. *Neuron* 62:802–813.
- Schlingloff D, Káli S, Freund TF, Hájos N, Gulyás AI (2014) Mechanisms of sharp wave

## REFERENCES

- initiation and ripple generation. *J Neurosci* 34:11385–11398.
- Schlusche AK (2011) Morphologische Charakterisierung zweier H-Strom defizienter Mauslinien. Diplomarbeit, Philipps-Universität Marburg.
- Schomburg EW, Anastassiou CA, Buzsáki G, Koch C (2012) The spiking component of oscillatory extracellular potentials in the rat hippocampus. *J Neurosci* 32:11798–11811.
- Schroeder BC, Kubisch C, Stein V, Jentsch TJ (1998) Moderate loss of function of cyclic-AMP-modulated KCNQ2/KCNQ3 K<sup>+</sup> channels causes epilepsy. *Nature* 396:687–690.
- Schulze-Bahr E, Neu A, Friederich P, Kaupp UB, Breithardt G, Pongs O, Isbrandt D (2003) Pacemaker channel dysfunction in a patient with sinus node disease. *J Clin Invest* 111:1537–1545.
- Sciancalepore M, Constanti A (1998) Inward-rectifying membrane currents activated by hyperpolarization in immature rat olfactory cortex neurones in vitro. *Brain Res* 814:133–142.
- Seelke A, Blumberg M (2010) Developmental appearance and disappearance of cortical events and oscillations in infant rats. *Brain Res* 1324:34–42.
- Seifert R, Scholten a, Gauss R, Mincheva a, Lichter P, Kaupp UB (1999) Molecular characterization of a slowly gating human hyperpolarization-activated channel predominantly expressed in thalamus, heart, and testis. *Proc Natl Acad Sci U S A* 96:9391–9396.
- Shah MM, Anderson AE, Leung V, Lin X, Johnston D (2004) Seizure-Induced Plasticity of h Channels in Entorhinal Cortical Layer III Pyramidal Neurons. *Neuron* 44:495–508.
- Shepherd GMG (2013) Corticostriatal connectivity and its role in disease. *Nat Rev Neurosci* 14:278–291.
- Shin M, Brager D, Jaramillo TC, Johnston D, M D (2009) Mislocalization of h channel subunits underlies h channelopathy in temporal lobe epilepsy. *October* 32:26–36.
- Sipilä ST, Huttu K, Soltesz I, Voipio J, Kaila K (2005) Depolarizing GABA acts on intrinsically bursting pyramidal neurons to drive giant depolarizing potentials in the immature hippocampus. *J Neurosci* 25:5280–5289.
- Sipilä ST, Huttu K, Voipio J, Kaila K (2006) Intrinsic bursting of immature CA3 pyramidal neurons and consequent giant depolarizing potentials are driven by a persistent Na<sup>+</sup> current and terminated by a slow Ca<sup>2+</sup>-activated K<sup>+</sup> current. *Eur J Neurosci* 23:2330–2338.
- Stark E, Roux L, Eichler R, Senzai Y, Royer S, Buzsáki G (2014) Pyramidal Cell-Interneuron Interactions Underlie Hippocampal Ripple Oscillations. *Neuron* 83:467–480.
- Stieber J, Herrmann S, Feil S, Löster J, Feil R, Biel M, Hofmann F, Ludwig A (2003) The hyperpolarization-activated channel HCN4 is required for the generation of pacemaker action potentials in the embryonic heart. *Proc Natl Acad Sci U S A* 100:15235–15240.
- Stieber J, Stöckl G, Herrmann S, Hassfurth B, Hofmann F (2005) Functional expression

## REFERENCES

- of the human HCN3 channel. *J Biol Chem* 280:34635–34643.
- Strata F, Atzori M, Molnar M, Ugolini G, Tempia F, Cherubini E (1997) A pacemaker current in dye-coupled hilar interneurons contributes to the generation of giant GABAergic potentials in developing hippocampus. *J Neurosci* 17:1435–1446.
- Strauss U, Kole MHP, Bräuer AU, Pahnke J, Bajorat R, Rolfs A, Nitsch R, Deisz RA (2004) An impaired neocortical Ih is associated with enhanced excitability and absence epilepsy. *Eur J Neurosci* 19:3048–3058.
- Stuart G, Spruston N (1998) Determinants of voltage attenuation in neocortical pyramidal neuron dendrites. *J Neurosci* 18:3501–3510.
- Sullivan D, Csicsvari J, Mizuseki K, Montgomery S, Diba K, Buzsaki G (2011) Relationships between Hippocampal Sharp Waves, Ripples, and Fast Gamma Oscillation: Influence of Dentate and Entorhinal Cortical Activity. *J Neurosci* 31:8605–8616.
- Tang B, Sander T, Craven KBK, Hempelmann A, Escayg A (2008) Mutation analysis of the hyperpolarization-activated cyclic nucleotide-gated channels HCN1 and HCN2 in idiopathic generalized epilepsy. *Neurobiol ...* 29:59–70.
- Tepper JM, Koos T, Wilson CJCJCJ, Koós T, Wilson CJCJCJ, Koos T (2004) GABAergic microcircuits in the neostriatum. *Trends Neurosci* 27:662–669.
- Thuault SJ, Malleret G, Constantinople CM, Nicholls R, Chen I, Zhu J, Panteleyev a., Vronskaya S, Nolan MF, Bruno R, Siegelbaum S a., Kandel ER (2013) Prefrontal Cortex HCN1 Channels Enable Intrinsic Persistent Neural Firing and Executive Memory Function. *J Neurosci* 33:13583–13599.
- Tsay D, Dudman JT, Siegelbaum SA (2007) HCN1 Channels Constrain Synaptically Evoked Ca<sup>2+</sup> Spikes in Distal Dendrites of CA1 Pyramidal Neurons. *Neuron* 56:1076–1089.
- Ulens C, Tytgat J (2001) Functional heteromerization of HCN1 and HCN2 pacemaker channels. *J Biol Chem* 276:6069–6072.
- Vaidya SP, Johnston D (2013) Temporal synchrony and gamma-to-theta power conversion in the dendrites of CA1 pyramidal neurons. *Nat Neurosci* 16:1812–1820.
- Valeeva G, Valiullina F, Khazipov R (2013) Excitatory actions of GABA in the intact neonatal rodent hippocampus in vitro. *Front Cell Neurosci* 7:20.
- Vasilyev D V, Barish ME (2002) Postnatal development of the hyperpolarization-activated excitatory current Ih in mouse hippocampal pyramidal neurons. *J Neurosci* 22:8992–9004.
- Wahl-Schott C, Biel M (2009) HCN channels: structure, cellular regulation and physiological function. *Cell Mol Life Sci* 66:470–494.
- Wainger BJ, Degennaro M, Santoro B, Siegelbaum SA, Tibbs GR (2001) Molecular mechanism of cAMP modulation of HCN pacemaker channels. *Nature* 411:805–810.
- Walaas SI, Lai Y, Gorelick FS, DeCamilli P, Moretti M, Greengard P (1988) Cell-specific localization of the alpha-subunit of calcium/calmodulin-dependent protein kinase II in Purkinje cells in rodent cerebellum. *Brain Res* 464:233–242.

## REFERENCES

- Wang M, Ramos BP, Paspalas CD, Shu Y, Simen A, Duque A, Vijayraghavan S, Brennan A, Dudley A, Nou E, Mazer J a, McCormick D a, Arnsten AFT (2007) Alpha2A-adrenoceptors strengthen working memory networks by inhibiting cAMP-HCN channel signaling in prefrontal cortex. *Cell* 129:397–410.
- Wang X, Zhang C, Szábo G, Sun QQ (2013) Distribution of CaMKII $\alpha$  expression in the brain in vivo, studied by CaMKII $\alpha$ -GFP mice. *Brain Res* 1518:9–25.
- Washio H, Takiguchi-Hayashi K, Konishi S (1999) Early postnatal development of substantia nigra neurons in rat midbrain slices: Hyperpolarization-activated inward current and dopamine-activated current. *Neurosci Res* 34:91–101.
- Watabe-Uchida M, Zhu L, Ogawa SK, Vamanrao A, Uchida N (2012) Whole-brain mapping of direct inputs to midbrain dopamine neurons. *Neuron* 74:858–873.
- Wilkars W, Liu Z, Lewis AS, Stoub TR, Ramos EM, Brandt N, Nicholson D a, Chetkovich DM, Bender R a (2012) Regulation of Axonal HCN1 Trafficking in Perforant Path Involves Expression of Specific TRIP8b Isoforms. *PLoS One* 7:e32181.
- Williams SR, Christensen SR, Stuart GJ, Hausser M (2002) Membrane potential bistability is controlled by the hyperpolarization-activated current I(H) in rat cerebellar Purkinje neurons in vitro. *J Physiol* 539:469–483.
- Xue T, Marbán E, Li R a. (2002) Dominant-Negative Suppression of HCN1- and HCN2-Encoded Pacemaker Currents by an Engineered HCN1 Construct: Insights Into Structure-Function Relationships and Multimerization. *Circ Res* 90:1267–1273.
- Yanagihara K, Irisawa H (1980) Inward current activated during hyperpolarization in the rabbit sinoatrial node cell. *Pflügers Arch Eur J Physiol* 385:11–19.
- Yang J-W, Hanganu-Opatz IL, Sun J-J, Luhmann HJ (2009) Three patterns of oscillatory activity differentially synchronize developing neocortical networks in vivo. *J Neurosci* 29:9011–9025.
- Ylinen a, Bragin a, Nádasdy Z, Jandó G, Szabó I, Sik a, Buzsáki G (1995) Sharp wave-associated high-frequency oscillation (200 Hz) in the intact hippocampus: network and intracellular mechanisms. *J Neurosci* 15:30–46.
- Zhang K, Peng BW, Sanchez RM (2006) Decreased IH in hippocampal area CA1 pyramidal neurons after perinatal seizure-inducing hypoxia. *Epilepsia* 47:1023–1028.
- Zhu JJ (2000) Maturation of layer 5 neocortical pyramidal neurons: amplifying salient layer 1 and layer 4 inputs by Ca<sup>2+</sup> action potentials in adult rat tuft dendrites. *J Physiol* 526 Pt 3:571–587.
- Zu T (2004) Recovery from Polyglutamine-Induced Neurodegeneration in Conditional SCA1 Transgenic Mice. *J Neurosci* 24:8853–8861.

## 6. Statistics

All tests were unpaired, two-tailed and significance accepted at  $P < 0.05$ . All  $P$  values above 0.1 were given as not significant (ns).

**Table 6-1: Neonatal hippocampal activity.**

Mann-Whitney  $U$  test to compare differences between control and mutant mice. Control  $n = 16$ , mutant  $n = 9$ . SPW, sharp wave; SRO, stratum radiatum oscillations.

Hippocampus	$U$	Group	$P$
SPW rate [Hz]	49.00		ns
SPW amplitude [mV]	50.00		ns
SRO rate [Hz]	56.00		ns
SRO mean length [ms]	47.00		ns
Time in SRO [%]	63.00		ns
SPW in SRO [%]	68.00		ns

**Table 6-2: Neonatal somatosensory cortex activity.**

Mann-Whitney  $U$  test to compare differences between control and mutant mice. Control  $n = 11$ , mutant  $n = 6$ . SAT, slow activity transient; SB, spindle burst.

Somatosensory cortex	$U$	Group	$P$
SAT I rate [counts/min]	28.00		ns
SAT II rate [counts/min]	19.50		ns
SB rate [counts/min]	22.00		ns

**Table 6-3: Neonatal visual cortex activity.**

Mann-Whitney  $U$  test to compare differences between control and mutant mice. Control  $n = 21$ , mutant  $n = 10$ . For SB mean length: control  $n = 16$ , mutant  $n = 4$ . SAT, slow activity transient; SB, spindle burst.

Visual cortex	$U$	Group	$P$
SAT rate [counts/min]	46.00		0.0114
SAT rate I [counts/min]	40.00		0.0040
SAT rate II [counts/min]	73.50		ns
SB rate [counts/min]	51.00		0.0183
SB mean length [ms]	26.00		ns

**Table 6-4: Adult hippocampal activity.**

One-way ANOVA having Group (control, mutant OFF, mutant ON/OFF) as between groups factor. Analysis was performed on the number of recordings obtained for each group. Slow wave sleep: control recordings n = 42, mutant OFF recordings n = 14, mutant ON/OFF recordings n = 17. REM sleep: control recordings n = 33, mutant OFF recordings n = 11, mutant ON/OFF recordings n = 17. SPW, sharp wave; SPW-R, sharp wave/ripple; or, stratum oriens; pyr, stratum pyramidale; rad, stratum radiatum; l.m., stratum lacunosum moleculare.

Slow wave sleep – SPW-R properties	F <sub>2,70</sub>	Group	
			P
Ripple frequency [Hz]	19.37		< 0.0001
Ripple duration [ms]	6.040		0.0038
SPW amplitude [normalized to mean minimum in radiatum]	6.064		0.0037
SPW-R occurrence rate [Hz]	6.463		0.0027

REM sleep – peak theta frequency	F <sub>2,12</sub>	Group	
			P
Peak theta or [Hz]	2.860		0.0654
Peak theta pyr [Hz]	3.722		0.0301
Peak theta rad [Hz]	1.400		ns
Peak theta l.m. [Hz]	2.520		0.0892

**Table 6-5: Adult hippocampal activity – coherence analysis.**

One-way ANOVA having group (control, mutant OFF, mutant ON/OFF) as between groups factor. Analysis was performed per recording. Control n = 33, mutant OFF n = 11, mutant ON/OFF n = 17.

REM sleep – coherence	F <sub>2,58</sub>	Group	
			P
L.m. – pyr theta	7.954		0.0009
L.m. – pyr beta	12.728		< 0.0001
L.m. – pyr gamma	10.336		0.0001
Rad – pyr theta	5.732		0.0054
Rad – pyr beta	6.565		0.0027
Rad – pyr gamma	6.583		0.0027
L.m. – rad theta	1.735		ns
L.m. – rad beta	2.035		ns
L.m. – rad gamma	1.303		ns

**Table 6-6: Activity in the home cage**

Student's *t* test to compare differences in home cage activity during the active phase of control OFF, mutant OFF and mutant ON/OFF mice. Control OFF n = 14, mutant OFF n = 14, mutant ON/OFF n = 13.

	<i>t</i>	<i>df</i>	<i>P</i>
control vs. mutant OFF	10.44	26	< 0.0001
control OFF vs. mutant ON/OFF	3.659	25	0.0012
mutant OFF vs. mutant ON/OFF	2.042	25	0.0519

**Table 6-7: Open field activity**

Student's *t* test to compare control and mutants of the OFF, ON/OFF and OFF/ON groups. Control OFF n = 29, mutant OFF n = 18, control ON/OFF n = 21, mutant ON/OFF n = 27, control OFF/ON n = 19, mutant OFF/ON n = 17.

	OFF			ON/OFF			OFF/ON		
	<i>t</i>	<i>df</i>	<i>P</i>	<i>t</i>	<i>df</i>	<i>P</i>	<i>t</i>	<i>df</i>	<i>P</i>
Distance moved [cm]	2.192	45	0.0336	1.680	46	0.0997	0.3868	34	ns
Run speed [cm/sec]	2.162	45	0.0360	2.633	46	0.0115	0.3626	34	ns
Rotations [n/min]	6.605	45	<0.0001	1.519	46	ns	1.331	34	ns
Time in border [%]	5.319	45	<0.0001	1.337	46	ns	2.344	34	0.0251
Time in center [%]	4.002	45	0.0002	0.537	46	ns	2.387	34	0.0227

**Table 6-8: Distance moved over time in the open field**

A two-way mixed ANOVA for repeated measurements with group (control and mutant) as between groups factor and time (3 x 5 min time bins) as within groups factor was performed. Control OFF n = 29, mutant OFF n = 18, control ON/OFF n = 21, mutant ON/OFF n = 27, control OFF/ON n = 19, mutant OFF/ON n = 17.

Distance moved	Group		Time		G x T	
	F <sub>1,45</sub>	P	F <sub>2,90</sub>	P	F <sub>2,90</sub>	P
control vs. mutant OFF	4.804	0.0336	7.559	0.0009	23.407	<0.0001

control vs. mutant ON/OFF	Group		Time		G x T	
	F <sub>1,46</sub>	P	F <sub>2,92</sub>	P	F <sub>2,92</sub>	P
	2.823	0.0997	10.455	<0.0001	0.209	ns

control vs. mutant OFF/ON	Group		Time		G x T	
	F <sub>1,34</sub>	P	F <sub>2,68</sub>	P	F <sub>2,68</sub>	P
	0.149	ns	3.112	0.0509	5.153	0.0082

**Table 6-9: Telemetric wake and sleep analysis.**

Mann Whitney U test to compare control and mutant mice. Control n = 4, mutant n = 3.

	% time in state		bout duration		bout numer	
	U	P	U	P	U	P
Wake	3.0	ns	3.0	ns	2.0	ns
Active wake	6.0	ns	0	0.0571	2.0	ns
Slow wave sleep	2.0	ns	4.0	ns	6.0	ns
REM sleep	0	0.0571	1.0	ns	3.0	ns

**Table 6-10: Spontaneous alternation in the Y maze.**

Student's t test to compare differences in the preference for the novel arm, and time needed for the total amount of alternations. Control OFF n = 31, mutant OFF n = 21, control OFF/ON n = 19, mutant OFF/ON n = 16, control ON/OFF n = 23, mutant ON/OFF n = 32.

	OFF			OFF/ON			ON/OFF		
	t	df	P	t	df	P	t	df	P
Novel arm choices [%]	1.427	50	ns	2.494	33	0.0178	1.186	53	ns
Time for alternation [s]	2.449	50	0.0179	1.044	33	ns	2.241	53	0.0292

**Table 6-11: Water maze performance in learning trials.**

Analysis was performed with a mixed two-way ANOVA for repeated measurements, having group (control and mutant) as between groups factor and trial (8 trials over 2 days) as within groups factor. Control OFF n = 22, mutant OFF n = 13, control ON/OFF n = 8, mutant ON/OFF n = 11, control OFF/ON n = 8, mutant OFF/ON n = 9.

OFF	Group		Trial		G x T	
	F <sub>1,33</sub>	P	F <sub>7,231</sub>	P	F <sub>7,231</sub>	P
Distance moved [cm]	34.478	<0.0001	5.349	<0.0001	2.587	0.0138
Escape latency [sec]	42.246	<0.0001	6.041	<0.0001	3.401	0.0018
Distance to border [cm]	10.605	0.0033	3.345	0.0020	2.290	0.0284
Distance to platform [cm]	32.346	<0.0001	16.701	<0.0001	2.174	0.0374
Rotations [n]	60.932	<0.0001	4.211	0.0002	1.058	ns
ON/OFF	Group		Trial		G x T	
	F <sub>1,17</sub>	P	F <sub>7,119</sub>	P	F <sub>7,119</sub>	P
Distance moved [cm]	2.710	ns	9.558	<0.0001	1.239	ns
Escape latency [sec]	1.168	ns	12.167	<0.0001	1.206	ns
Distance to border [cm]	0.012	ns	4.389	0.0002	0.726	ns
Distance to platform [cm]	0.619	ns	23.499	<0.0001	0.537	ns
Rotations [n]	4.267	0.0545	12.485	<0.0001	1.128	ns
OFF/ON	Group		Trial		G x T	
	F <sub>1,15</sub>	P	F <sub>7,105</sub>	P	F <sub>7,105</sub>	P
Distance moved [cm]	4.029	0.0631	1.248	ns	0.783	ns
Escape latency [sec]	4.117	0.0606	1.178	ns	0.757	ns
Distance to border [cm]	1.322	ns	4.023	0.0006	1.130	ns
Distance to platform [cm]	5.769	0.0297	4.675	0.0001	0.925	ns
Rotations [n]	8.284	0.0077	1.079	ns	0.235	ns

**Table 6-12: Water maze, probe trial.**

Time spent in each of the four different quadrants (target, right, left, opposite) was expressed as percentage of total trial duration. The times spent in each quadrant for control and mutant mice were compared with Student's *t* test. Control OFF n = 22, mutant OFF n = 13, control ON/OFF n = 8, mutant ON/OFF n = 11, control OFF/ON n = 15, mutant OFF/ON n = 14.

	OFF			ON/OFF			OFF/ON		
	<i>t</i>	df	P	<i>t</i>	df	P	<i>t</i>	df	P
Target [%]	1.108	33	ns	0.276	17	ns	1.371	27	ns
Right [%]	0.186	33	ns	1.110	17	ns	1.716	27	0.0976
Left [%]	0.857	33	ns	1.810	17	0.0880	1.477	27	ns
Opposite [%]	0.766	33	ns	0.678	17	ns	1.204	27	ns

**Table 6-13: Contextual fear conditioning.**

Student's *t* test to compare OFF and ON/OFF animals. Mann-Whitney U test to compare OFF/ON animals. Baseline and footshock: Control OFF *n* = 24, mutant OFF *n* = 16; Recall: control OFF *n* = 27, mutant OFF *n* = 19. Control OFF/ON *n* = 6, mutant OFF/ON *n* = 5. Baseline and footshock: Control ON/OFF *n* = 11, mutant ON/OFF *n* = 18. Recall: control ON/OFF *n* = 15, mutant ON/OFF *n* = 24.

Freezing [%]	OFF			OFF/ON		ON/OFF		
	<i>t</i>	<i>df</i>	<i>P</i>	<i>U</i>	<i>P</i>	<i>t</i>	<i>df</i>	<i>P</i>
Baseline	0.226	38	ns	10.00	ns	1.364	27	ns
After footshock	0.128	38	ns	12.00	ns	0.776	27	ns
Recall	1.795	44	0.0796	10.00	ns	0.478	37	ns

**Table 6-14: Pole test performance**

The Fisher's exact probability test was used to compare between groups the number of mice successfully climbing down the pole with the number of mice not being able to climb down. Total number of mice per group is indicated in the table. Con = control, mut = mutant.

	Trial 1			Trial 2			Trial 3		
	<i>n</i>	<i>n</i>	<i>P</i>	<i>n</i>	<i>n</i>	<i>P</i>	<i>n</i>	<i>n</i>	<i>P</i>
con vs. mut male OFF	23/30	1/13	0.0000	28/30	3/13	0.0000	25/30	2/13	0.0000
con vs. mut female OFF	23/30	4/7	ns	28/30	3/7	0.0068	25/30	5/7	ns
mut male vs. female OFF	1/13	4/7	0.0307	3/13	3/7	ns	2/13	5/7	0.0223
con vs. mut ON/OFF	10/12	13/16	ns	12/12	16/16	-	7/12	12/16	ns
con vs. mut OFF/ON	12/17	7/15	ns	14/17	7/15	0.0617	15/17	6/15	0.0057

**Table 6-15: Rotarod performance**

A two-way mixed ANOVA for repeated measurements with Group (control and mutant) as between groups factor and Trial (Trials 1 to 4) as within groups factor was performed. Male and female mutants OFF were separately compared to controls OFF. Control OFF *n* = 30, mutant female OFF *n* = 7, mutant male OFF *n* = 13, control ON/OFF *n* = 17, mutant ON/OFF *n* = 23, control OFF/ON *n* = 17, mutant OFF/ON *n* = 10.

Latency to fall [s]	Group		Trial		G x T	
	<i>F</i> <sub>2,47</sub>	<i>P</i>	<i>F</i> <sub>3,141</sub>	<i>P</i>	<i>F</i> <sub>6,141</sub>	<i>P</i>
control vs. mutant male vs. mutant female OFF	10.21	0.0002	7.64	0.0000	0.73	ns
control vs. mutant ON/OFF	Group		Trial		G x T	
	<i>F</i> <sub>1,38</sub>	<i>P</i>	<i>F</i> <sub>3,114</sub>	<i>P</i>	<i>F</i> <sub>3,114</sub>	<i>P</i>
control vs. mutant ON/OFF	0.00	ns	3.05	0.0316	0.99	ns
control vs. mutant OFF/ON	Group		Trial		G x T	
	<i>F</i> <sub>1,30</sub>	<i>P</i>	<i>F</i> <sub>3,90</sub>	<i>P</i>	<i>F</i> <sub>3,90</sub>	<i>P</i>
control vs. mutant OFF/ON	6.89	0.0135	5.66	0.0013	3.01	0.0342

**Table 6-16: Rotarod performance in control mice**

A two-way mixed ANOVA for repeated measurements with Group (OFF, ON/OFF, OFF/ON) as between groups factor and Trial (Trials 1 to 4) as within groups factor was performed. Control OFF *n* = 30, control ON/OFF *n* = 17, control OFF/ON *n* = 17.

Latency to fall [sec]	Group		Trial		G x T	
	<i>F</i> <sub>2,61</sub>	<i>P</i>	<i>F</i> <sub>3,183</sub>	<i>P</i>	<i>F</i> <sub>6,183</sub>	<i>P</i>
Latency to fall [sec]	22.44	0.0000	12.70	0.0000	1.20	ns

**Table 6-17: Grip test**

Student's *t* test to compare differences in forelimb strength. Control OFF *n* = 30, mutant OFF *n* = 20, control ON/OFF *n* = 8, mutant ON/OFF *n* = 11, control OFF/ON *n* = 17, mutant OFF/ON *n* = 15.

	<i>t</i>	<i>df</i>	<i>P</i>
control vs. mutant OFF	7.379	48	< 0.0001
control vs. mutant ON/OFF	2.196	17	0.0423
control vs. mutant OFF/ON	2.774	30	0.0094

**Table 6-18: Gait analysis**

Student's *t* test to compare differences in gait parameters. Control OFF *n* = 6, mutant OFF *n* = 6, control ON/OFF *n* = 10, mutant ON/OFF *n* = 13, control OFF/ON *n* = 17, mutant OFF/ON *n* = 15.

	OFF			ON/OFF			OFF/ON		
	<i>t</i>	<i>df</i>	<i>P</i>	<i>t</i>	<i>df</i>	<i>P</i>	<i>t</i>	<i>df</i>	<i>P</i>
Running speed [cm/s]	1.404	10	ns	1.578	21	ns	0.631	31	ns
Stand [s]	2.214	10	0.0512	0.018	21	ns	2.133	31	0.0410
Step cycle [s]	2.173	10	0.0549	0.373	21	ns	2.066	31	0.0473
Stride length [cm]	2.109	10	0.0611	1.005	21	ns	2.922	31	0.0064
BOS [cm]	2.683	10	0.0230	1.877	21	0.0745	2.332	31	0.0264
Regularity index [%]	1.783	10	ns	0.776	21	ns	2.308	31	0.0279

Mann-Whitney *U* test to compare differences in step sequence patterns.

	OFF		ON/OFF		OFF/ON	
	<i>U</i>	<i>P</i>	<i>U</i>	<i>P</i>	<i>U</i>	<i>P</i>
Step sequence Ab [%]	6	0.0584	33.50	0.0512	85	0.0815
Step sequence Rb [%]	12	ns	56	ns	85.5	0.0084

**Table 6-19: Pole test performance of mice with PC-restricted I(h) deficiency**

The Fisher's exact probability test was used to compare between groups the number of mice successfully climbing down the pole with the number of mice not being able to climb down. Total number of mice per group is indicated in the table. Control OFF *n* = 8, mutant OFF *n* = 9, mutant ON/OFF *n* = 11. Con = control, mut = mutant.

	Trial 1			Trial 2			Trial 3		
	<i>n</i>		<i>P</i>	<i>n</i>		<i>P</i>	<i>n</i>		<i>P</i>
con OFF vs. mut OFF	4/8	2/9	ns	7/8	7/9	ns	7/8	6/9	ns
con OFF vs. mut ON/OFF	4/8	4/11	ns	7/8	6/11	ns	7/8	10/11	ns
mut OFF vs. mut ON/OFF	2/9	4/11	ns	7/9	6/11	ns	6/9	10/11	ns

**Table 6-20: Rotarod performance of mice with PC-restricted I(h) deficiency**

A two-way mixed ANOVA for repeated measurements with Group (control OFF, mutant OFF, and mutant ON/OFF) as between groups factor and Day (Days 1 to 4) as within groups factor was performed. Control OFF *n* = 8, mutant OFF *n* = 9, mutant ON/OFF *n* = 11.

	Group		Day		G x D	
	<i>F</i> <sub>2, 25</sub>	<i>P</i>	<i>F</i> <sub>3, 75</sub>	<i>P</i>	<i>F</i> <sub>6, 75</sub>	<i>P</i>
Latency to fall [s]	3.99	0.0312	45.03	0.0000	1.68	0.1375

**Table 6-21: Gait analysis of mice with PC-restricted I(h) deficiency**

One-way ANOVA with Group (control OFF, mutant OFF, mutant ON/OFF) as between groups factor. Control OFF *n* = 8, mutant OFF *n* = 9, mutant ON/OFF *n* = 11.

	Group	
	<i>F</i> <sub>2, 25</sub>	<i>P</i>
Running speed [cm/s]	1.49	ns
Stand [s]	0.99	ns
Step cycle [s]	1.09	ns
Stride length [cm]	3.99	0.0312
BOS [cm]	0.86	ns
Regularity index [%]	0.71	ns
Alternating step sequence [%]	1.08	ns

## 7. Index

Abstract.....	i
1. Introduction.....	1
1.1. Hyperpolarization-activated cyclic nucleotide-gated cation channels.....	1
1.1.1. HCN channel-mediated currents – I(h).....	1
1.1.2. HCN channel family and regulation.....	4
1.1.3. HCN channel expression pattern.....	5
1.2. Physiological roles of I(h).....	7
1.2.1. From excitability to behavior.....	7
1.2.2. HCN channel dysfunction is associated with disease.....	10
1.2.3. Role of I(h) in CNS development.....	11
1.3. Aims of the study.....	14
2. Material and Methods.....	16
2.1. Animals and husbandry.....	16
2.2. Genotyping.....	16
2.2.1. Isolation of genomic DNA from tail biopsies.....	16
2.2.2. Isolation of genomic DNA from ear biopsies.....	16
2.2.3. Polymerase chain reaction.....	17
2.2.4. Agarose gel electrophoresis.....	17
2.3. <i>In situ</i> hybridisation.....	19
2.3.1. Preparation of probe.....	19
2.3.2. Hybridisation protocol.....	19
2.4. Western blot.....	21
2.5. Histology.....	22
2.5.1. Perfusion.....	22
2.5.2. Slice preparation.....	22

2.5.3.	Immunolabeling .....	22
2.5.4.	Microscopy .....	23
2.6.	Whole-cell patch clamp recordings .....	23
2.6.1.	Electrophysiological recordings from neonatal CA1 pyramidal neurons	23
2.6.2.	Electrophysiological recordings from adult CA1 pyramidal neurons.....	24
2.6.3.	Electrophysiological recordings from adult entorhinal cortex layer III pyramidal neurons .....	24
2.7.	<i>In vivo</i> depth recordings.....	25
2.7.1.	<i>In vivo</i> depth recordings in neonatal head-fixed mice .....	25
2.7.2.	<i>In vivo</i> depth recordings in adult behaving mice .....	26
2.7.3.	Data acquisition and analysis.....	27
2.8.	Telemetric electrocorticogram recordings .....	28
2.8.1.	Implantation of radio transmitters.....	28
2.8.2.	Data analysis.....	28
2.9.	Behavioral analysis.....	29
2.9.1.	Home cage activity .....	29
2.9.2.	Grip strength .....	29
2.9.3.	Pole test.....	30
2.9.4.	Rotarod .....	30
2.9.5.	Beam walk .....	31
2.9.6.	Catwalk.....	31
2.9.7.	Open field .....	32
2.9.8.	Spontaneous alternation.....	32
2.9.9.	Water maze .....	32
2.9.10.	Contextual fear conditioning .....	33
2.10.	Statistics.....	33
3.	Results .....	35

3.1.	I(h) deficiency causes hyperexcitability in forebrain projection neurons.....	37
3.1.1.	Mice with forebrain-restricted I(h) deficiency in projection neurons.....	37
3.1.2.	Localization of HCN-DN expression via EGFP in forebrain regions.....	40
3.1.3.	HCN-DN expression causes hyperexcitability in brain slices .....	44
3.2.	<i>In vivo</i> cortical and hippocampal activity is affected by I(h) deficiency .....	47
3.2.1.	Functional suppression of I(h) alters spontaneous local field potential activity in neonatal mice .....	47
3.2.2.	Adult network activity is affected by I(h) deficiency .....	51
3.3.	I(h) deficiency causes behavioral abnormalities.....	54
3.3.1.	General behavioral hyperactivity .....	54
3.3.2.	Sleep behavior .....	57
3.4.	Cognitive deficits are dependent on age of onset of I(h) deficiency .....	59
3.4.1.	Working memory .....	59
3.4.2.	Spatial learning and memory in the water maze .....	60
3.4.3.	Contextual fear conditioning .....	62
3.5.	I(h) exerts functional roles in motor coordination and motor learning.....	64
3.5.1.	Gait abnormalities develop at early postnatal ages.....	64
3.5.2.	I(h) deficiency during development affects motor learning.....	66
3.5.3.	I(h) ablation in cerebellar Purkinje cells does not affect motor behavior	69
4.	Discussion.....	72
4.1.	Advantages and limitations of functional I(h) ablation by HCN-DN expression	72
4.1.1.	HCN-DN subunit expression functionally ablates endogenous HCN1-4 channel-mediated currents .....	72
4.1.2.	The transgenic CaMKII $\alpha$ promoter line limits HCN-DN expression to a smaller subset of the endogenously CaMKII $\alpha$ -expressing neuronal population .....	74
4.2.	HCN-DN-mediated neuronal hyperexcitability affects neonatal and adult network activity .....	76

4.2.1.	I(h) ablation reduces neonatal spontaneous cortical activity .....	76
4.2.2.	I(h) contributes to sharp wave-ripple properties .....	78
4.2.3.	I(h) contributes to theta frequency oscillations.....	80
4.3.	Implications for the role of I(h) in learning and memory .....	82
4.4.	Motor function deficits and hyperactivity suggest roles of I(h) in cortico-basal ganglia communication.....	83
4.4.1.	Role of I(h) in the cortico-basal ganglia-thalamocortical loop .....	86
4.4.2.	Role of I(h) in cerebellar motor control.....	88
4.5.	I(h) is necessary during early postnatal development.....	89
5.	References.....	92
6.	Statistics.....	106
7.	Index .....	112
8.	Figure index .....	116
9.	Table index .....	117
10.	Abbreviations.....	118
	Acknowledgement .....	124
	Declaration.....	125

## 8. Figure index

Figure 1-1: Characteristics of I(h) conductance under experimental conditions. ....	3
Figure 1-2: Structure of HCN channels. ....	5
Figure 3-1: Tet-Off system to study I(h) deficiency at different developmental stages. .	36
Figure 3-2: Mice with forebrain-specific I(h) ablation. ....	39
Figure 3-3: EGFP expression in cortical regions. ....	41
Figure 3-4: EGFP expression in the hippocampus. ....	42
Figure 3-5: EGFP expression in subcortical regions. ....	43
Figure 3-6: Lack of I(h) increases entorhinal cortex layer 3 pyramidal neuron excitability <i>in vitro</i> . ....	45
Figure 3-7: I(h) ablation affects integration of EPSPs. ....	46
Figure 3-8: Hippocampal local field potential activity is not affected by I(h) ablation. ...	48
Figure 3-9: Activity in somatosensory cortex is slightly affected by suppressed I(h). ....	49
Figure 3-10: Spontaneous activity in visual cortex is attenuated upon I(h) deficiency. ...	50
Figure 3-11: Hippocampal LFP sleep patterns in adult mice. ....	52
Figure 3-12: Ripple frequency is reduced upon developmental I(h) attenuation. ....	53
Figure 3-13: Theta oscillations during REM sleep are affected by I(h) deficiency. ....	54
Figure 3-14: Behavioral hyperactivity upon I(h) deficiency. ....	56
Figure 3-15: Distribution of waking and sleeping behavior over the day. ....	58
Figure 3-16: Working memory performance in the spontaneous alternation task. ....	59
Figure 3-17: Spatial learning in the water maze is dependent on age of onset of I(h) deficiency. ....	61
Figure 3-18: Context-dependent fear memory does not rely on I(h). ....	63
Figure 3-19: Gait abnormalities upon I(h) deficiency during early development. ....	65
Figure 3-20: Motor function deficits were partially linked to early developmental I(h) ablation. ....	68
Figure 3-21: Mice with cerebellar Purkinje cell-specific I(h) ablation. ....	70
Figure 3-22: Cerebellar Purkinje cell-specific I(h) ablation does not affect gait properties or motor learning. ....	71

## 9. Table index

Table 2-1: Nucleotide sequences of oligonucleotides used for PCR and expected product size.....	18
Table 2-2: Touchdown PCR protocol to amplify the tTA transgene.....	18
Table 2-3: PCR protocol to amplify hHCN4-G480S transgene.....	18
Table 2-4: Primer for <i>in situ</i> hybridization probe specific to hHCN4-G480S.....	20
Table 6-1: Neonatal hippocampal activity.....	106
Table 6-2: Neonatal somatosensory cortex activity.....	106
Table 6-3: Neonatal visual cortex activity.....	106
Table 6-4: Adult hippocampal activity.....	107
Table 6-5: Adult hippocampal activity – coherence analysis.....	107
Table 6-6: Activity in the home cage.....	107
Table 6-7: Open field activity.....	107
Table 6-8: Distance moved over time in the open field.....	108
Table 6-9: Telemetric wake and sleep analysis.....	108
Table 6-10: Spontaneous alternation in the Y maze.....	108
Table 6-11: Water maze performance in learning trials.....	109
Table 6-12: Water maze, probe trial.....	109
Table 6-13: Contextual fear conditioning.....	110
Table 6-14: Pole test performance.....	110
Table 6-15: Rotarod performance.....	110
Table 6-16: Rotarod performance in control mice.....	110
Table 6-17: Grip test.....	110
Table 6-18: Gait analysis.....	111
Table 6-19: Pole test performance of mice with PC-restricted I(h) deficiency.....	111
Table 6-20: Rotarod performance of mice with PC-restricted I(h) deficiency.....	111
Table 6-21: Gait analysis of mice with PC-restricted I(h) deficiency.....	111

## 10. Abbreviations

°	degree
°C	degree Celsius
μl	microliter
μm	micrometer
A	Ampere
AAA	alanine-alanine-alanine
ACSF	artificial cerebrospinal fluid
ADHD	attention deficit/hyperactivity disorder
AMPA	α-amino-3-hydroxy-5-methyl-4-isoxazolepropionic acid
ANOVA	analysis of variance
ap	apathetic
APV	DL-2-amino-5-phosphonovaleric acid
ASD	autism spectrum disorder
BCA	bicinchoninic acid
BOS	base of support
bp	base pair
BSA	bovine serum albumin
CA1	cornu ammonis region 1
CAMKII	Ca <sup>2+</sup> /calmodulin-dependent protein kinase II
CaMKIIα, CamK2α	Ca <sup>2+</sup> /calmodulin-dependent protein kinase II alpha
cAMP	cyclic adenosine monophosphate
CCD	charge-coupled device
cm	centimeter
cmp	counts per minute
CNBD	cyclic nucleotide-binding domain
CNQX	6-cyano-7-nitroquinoxaline-2,3-dione
CNS	central nervous system
CP	caudoputamen
Cs	cesium
CSD	current-source-density
CST	corticospinal tract

C-terminus	COOH-terminus, carboxy terminus
Da	Dalton
DAPI	4',6-diamidino-2-phenylindole
DG	dentate gyrus
DIG	digoxigenin
DN	dominant-negative
DNA	deoxyribonucleic acid
dox	doxycycline
DRG	dorsal root ganglion
DTT	dithiothreitol
EC L3	entorhinal cortex layer 3
ECG	electrocardiogram
ECoG	electrocorticogram
EDTA	ethylenediaminetetraacetic acid
EEG	electroencephalogram
EGFP	<i>Enhanced Green Fluorescent Protein</i>
EIEE	early infantile epileptic encephalopathy
ENO	early network oscillation
EPSP	excitatory postsynaptic potential
fig	figure
FVB	mouse line sensitive to the Friend leukemia virus B strain
g	acceleration relative to free-fall
GABA	gamma-Aminobutyric acid
GDP	giant depolarizing potential
GPe	globus pallidus external segment
GPi	globus pallidus internal segment
GTP	Guanosine-5'-triphosphate
gr	granule cell layer
GYG	glycine-tyrosine-glycine
GYS	glycine-tyrosine-serine
h	hour
HA	RNase
HCN	hyperpolarization-activated cyclic nucleotide-gated
HEK	human embryonic kidney

HRP	horse radish peroxidase
Hz	Hertz
I(f)	funny current
I(h)	hyperpolarizing current
I(q)	queer current
i.e.	id est
IGE	generalized idiopathic epilepsy
IgG	Immunoglobulin G
IPSP	inhibitory postsynaptic potential
IR-DIC	infrared-differential interference contrast
ISI	intersession interval
ITI	intertrial interval
K	potassium
KCNQ1	Potassium voltage-gated channel subfamily KQT member 1
KO	knock-out
Kv7	voltage-gated potassium channel 7
LD	learning day
l.m.	stratum lacunosum moleculare in CA1
LFP	local field potential
LTP	long term potentiation
luc	stratum lucidum in CA3
M	mega
M	molar
mA	milliampere
M-current	muscarinic acetylcholine receptor activation dependent non-inactivating potassium current
MeOH	methanol
mg	milligram
min	minute
MiRP1	min-K related protein 1
ml	milliliter
mM	millimolar
mo	molecular layer

MRC	Minimum resolvable contrast
mRNA	messenger RNA
mV	millivolt
MΩ	Ohm
n	number
Na	sodium
NMDA	N-Methyl-D-aspartic acid
N-terminus	amino terminus, NH <sub>4</sub> -terminus
ori	stratum oriens in CA1
<i>P</i>	probability
P	postnatal day
p	pico
P	pore forming region
PAGE	polyacrylamide gel electrophoresis
PBS	phosphate buffered saline
pc	Purkinje cell layer
PCP2	Purkinje cell protein-2
PCR	Polymerase chain reaction
PD	Privatdozent
PD	Parkinsons disease
PFA	paraformaldehyde
pH	potentia Hydrogenii
PIP <sub>2</sub>	phosphatidylinositol-4, 5-bisphosphate
PKA	protein kinase A
PKC	protein kinase C
po	polymorph layer of DG
py	pyramidal tract
pyr	stratum pyramidale in CA1
QT interval	time between start of Q wave and end of T wave in ECG
Rab8b	member of RAS oncogenes family
rad	stratum radiatum in CA1
rcf	relative centrifugal force
REM	rapid eye movement
R <sub>in</sub>	input resistance

RMP	resting membrane potential
RN	raphe nucleus
RNA	Ribonucleic acid
RNase	ribonuclease
rpm	rounds per minute
s	second
S	sulphure
S.E.M	standard error of the mean
S1, S2, S3...	transmembrane segment 1, 2, 3...
S1HL	somatosensory hind limb
SAN	sinoatrial node
SAT	slow activity transients
SB	spindle burst
SDS	sodium dodecyl sulfate
SNc	substantia nigra pars compacta
SNr	substantia nigra pars reticulata
SPW	sharp wave
SPW-R	sharp wave-ripple
SRO	stratum radiatum oscillation
SSC	saline sodium citrate buffer
STN	subthalamic nucleus
T7	T7 bacteriophage
TAE	tris-acetic acid-EDTA
TBS	tris-buffered saline
Terd	conserved part of the delta chain of the T cell receptor
tet	tetracycline
tetO	tetracycline operator
Tg	transgene
TLE	temporal lobe epilepsy
TRE	tetracycline-response element
TRIP8b	tetratricopeptide repeat-containing Rab8b interacting protein
tRNA	transfer RNA
tTA	transcriptional transactivator

UTP	Uridine-5'-triphosphate
UV	ultraviolet
V	Volt
V1	primary visual cortex
$V_{1/2}, V_{0,5}$	voltage of half-maximal activation
VGCC	voltage-gated calcium channel
$V_m$	membrane potential
ZMNH	<i>Zentrum für molekulare Neurobiologie Hamburg</i>

## Acknowledgement

I first have to heartily thank Prof. Dr. Arp Schnittger and Prof. Dr. Dirk Isbrandt for agreeing to co-supervise this thesis and to additionally thank PD Dr. Sabine Hoffmeister-Ullerich and Dr. Fabio Morellini for support and scientific suggestions that made the writing of this thesis possible.

Special thanks go to Prof. Dr. Dirk Isbrandt for providing me the opportunity to work on a fascinating project in his laboratory. I want to also thank him for his significant guidance, support, inspiration and his inexhaustible help in any matter, scientific and otherwise, and most of all for his trust in me as a scientist.

I want to thank the collaborators from the laboratory of Prof. Mala Shah (including Dr. Zhuo Huang), and Dr. Steffi Sandke, PD Dr. Axel Neu and Prof. Dr. Jochen Roeper for their input and work on this project.

Many thanks go to all the wonderful people of the ENP team in Cologne and Hamburg, who have become valuable colleagues and friends and who are always understanding, supportive, helpful and inspiring.

Over the past five years I have had the pleasure to meet many great people with whom I became colleagues, but more so, friends. I must especially thank Dr. Katharine Miller and Anna Katharina Schlusche for their friendship and caring support during the entire time of my PhD.

Most importantly, I want to thank my dear friend Dr. Stephan Marguet. Without him I would not be where I am today, or the person that I am today. All my love goes to him.

## Declaration

I hereby declare, on oath, that the present dissertation titled “HCN/h-channel deficiency in forebrain neurons impairs early postnatal development and alters neuronal network activity in mice (*Mus musculus*, Linnaeus 1758)” does not contain materials written or published by another person, except where due reference is given in the text.

Hamburg, April 15<sup>th</sup> 2016

---

Andrea Merseburg